

THESIS

OLEOPHILIC BIO BARRIERS (OBBS) FOR CONTROL OF HYDROCARBON SHEENS AT GROUNDWATER-  
SURFACE WATER INTERFACES

Submitted by

Marc William Chalfant

Department of Civil and Environmental Engineering

In partial fulfillment of the requirements

For the Degree of Master of Science

Colorado State University

Fort Collins, Colorado

Summer 2015

Master's Committee:

Advisor: Tom Sale

Greg Butters

Michael Gooseff

Copyright by Marc William Chalfant 2015

All Rights Reserved

## ABSTRACT

### OLEOPHILIC BIO BARRIERS (OBBS) FOR CONTROL OF HYDROCARBON SHEENS AT GROUNDWATER-SURFACE WATER INTERFACES

Sheens are a common problem at petroleum facilities located adjacent to surface water bodies. Thin, iridescent films of Non-Aqueous Phase Liquid (**NAPL**) can form on surface water sporadically and unpredictably via three processes: seeps, ebullition, and/or shoreline erosion. Because the appearance of sheens can elicit a notice of violation of the Clean Water Act, a suite of remedies has been used to address them. Common remedies are often predicated on physical barriers and sorbent barriers, both of which can be expensive and/or prone to failure due to bypass and/or finite storage capacities.

Groundwater-Surface water Interfaces (**GSIs**) are active biological zones where NAPL fluxes are attenuated via aerobic biological degradation. Physical and sorptive barriers can inhibit aerobic degradation processes by causing NAPL to accumulate, preventing oxygen delivery or introducing organic matter that exerts an oxygen demand. Shortcomings of current sheen remedies motivate the research presented herein, exploring the concept of aerobic reactive barriers at GSIs. Specifically, the concept of an Oleophilic Bio Barrier (**OBB**) is advanced. An OBB prevents sheens due to seeps, ebullition, and erosion by employing 1) an oleophilic geocomposite to sorb NAPL, 2) aerobic degradation of NAPL via naturally occurring microbes, and 3) structural cover to mitigate erosion. A full US patent detailing these concepts was submitted to the US patent office in September 2014 (Zimbron et al., 2014).

The work presented herein includes laboratory studies, a preliminary field study, a full-scale field demonstration and a general estimate of construction costs. Results of the lab studies provided proof-of-concept that a geocomposite material in an OBB could prevent sheens. The geocomposite was shown

to have a capacity of 3L of NAPL/m<sup>2</sup>. The geocomposite was also shown to reduce dissolved hydrocarbon concentrations by up to 77%. The preliminary field study showed that an OBB could be used to prevent sheens in a field setting. Four 1m x 1m OBBs were installed in March 2013 and monitored through August 2013. In August, NAPL saturations of up to 1.6 L/m<sup>2</sup> were measured in the OBBs, demonstrating their ability to prevent sheens. The geocomposite maintained structural integrity, suggesting chemical compatibility with the NAPL. A low redox potential (62 mV) and the presence of dissolved iron (9.0 mg/L) at 90 cm depth showed that subsurface sediments were anaerobic. Redox potentials ranging from 302 to 423 mV were measured in the OBB water, demonstrating that aerobic degradation could occur and deplete NAPL on the OBBs. Results from the full-scale (36 ft x 18 ft) OBB module study demonstrated sheen prevention and microbial activity. Of 26 visual inspections for sheens, no sheens were observed sourcing from the OBB, while 3 inspections yielded sheen observations on adjacent shoreline. Seasonal changes in sorbed NAPL composition were consistent with patterns of microbial degradation and correlated to decreased redox potentials and warm temperatures. Microbial populations in the OBB were comparable to adjacent and underlying sediments but showed increased diversity of hydrocarbon-degrading microbes. In addition, structural cover was shown to mitigate erosion associated with ice-scour, while sustaining minimal damage and sedimentation. Costs for OBB construction were estimated to be on the order of \$100,000 per acre, making more affordable than organoclay barriers and sheet pile barriers. The primary conclusion of this thesis is that OBBs are a viable technology from both cost and performance perspectives.

Recommendations for future work include OBB design modifications for improved sediment control, greater compatibility with natural environments, and enhanced NAPL retention capacity. Simplified performance monitoring, research on governing processes, methods for characterizing sheen sources, and the development of a model to support OBB design optimization are also recommended.



Ongoing consideration of expanding the full-scale OBB module and active consideration of OBB remedies at other sites provide promising opportunities for further development.

## ACKNOWLEDGMENTS

I'd like to thank the following people for their help and support:

**Dr. Tom Sale**, for the opportunity to work on such a unique and interesting project and for his continued support and guidance

**Mark Lyverse**, for his technical guidance and collaborative efforts

The **Chevron Energy Technology Company** for providing funding for this research

**Dr. Julio Zimbron**, for his vision and advice getting started

**Alison Hawkins**, for her foundation work on the topic of sheens

- Collaborators at **ARCADIS**:
  - **Matt Biondolillo**, Lauren Vogel and Caron Koll for their operational and planning support:
  - **Matt Schnobrich** and Julie Sueker for generously donating their time and technical advice
  - **Tyler Howe** and Katie Bidwell for their perseverance and support in the field

**Maria Irianni-Renno**, for her hard work on microbial ecology valuable insights

**Dr. Kevin Saller**, **Gary Dick**, and particularly **Dr. Mitch Olson**, for their continued advice and assistance in designing experiments, constructing apparatuses and learning to use analytical machines

My fellow students at the Center for Contaminant Hydrology, for supporting me through coursework, lending a helping hand and offering any words of wisdom they may have offered me along the way

My family and friends, for their love, support, patience and perspectives

## TABLE OF CONTENTS

Abstract.....	ii
Acknowledgements.....	iii
List of Tables.....	xii
List of Figures.....	xiii
1 Introduction .....	1
1.1 Hypothesis.....	2
1.2 Objective .....	2
1.3 Content and Organization .....	3
2 Problem Statement.....	6
2.1 History .....	6
2.2 Regulation .....	7
2.3 Governing Processes .....	7
2.3.1 Sheens on Water Surfaces .....	7
2.3.2 Seeps .....	8
2.3.3 Ebullition .....	9
2.3.4 Erosion .....	9
2.3.5 Confidential Sheens Survey.....	10
2.4 Mass Balance Conceptual Model.....	11
2.5 Existing Options for Sheen Management .....	13

2.6	Groundwater-Surface Water Interfaces .....	17
2.7	Permeable Reactive Barriers.....	19
2.8	Design Concepts of an Oleophilic Bio Barrier .....	19
2.8.1	Erosion sheen prevention .....	19
2.8.2	Oxygen Delivery .....	20
2.8.3	Temperature .....	20
2.8.4	Retention Time.....	21
2.8.5	Oleophilic Material.....	21
3	Lab Studies .....	23
3.1	Oleophilic Capacity Tests .....	23
3.1.1	Objectives.....	23
3.1.2	Methods.....	23
3.1.3	Results .....	24
3.2	Sand Tank Experiments.....	26
3.2.1	Objectives.....	26
3.2.2	Materials .....	26
3.2.3	Methods.....	28
3.2.4	Results.....	29
3.3	Aqueous Sorption Experiment.....	32
3.3.1	Objectives.....	32

3.3.2	Methods.....	33
3.3.3	Results.....	34
4	Preliminary OBB Field Study .....	37
4.1	Site Description .....	37
4.2	Preliminary Field Study Objectives .....	39
4.3	Preliminary OBB Installation and Monitoring Equipment .....	39
4.3.1	Geocomposite and Sampling Tubes.....	40
4.3.2	Monitoring System.....	40
4.3.3	Thermocouples .....	40
4.3.4	Placement and Anchoring.....	41
4.4	Data Collection and Analysis .....	41
4.4.1	Sheen Monitoring .....	42
4.4.2	Water Quality.....	42
4.4.3	UV Fluorescence Survey.....	44
4.4.4	Hydrocarbon Analysis .....	44
4.4.5	Temperatures.....	47
4.5	Results.....	47
4.5.1	Inspection of Anchoring and Structure .....	47
4.5.2	Geochemistry and Temperatures .....	49
4.5.3	Sheen Prevention via NAPL Sorption .....	52

5	Full-Scale OBB Field Demonstration .....	54
5.1	Objectives.....	54
5.2	OBB Construction Methods and Monitoring Equipment.....	55
5.2.1	Full-Scale OBB Design.....	55
5.2.2	Sampling Port Design .....	58
5.2.3	OBB Construction.....	60
5.3	Performance Monitoring Plan and Schedule .....	61
5.3.1	Selection of Ports for Continued Analysis.....	63
5.3.2	Southwest Corner Sampling.....	64
5.4	Performance Monitoring Methods.....	65
5.4.1	Visual Observations.....	65
5.4.2	Sedimentation.....	65
5.4.3	Temperature Data.....	66
5.4.4	Pore Pressure Data.....	66
5.4.5	Water Quality Analysis.....	66
5.4.6	UV Survey.....	67
5.4.7	Geocomposite and Sediment Sampling.....	67
5.4.8	Hydrocarbon Analysis .....	68
5.4.9	Characterization of Microbial Ecology .....	71
5.5	Results.....	74

5.5.1	Visual Sheen Observations.....	74
5.5.2	Temperature .....	74
5.5.3	Structural Integrity and Anchoring .....	76
5.5.4	UV Survey.....	78
5.5.5	Hydrocarbon Quantification .....	79
5.5.6	Hydrocarbon Forensics .....	80
5.5.7	Pressure Data .....	82
5.5.8	Water Quality.....	83
5.5.9	Microbial Characterization.....	85
6	Construction Cost Estimate for a Full-Scale OBB .....	90
7	Conclusions and Recommendations .....	92
7.1	Basic Concepts and Approach.....	92
7.2	Laboratory Studies .....	93
7.3	Preliminary Field Study .....	93
7.4	Full-Scale Field Demonstration .....	95
7.5	Construction Cost Estimate.....	96
7.6	Recommendations for Future Work .....	96
8	References .....	99
	Appendix A: Confidential Sheens Survey Summary.....	108
	Appendix B: Supplemental Lab Study Data .....	111

Appendix C: As-built drawing of a small-scale OBB .....	112
Appendix D: Preliminary OBB study UV survey and sampling forms.....	113
Appendix E: Notes on preliminary study sediment hydrocarbon analysis .....	117
Appendix F: Full-scale field demonstration construction documents .....	118
Appendix G: Monitoring system parts list and assembly instructions.....	120
Appendix H: Full-scale OBB product data sheets and construction photos .....	126
Appendix I: 454 Pyrosequencing Data Analysis Methodology .....	138
Appendix J: Full-Scale OBB supplemental data.....	160



## LIST OF TABLES

Table 1: Classes of geochemical reactions with examples relevant to contaminant transport at a GSI (EPA, 2005).....	18
Table 2: Summary of Capacity Test Results .....	25
Table 3: Summary of sand tank experiment results .....	32
Table 4: Hydrocarbon concentration reduction due to geocomposite treatment.....	36
Table 5: Preliminary study monitoring and sampling plan .....	42
Table 6: ORP and pH values .....	50
Table 7: Selected OBB fluorescence photos and concentrations .....	53
Table 8: Full-Scale OBB performance monitoring plan.....	62
Table 9: Sampling Schedule Summary. Letters represent ports sampled. SW refers to sample collection described in Section 5.3.2 .....	64
Table 10: Mass/area of geocomposite samples .....	78
Table 11: Full-scale OBB hydrocarbon concentrations.....	79
Table 12: Results summary of hydrocarbon forensics.....	80
Table 13: Descriptions of microbes found in site samples .....	88
Table 14: Sheen Remedy Cost Comparison .....	91
Table 15: Parts List for monitoring port system .....	120
Table 16: Key for identifying aromatic hydrocarbons.....	160
Table 17: Microbial DNA 454 pyrosequencing data from full-scale OBB study.....	164

## LIST OF FIGURES

Figure 1: A hydrocarbon sheen .....	1
Figure 2: Sheen formation via a seep .....	8
Figure 3: Dyed green NAPL is the intermediate wetting phase in a system with sand, water and air.....	8
Figure 4: Sheen formation via ebullition.....	9
Figure 5: Sheen formation via shoreline erosion.....	9
Figure 6: Highlights from Sheens Survey .....	10
Figure 7: Conceptual mass balance of NAPL at a GSI.....	11
Figure 8: Geonet core structure.....	21
Figure 9: Chemical structure of polypropylene .....	22
Figure 10: Geocomposite capacity test configuration .....	24
Figure 11: Summary of Capacity Test Results .....	25
Figure 12: Sand tank setup with geocomposite.....	26
Figure 14: Closeup of Geocomposite retaining NAPL in contact with water surface.....	30
Figure 13: NAPL wicking up geocomposite during a rising tide over 30 min.....	30
Figure 15: Comparison of OBB tank experiments prior to failure .....	31
Figure 16: Column setup for sorption experiment .....	33
Figure 17: Flow-through sampling .....	34
Figure 18: o-xylene effluent concentrations for a control column and a column treated with geocomposite.....	35
Figure 19: Site layout and hydrocarbon heat map (ARCADIS).....	37
Figure 20: Conceptual Model of the site (ARCADIS).....	38
Figure 21: Sampling tube configuration. The white dots are sampling tube ends wrapped with filter cloth. ....	40

Figure 22: Waterproof housing for data loggers and sampling ports.....	40
Figure 23: Small-scale OBBs .....	41
Figure 24: Flow-thru vial filler .....	43
Figure 25: Custom peristaltic pump driven by a cordless drill.....	43
Figure 26: Consistent headspace sampling.....	46
Figure 27: Monitoring equipment damaged by river debris.....	47
Figure 28: Microbial growth patterning on top of geocomposite from OBB A .....	48
Figure 29: OBB Temperatures from March 21 to August 13 .....	49
Figure 30: Mean and standard error of ion concentrations from the preliminary study. August 30cm Cl column is truncated. ....	51
Figure 31: Fluorescing geocomposite .....	52
Figure 32: Plan view UV fluorescence and sampling location key. Numbered regions used to ID samples. .....	52
Figure 33: Full-scale OBB construction drawing (modified from ARCADIS).....	56
Figure 34: Full-scale OBB covered in ice, January 2015 .....	57
Figure 35: Schematic of OBB layers and sampling port .....	57
Figure 36: Flange with 6 inch PVC pipe.....	58
Figure 37: a) geocomposite disc cut with hole saw b) disc placed back in hole.....	59
Figure 38: a) OBB sampling port b) sampling port insert.....	59
Figure 39: Cavity formed by sediment sampling .....	63
Figure 40: Sheen observed in August, adjacent to SW corner of OBB .....	64
Figure 41: PAH biomarker fingerprints .....	70
Figure 42: Summary of sheen observations, Dec 2013 to Jan 2015 .....	74
Figure 43: November 2013 – May 2014 temperature profile .....	75

Figure 44: Summer 2014 temperature profile.....	76
Figure 45: Reno mattress with bent panel.....	77
Figure 46: Tops of geocomposite samples displaying different levels of sedimentation: a) E port, May b) E port, November and c) Southwest corner, November .....	78
Figure 47: Fluorescence observed on November geocomposite sample B.....	78
Figure 48: June 2014 river stage and pore pressure fluctuations .....	82
Figure 49: ORP data for each sampling port. Readings are labeled by port and depth in feet. ....	84
Figure 50: Dissolved metals mean values and standard errors .....	85
Figure 51: Sulfate mean values and standard errors.....	85
Figure 52: Summary of average bacteria and archaea gene counts and standard errors.....	86
Figure 53: Composition of identified bacterial community for each sample taken in May 2014 .....	87
Figure 54: Composition of identified archaeal community for each sample taken in May 2014.....	87
Figure 55: Aqueous sorption study treated column breakthrough curves.....	111
Figure 56: Aqueous sorption study untreated column breakthrough curves .....	111
Figure 57: As-built drawing of small-scale OBB .....	112
Figure 58: Preliminary study final sampling log: OBB A.....	113
Figure 59: Preliminary study final sampling log: OBB B.....	114
Figure 60: Preliminary study final sampling log: OBB C.....	115
Figure 61: Preliminary study final sampling log: OBB D.....	116
Figure 62: Sediment hydrocarbon chromatograms.....	117
Figure 63: OBB Layout Plan.....	118
Figure 64: OBB Profile, Section, and Specifications .....	119
Figure 65: PVC flange modified to receive 1 1/4" PVC tubes. Flange is centered over hole in geocomposite. Note: edging spike is not relevant to port assembly .....	121

Figure 66: a) Hose clamp and screw fasten grate to pipe b) hose clamp tightener c) hose clamp tightener removed .....	122
Figure 67: Handle assembly .....	122
Figure 68: Water sampling port .....	122
Figure 69: BaroLogger pressure vessel .....	123
Figure 70: Modified plunger tip a) side sawed-off of plunger b) side with cut rubber .....	123
Figure 71: Thermocouples through Swagelok fitting.....	123
Figure 72: Thermocouple plug assembly .....	123
Figure 73: Location of porewater sampler/thermocouple holes .....	125
Figure 74: Top view schematic of sampling port .....	125
Figure 75: Geocomposite Product Sheet .....	126
Figure 76: Sand gradation data .....	127
Figure 77: Reno mattress product sheet page 1/2 .....	128
Figure 78: Reno mattress product sheet page 2/2 .....	129
Figure 79: Duckbill anchors product sheet .....	130
Figure 80: Porewater sampler product sheet .....	131
Figure 81: OBB construction materials                      Figure 82: Temporary construction barriers.....	132
Figure 83: Reno mattress anchor installation .....	134
Figure 84: Digging a trench to integrate the edges of the reno mattress .....	135
Figure 85: Installation of the geocomposite, monitoring ports and sand .....	136
Figure 86: The completed OBB module .....	137
Figure 87: Record of sheen observation from 8/13/2014 .....	161

# 1 Introduction

Petroleum hydrocarbons have been used as a fuel source for thousands of years (Encyclopædia Britannica, 2005). Although modern technologies have reduced the frequency of petroleum releases to the environment, accidental releases still occur. When released into a shallow environment, the physical properties of petroleum liquids often cause them to percolate into soils and sediments and reach the water table. Fortunately, most petroleum hydrocarbons readily degrade in shallow environments and in surface water via natural processes. Where natural depletion processes are insufficient, petroleum releases have the potential to result in adverse impacts to human health and the environment.

Petroleum sheens (Figure 1) are frequently encountered in surface water near facilities where historical subsurface petroleum releases have occurred. Sheens are defined as thin (0.1 - 100 micron) iridescent layers of Non-Aqueous Phase Liquid (**NAPL**) that spread across air-water interfaces. The occurrence of petroleum sheens in surface waters can result in notices of violation and fines issued by regulatory agencies, as well as undesired publicity and aesthetic issues. In many cases, a rapid and often costly response is necessary.



Figure 1: A hydrocarbon sheen

Given diverse conditions controlling sheens at a site, a suite of remedies has been developed to address sheens. Common remedies include adsorbent booms, physical barriers, hydraulic controls and/or excavation of impacted soils. These remedies can often be costly, less effective than desired, and/or require ongoing operation and maintenance. The shortcomings of common sheen remedies will be discussed in greater detail in Section 2.5 .

## 1.1 Hypothesis

Given the limitations of common sheen remedies, this thesis explores a novel remedy for sheens that is centered on the premise of enhancing NAPL retention and degradation at Groundwater Surface-water Interfaces (**GSIs**). Specifically, the hypothesis for this work is that reactive barriers enhancing both sorption and degradation processes are a viable strategy for managing sources of sheens at GSIs.

In more detail, unique environmental conditions at GSIs give rise to processes that can attenuate petroleum liquids as they move towards surface water. Conditions often transition from anaerobic, sub-surface conditions to surface conditions characterized by the presence of oxygen. Porous media composition also transitions from largely inorganic minerals to marine, riverine or lacustrine sediments rich in organic matter. Transmissivity and heterogeneity of the media can also change drastically. In this transition zone, steep chemical, thermal and hydraulic gradients can be found (EPA, 2005). These gradients can give rise to an environment with a diverse microbiological community and a high capacity for attenuating hydrocarbon contaminants (Kostka et al., 2011). Reactive barriers that rely on natural processes to deplete NAPL could be a sustainable, low-cost strategy for managing sheens.

## 1.2 Objective

The objective of this work is to construct a permeable reactive barrier at a GSI to mitigate petroleum hydrocarbon sheen formation on surface water. In particular, the concept of an Oleophilic Bio Barrier (**OBB**) is advanced herein. An OBB is a reactive barrier that utilizes sorption and natural biological degradation to sustainably attenuate NAPL. In doing so, the author seeks addresses the need for inexpensive, effective and sustainable sheen remedies. Concepts investigated herein that may affect the efficacy of an OBB include:

- Chemical gradients

- Temperature profiles
- Microbial communities
- Oleophilic materials
- Layered design
- Hydraulic transmissivity
- Structural cover
- Permeability reduction

### **1.3 Content and Organization**

Herein you will find:

#### Chapter 2: Problem Statement

The problem statement sets a foundation of terminology and concepts that underpin subsequent developments. Included in Chapter 2 are:

- Summary of a survey of sheen site managers that helps to inform formation processes
- Description of processes that lead to sheen formation
- Introduction of conceptual model for sheen formation
- Outline of the shortcomings of current sheen solutions
- Design features of an OBB

#### Chapter 3: Lab Studies

Lab studies provide a proof-of-concept demonstration that supports field studies. Included in Chapter 3 are:

- Quantification of the geocomposite's sorption capacity in a lab setting



- Demonstration of an oleophilic geocomposite's potential for sheen prevention
- Investigation of the geocomposite's effect on dissolved hydrocarbons

#### Chapter 4: Preliminary OBB Field Study

Motives for a preliminary field study include investigating the feasibility of an OBB under field conditions and the development of techniques for monitoring OBBs. Included in Chapter 4 are:

- A description of the field site where both field studies occurred
- Methods for constructing the preliminary, small-scale OBBs
- Methods for the performance monitoring of an OBB
- Results evaluating the potential of an OBB to mitigate sheens via petroleum sorption
- Data characterizing the geochemistry and temperatures of the field site

#### Chapter 5: Full-Scale OBB field demonstration

Motives for the field demonstration include exploring feasibility of a full-scale OBB, development of techniques for monitoring OBBs, and gaining insights for future OBB design. Included in Chapter 5 are:

- Methods for the construction of a full-scale OBB module
- Methods for and lessons learned from monitoring the performance of an OBB
- Evaluation of the OBB's ability to prevent sheens via NAPL sorption and shoreline armoring
- Characterization of the diversity and abundance of microbes in an OBB
- Documentation of changes in sorbed NAPL composition corresponding to biological degradation

## Chapter 6: Cost Estimate

To provide a basis for comparison to other sheen remedies, an OBB cost estimate is provided.

Included in Chapter 6 is:

- Construction cost estimate of an OBB

## Chapter 7: Conclusions and Recommendations

The synthesis of conclusions from information gathered provide a basis for the design and implementation of future OBBs. Included in Chapter 7 are:

- Basic concepts and approach taken
- Conclusions from laboratory studies
- Conclusions from the preliminary field study
- Conclusions from the full-scale field demonstration
- Conclusions from the OBB cost estimate
- Recommendations for future work

## **2 Problem Statement**

This chapter establishes the importance of and basis for the work presented. A historical background of sheen regulation is provided, followed by a description of physical processes governing sheen formation. A conceptual mass-balance model is presented and utilized to evaluate the advantages and disadvantages of current sheen remedies. Background information on the natural attenuative capacity of GSIs leads into a discussion of reactive barriers at GSIs. Last, the foundational principles and concepts of an OBB are established.

### **2.1 History**

The use of petroleum began more than 5000 years ago in what is now Iraq (Encyclopædia Britannica, 2005). The towers of Babylon and the first roads of Baghdad were constructed from asphalt. By the first millennia AD, petroleum was being produced and exported in industrial quantities near what is now Baku, Azerbaijan. Distillation had also begun by the first millennia, leading to the multitude of petroleum products found in modern society. The boom in oil production associated with the industrial revolution began in 1859 (AO&GHS, 2014). Since then, the use of petroleum has been inextricably linked to the expansion of the global economy. Global consumption is still on the rise today, especially in developing nations, the demand of which has surpassed developed nations' (Sheppard, 2013).

Production, transmission, refining and storage of petroleum have led to releases of NAPL to soil and groundwater. Underground petroleum contaminants can pose threats to human health and the environment. Many of the compounds found in petroleum are carcinogenic to humans and toxic to aquatic organisms (Hoffman and Albers, 1984; Long et al., 1995; Pashin and Bakhitova, 1979). Petroleum compounds can be transported with water, either as a dissolved phase or as a NAPL

(Schwarzenbach, 2005; Hawkins, 2013). The transport of NAPLs in the subsurface will be explained in greater depth in Section 2.3.2.

## **2.2 Regulation**

Rigorous regulation of petroleum releases did not arrive until the late 20<sup>th</sup> century. Environmental regulations pertaining to petroleum began to surface in the early 20<sup>th</sup> century. These regulations were largely inconsequential, and only served to uphold the status quo of “good oil field practice” (Gao, 1998). Modern environmental petroleum policy began to take shape in the 1950s, during the 1954 International Convention for the Prevention of Pollution of the Sea by Oil and the 1958 Geneva conventions. A highly publicized oil fire on the Cuyahoga River, as well as the Santa Barbara oil spill in 1969, led to the creation of the National Environmental Policy Act (NEPA), Environmental Protection Agency (EPA), and ultimately the Clean Water Act of 1972 (Adler, 2002). The Clean Water Act was the US’s first comprehensive regulation governing petroleum releases. In the Clean Water Act, the Discharge of Oil regulation stipulates that a sheen on the surface of a water body is a discharge of oil in such quantities as “may be harmful”, and should be reported to the EPA. Although sheens are only one potential form of contamination, they are a strong visual indication of contamination as well as a driver for decision-making at contaminated sites.

## **2.3 Governing Processes**

Understanding how and why sheens form is paramount to designing an effective solution.

### **2.3.1 *Sheens on Water Surfaces***

As defined by the Clean Water Act, a sheen is an “iridescent appearance on the surface of water” caused by NAPL. Sheens consist of a thin (0.1-100 micron) layer of NAPL. Iridescence is caused by the refraction of light through the petroleum film. Following Sale and Lyverse (2014), common mechanisms of sheen formation include seeps, ebullition, and shoreline erosion. These mechanisms are illustrated in

Figure 2, Figure 4, and Figure 5. Timing of sheen release can be chronic, periodic, or sporadic, depending on the mechanism of release and source of NAPL.

### 2.3.2 Seeps

A seep occurs when NAPL flows out of the subsurface and onto a water surface, as illustrated in Figure 2. Seeps can occur from sediments containing NAPL at any concentration. In sediments that contain NAPL as a continuous phase, hydraulic

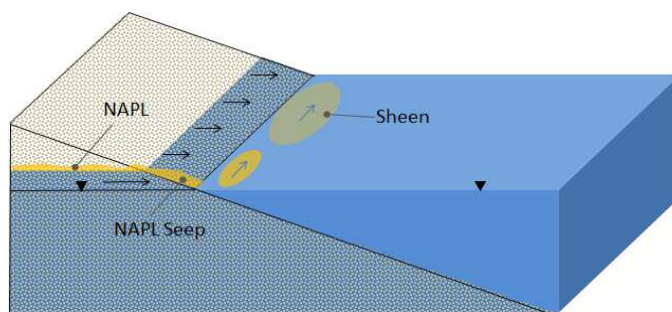


Figure 2: Sheen formation via a seep

head can drive the NAPL into surface water. Groundwater flow can also flush NAPL into the surface water, particularly after high intensity precipitation events. In porous media at GSIs, NAPL, air, and water are often present as a three-phase system. Water is typically present as the wetting phase, in



Figure 3: Dyed green NAPL is the intermediate wetting phase in a system with sand, water and air

contact with the porous media. NAPL is typically present as an intermediate wetting phase between water and air, as shown in Figure 3. By comparing the interfacial force between water and air to that of NAPL and air, one can determine whether the NAPL will tend to spread along the air-water interface. Most petroleum NAPLs tend to spread on water.

The process of spreading is also known as wetting or spontaneous imbibition. Seeps related to sheens commonly occur as water levels fall. Although any level of NAPL saturation can cause sheens, NAPLs at higher saturations transport more easily (Hawkins, 2013). Depending on the temporal nature of water table fluctuations at the GSI, seeps may be chronic, periodic, or sporadic.

### 2.3.3 Ebullition

Ebullition begins with the formation of gas bubbles within saturated media. Often, these gasses are  $\text{CO}_2$  and  $\text{CH}_4$ , the byproducts of anaerobic degradation of NAPL. As a bubble forms, NAPL can wet the interior of the bubble, present as an intermediate wetting phase between the gas and the water. As illustrated in Figure 4, the buoyancy of the bubble carries the NAPL through the sediment and water column to the water surface, where it can rupture and cause a sheen (Amos and Mayer, 2006). Since ebullition is dependent on the formation of subsurface gases, it tends to be periodic. In select cases, ebullition sheens can be sporadic or chronic.

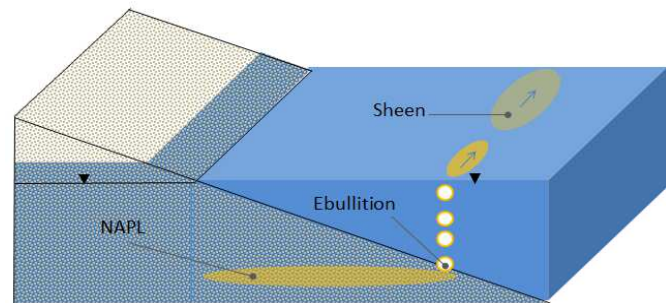


Figure 4: Sheen formation via ebullition

### 2.3.4 Erosion

The erosion of sediments containing NAPL can also cause sheens. As impacted sediments erode into surface water, NAPL contained in the pore space enters the water. Light NAPLs may float to the surface, causing sheens (Figure 5). Erosion can occur due to high river flows, storm-related wave action, construction activities, and/or ice scour. Sheens associated with erosion can therefore be periodic, sporadic, or chronic.

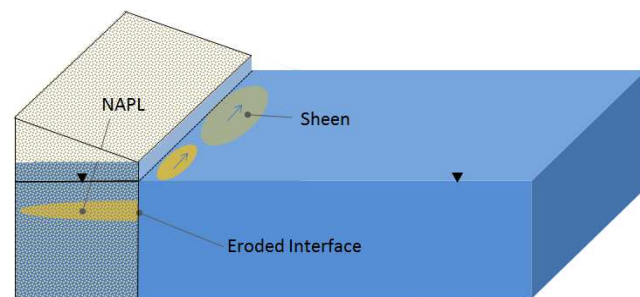


Figure 5: Sheen formation via shoreline erosion

It is important to note that a successful sheen remedy may need to address all three sheen formation processes.

### 2.3.5 Confidential Sheens Survey

A confidential sheen survey was completed by the managers of 10 petroleum facilities where sheens have occurred. The survey was designed to gain insights into why sheens form and how they are currently managed. Figure 6 shows some highlights from the survey. A more complete summary of results can be found in Appendix A.

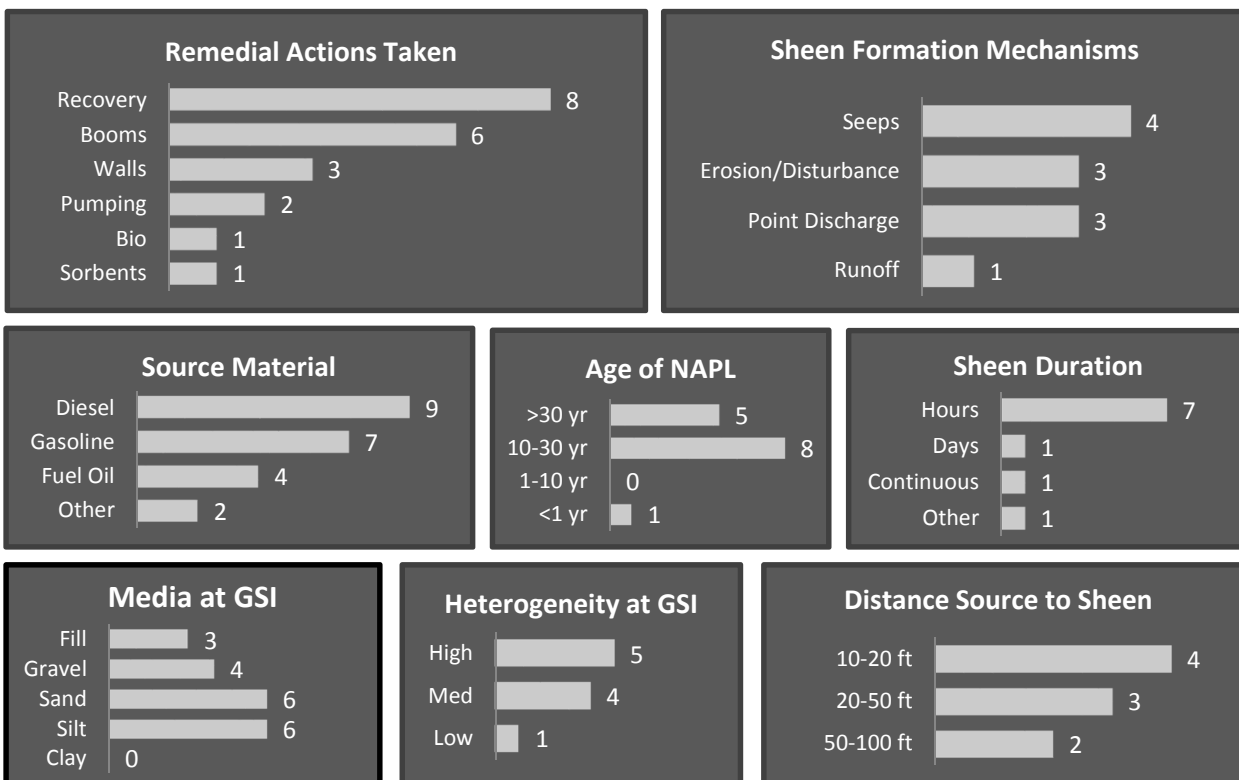


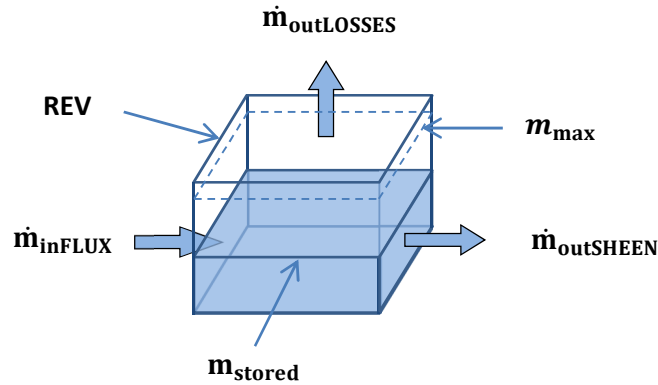
Figure 6: Highlights from Sheens Survey

Sheens form from materials coarser than clays, with medium to high heterogeneity. All study sites experienced water table fluctuations, 7 of which were tidal. Source zones tended to be older and contain heavier hydrocarbons. Older age and heavier composition are consistent with a pattern of weathering, which has been observed to result in a composition shift towards heavier compounds (Jonker et al., 2005). This combination of tidal fluctuations at late-stage sites with residual NAPL helps to explain why sheens tend to occur sporadically, and can last for limited periods. In addition, the survey shows that remedies may be expensive and/or ineffective; 9 out of 10 managers anticipated

ongoing costs associated with operation and maintenance, while 3 out of 10 say current remedies are not meeting their needs. In summary, the spatial and temporal variability of sheens makes them difficult to address, and there is a need for more effective, sustainable and lower cost sheen remedies.

## 2.4 Mass Balance Conceptual Model

A conceptual mass balance model for sheen formation by seeps is advanced in Figure 7 and Equation 1. The model provides a framework to understand current sheen remedies (discussed in Section 2.5 ) and to explore promising alternatives. Although seeps can occur at any NAPL saturation, the mass balance is based on the concept that NAPL transport increases once saturations exceed a threshold of residual saturations (Mercer and Cohen, 1990). Figure 7 and Equation 1 present a Representative Element of Volume (REV) of porous media at a GSI and a general governing equation.



$$\dot{m}_{in} - \dot{m}_{outLOSSES} - \dot{m}_{outSHEEN} = \frac{d}{dt} m_{stored} \quad (1)$$

Figure 7: Conceptual mass balance of NAPL at a GSI

Variables:

- $\dot{m}_{in}$ : Influx of NAPL from upland source zone or active release [M/T]
- $\dot{m}_{outLOSSES}$ : Losses of NAPL via biological degradation, dissolution or volatilization [M/T]
- $\dot{m}_{outSHEEN}$ : NAPL release to surface water, causing a sheen [M/T]



- $\dot{m}_{\text{stored}}$ : NAPL stored in the REV [M]
- $\dot{m}_{\text{max}}$ : Maximum NAPL stored in REV before release to surface water [M]

Constraints:

- For no sheens to form,  $0 \leq m_{\text{stored}} \leq m_{\text{max}}$ , where  $m_{\text{max}}$  is positive and finite
- All  $\dot{m}$  terms are non-negative

To gain insights about the mass stored at a given time, we start by solving the following differential equation:

$$\dot{m}_{\text{in}} - \dot{m}_{\text{outLOSSES}} - \dot{m}_{\text{outSHEEN}} = \frac{d}{dt} m_{\text{stored}} \quad (1)$$

To solve, we separate and integrate.

$$\int_{t_1}^{t_2} (\dot{m}_{\text{in}} - \dot{m}_{\text{outLOSSES}} - \dot{m}_{\text{outSHEEN}}) dt = \int_{m_{\text{stored}}(t_1)}^{m_{\text{stored}}(t_2)} dm_{\text{stored}} \quad (2)$$

$$\int_{t_1}^{t_2} (\dot{m}_{\text{in}}) dt - \int_{t_1}^{t_2} (\dot{m}_{\text{outLOSSES}}) dt - \int_{t_1}^{t_2} (\dot{m}_{\text{outSHEEN}}) dt = m_{\text{stored}}(t_2) - m_{\text{stored}}(t_1) \quad (3)$$

Rearranging,

$$\int_{t_1}^{t_2} (\dot{m}_{\text{in}}) dt - \int_{t_1}^{t_2} (\dot{m}_{\text{outLOSSES}}) dt - \int_{t_1}^{t_2} (\dot{m}_{\text{outSHEEN}}) dt + m_{\text{stored}}(t_1) = m_{\text{stored}}(t_2) \quad (4)$$

This equation represents the concept that the mass stored at any time is equal to the integral of the fluxes since some initial time, plus the mass stored at that initial time.

To consider the case where no sheens form ( $\dot{m}_{\text{outSHEEN}} = 0$ ), the following condition must be met at all times  $t_2$ :

$$m_{\text{stored}}(t_2) \leq m_{\text{capacity}}$$

Which yields the following relation:

$$\boxed{\int_{t_1}^{t_2} (\dot{m}_{\text{in}}) dt - \int_{t_1}^{t_2} (\dot{m}_{\text{outLOSSES}}) dt + m_{\text{stored}}(t_1) \leq m_{\text{capacity}}} \quad (5)$$

Although not evaluated quantitatively, the conceptual model developed serves as a tool to evaluate sheen remedies. It is important to note that  $\dot{m}_{in}$ ,  $\dot{m}_{outLOSSES}$ , and even  $m_{capacity}$  are potentially time-dependent, highly variable and can be influenced by many confounding factors. The model suggests that sheens will form from REV's with a positive  $\dot{m}_{in}$  and no  $\dot{m}_{outLOSSES}$  term. Analysis of the model also yields the following strategies for preventing sheens:

1. Increasing  $m_{capacity}$  – This can be accomplished by adding a sorbent at the interface, whereby NAPL can accumulate without release into surface water.
2. Reducing  $\dot{m}_{in}$  – This can be achieved by removing or addressing upland NAPL sources.
3. Enhancing  $\dot{m}_{outLOSSES}$  – Increased losses can prevent  $m_{stored}$  from exceeding  $m_{capacity}$ .
4. Reducing  $m_{stored}(t_1)$  – Using hydraulic recovery or other depletion methods to lower the initial mass stored could buffer future influxes.

These basic concepts will be used to conceptually analyze current remedies in the following section.

## 2.5 Existing Options for Sheen Management

Frequent observations of sheen formation at petroleum facility sites have led to a suite of remedies. Current sheen remedies are summarized below. For each option, pros and cons are noted. Often, these methods are expensive and/or ineffective in preventing sheens. Concerns regarding efficiency and cost are highlighted when one considers the limited mass of NAPL associated with sheens.

**Physical barriers** physically obstruct flow of NAPL.

Examples: sheet piles, grout curtains

- Pros
  - Simple design/installation

- Long-lasting
- Low ongoing cost
- Cons
  - Initial cost
  - Installation can spread contamination
  - Barriers can inadvertently affect flow patterns
  - High intensity rainfall can lead to bypass
  - Accumulation of NAPL can lead to bypass (exceedance of  $m_{capacity}$ )
  - Development of anoxic zone, potentially reducing  $\dot{m}$
  - Need for active management, operation, maintenance, and monitoring

**Hydraulic barriers** alter the flow of NAPL by manipulating the hydraulic gradient

Example: Line drains

- Pros
  - Simple design/installation
  - Potentially positive  $\dot{m}_{outLOSSES}$
  - Low ongoing cost
- Cons
  - Installation can spread contamination
  - Accumulation of NAPL can lead to bypass (exceedance of  $m_{capacity}$ )
  - Exceptionally dry or wet weather can undermine effectiveness
  - Development of anoxic zone, potentially reducing  $\dot{m}_{outLOSSES}$
  - Need for active management, operation, maintenance, and monitoring

**Capillary barriers** utilize capillary rise in fine-grained sediments to create a wall of water-wet media that extends above the top of the capillary fringe in the NAPL-containing formation. The necessary condition for a capillary barrier is that the pressure required for NAPL to displace water in the barrier is greater than the capillary pressure of the NAPL.

- Pros
  - Simple design
  - Low ongoing cost
- Cons
  - Difficult to construct well
  - Installation can spread contamination
  - Accumulation of NAPL can lead to bypass (exceedance of  $m_{capacity}$ )
  - Exceptionally dry or wet weather can undermine effectiveness
  - Development of anoxic zone, potentially reducing  $\dot{m}_{outLOSSES}$
  - Need for active management, operation, maintenance, and monitoring

**Sorptive barriers** make use of sorbents like organoclay or activated carbon to sequester the contaminant by irreversibly sorbing it.

- Pros
  - Simple installation
- Cons
  - Finite capacity leads to failure in long-term
  - Losses of organics in clay through time reduces  $m_{capacity}$

- Organoclay can induce an oxygen demand that competes with aerobic hydrocarbon degradation, reducing  $\dot{m}_{outLOSSES}$
- Designed  $m_{capacity}$  can be overestimated due to poor contact
- Hydraulic short-cuts can lead to failure

**In-situ remediation** diminishes NAPL either by reduction, oxidation, vaporization, or combustion.

Examples: Permanganate injection, soil vapor extraction

- Pros
  - Effectively reduces initial contaminant mass ( $m_{stored}(t_1)$ )
- Cons
  - Does not address ongoing releases (*positive*  $\dot{m}_{in}$ )
  - Difficult to achieve target reductions ( $m_{stored}(t_1)$ )
  - Difficult to affect entirety of target zone (contact/sweep)
  - Introduction of potentially harmful chemicals or high heats to sensitive environments
  - Potentially high costs

**NAPL removal** can occur via wells, drains or excavation.

Examples: Recovery wells, dredging

- Pros
  - Effectively reduces initial contaminant mass ( $m_{stored}(t_1)$ )
- Cons
  - High cost, either initial (excavation) or ongoing (recovery)
  - Decline of recovery rates ( $\dot{m}_{outLOSSES}$ ) and diminishing marginal return on associated costs
  - Poor site characterization can lead to incomplete removal of contaminant

One important aspect of sheen management that is not utilized by the methods presented above is the incorporation of natural aerobic degradation of NAPL. As discussed in the following section, microbes occurring naturally at GSIs can heavily influence contaminant fluxes to surface water. Many of the commonly used methods discussed above create conditions that inhibit aerobic degradation processes. Without diffusion or water flow, oxygen cannot be replenished, and the affected area can become anaerobic if oxygen is depleted. In terms of the mass balance, this is effectively trading  $\dot{m}_{outLOSSES}$  for an improvement in  $m_{max}$ . Over the long-term, remedies without a  $\dot{m}_{outLOSSES}$  term eventually fail. The method presented herein aims to create an effective remedy by enhancing both  $\dot{m}_{outLOSSES}$  and  $m_{max}$ .

## 2.6 Groundwater-Surface Water Interfaces

Building on the work presented herein, GSIs can be microbially and chemically dynamic environments with a natural ability to attenuate hydrocarbon contamination. For the purposes of this thesis, the GSI will be defined as the zone of sediments that is chemically and microbially influenced by adjacent surface water. At this interface, rapid changes in geochemistry can lead to a number of relevant processes affecting NAPL fate and transport. One of the first detailed studies to characterize groundwater-surface water interaction with respect to contaminant hydrology studied tetrachloroethylene transport through a shallow aquifer and water within a river channel in high resolution (Conant, Cherry and Gillham, 2004). Extensive biodegradation occurred within 2.5m of the streambed when transported from an otherwise inactive aquifer. At least one other study corroborates this finding (Gavaskar et al., 2000).

Table 1, reproduced from an EPA report on GSIs, provides examples of different classes of these processes and their corresponding reactions. Of particular importance are oxidation-reduction (redox

reactions), biodegradation, and gas dissolution. These processes control NAPL fluxes into surface water and are crucial to designing effective remedies.

**Table 1: Classes of geochemical reactions with examples relevant to contaminant transport at a GSI (EPA, 2005)**

Geochemical Reaction	Relevant Process	Example Reaction
Acid-Base	Acid neutralization by aqueous carbonate alkalinity	$\text{HCO}_3^- + \text{H}^+ = \text{H}_2\text{CO}_3$
Precipitation-Dissolution of Minerals	Precipitation of metal sulfide	$\text{Zn}^{2+} + \text{HS}^- = \text{ZnS}_{(s)} + \text{H}^+$
Sorption and Ion Exchange	Ion exchange on feldspars	$\text{KAlSi}_3\text{O}_{8(s)} + \text{NH}_4^+ = \text{NH}_4\text{AlSi}_3\text{O}_{8(s)} + \text{K}^+$
Oxidation-Reduction	Reductive dissolution of iron oxide coupled to organic carbon oxidation	$4\text{Fe}(\text{OH})_{3(s)} + 8\text{H}^+ + \text{CH}_2\text{O} = 4\text{Fe}^{2+} + \text{CO}_{2(g)} + 11\text{H}_2\text{O}$
Biodegradation	Benzene oxidation coupled to denitrification	$\text{C}_6\text{H}_6 + 6\text{NO}_3^- + 6\text{H}^+ = 6\text{CO}_{2(g)} + 6\text{H}_2\text{O} + 3\text{N}_{2(g)}$
Gas Dissolution and Exsolution	Ammonia gas-water exchange	$\text{NH}_{3(g)} + \text{H}_2\text{O} = \text{NH}_4^+ + \text{OH}^-$

Surface water commonly contains dissolved oxygen at or near solubility (about 8 mg/L). Important exceptions occur when surface water has high levels of organic carbon. The abundance of oxygen in the atmosphere and surface waters helps to define environmental redox conditions. Since atmospheric oxygen will lead to the oxidation of compounds more reduced than it, it commonly stands as the most oxidized molecule in abundance. Many naturally occurring microbes have evolved to oxidize hydrocarbons by respiring on oxygen. These microbes include bacteria, fungi, and algae (Rojo, 2009). The activity of hydrocarbon-degrading microbes is often temperature-dependent (Atmos and Bartha, 1992; Margesin and Schinner, 2001; Zeman et al., 2014), with higher temperatures generally leading to faster degradation due to increased bioavailability (Atlas and Bartha, 1972; Perfumo et al., 2007). Surface water temperatures fluctuate with atmospheric conditions, while subsurface temperatures are depth-dependent. Thus, degradation rates are likely both seasonally variable and depth-dependent.

Subsurface environments are often characterized by an absence of oxygen. In the subsurface, nitrate, sulfate, ferric iron (3+) and manganese (4+) may serve as electron acceptors in anaerobic degradation processes. Hydrocarbon degradation under anaerobic conditions tends to be slow (Coates

et al., 1996). Subsurface water temperatures vary widely with depth and season. Generally, subsurface water temperatures approach mean annual temperatures at depths greater than 10m.

## **2.7 Permeable Reactive Barriers**

The premise of this research is that engineered reactive barriers can be used to enhance natural processes that attenuate NAPL fluxes at GSIs. As discussed in Section 2.6, GSIs can have a high capacity to attenuate NAPL fluxes. These natural processes, dependent on near-surface conditions, can be enhanced by engineering a reactive barrier. Permeable Reactive Barriers (**PRBs**) have been used to treat organic contaminants in groundwater plumes. Some of the earliest and best known examples are those designed by Robert Gillham (1990). Iron PRBs rely on natural gradients to carry chlorinated solvents through bodies of zero-valent iron that drive reductive dechlorination. This concept has seen a number of variations, including barriers filled with other minerals, electron acceptor-releasing compounds, and even microbes (Ahmad, Schnikter and Newell, 2007; Tratnyek et al., 2003). The long-term success and passive nature of PRBs are attractive features that are suited to the challenges of sheen prevention.

## **2.8 Design Concepts of an Oleophilic Bio Barrier**

Building on the concept of a PRB, the idea advanced herein is to employ a sorptive, oleophilic material to increase  $m_{max}$ , to enhance  $\dot{m}_{outLOSSES}$  by storing the NAPL in an active aerobic zone, and to prevent erosion-caused sheens. To design an OBB that maximizes  $\dot{m}_{outLOSSES}$  via aerobic degradation, the following REV characteristics must be considered: 1) oxygen delivery, 2) temperature, and 3) retention time of target compounds.

### ***2.8.1 Erosion-associated sheen prevention***

While seeps and ebullition may be addressed by sorbing and storing NAPL, sheens associated with erosion must be addressed separately. Protective armoring is often used to prevent shoreline erosion.



Vegetation, rip-rap and gabion-style armoring are all commonly recommended to protect shorelines from erosion. Choice of anchoring is dependent on site conditions and mechanisms of erosion.

### **2.8.2 Oxygen Delivery**

Oxygen is typically an abundant and powerful oxidant in natural surface or near-surface environments. Ideally, delivery of oxygen into the interface should be maximized. While systems designed to actively pump oxygenated air into the interface may work, this approach can be energy intensive, maintenance intensive, and incur ongoing costs. Designing a remedy that maximizes natural oxygen delivery processes could eliminate those costs, while maintaining a sufficient oxygen supply. Barrier remedies that inhibit mixing and diffusion prevent the replenishment of oxygen. By constructing an OBB with hydraulically transmissive materials in an actively flowing zone, one can capitalize on natural oxygen-delivering processes. Designs could even incorporate a passive piping system that is driven by natural streamflow or tidal water fluctuations.

### **2.8.3 Temperature**

As mentioned in Section 2.6 , degradation processes can be temperature dependent, with higher temperatures generally leading to a higher  $\dot{m}_{outLOSSES}$ . Constructing an OBB with materials that absorb solar radiation or insulate could increase average temperatures. Increased temperatures could increase loss rates or extend the warm, microbially active season during which losses occur. Temperature fluctuations have also been associated with faster hydrocarbon degradation rates when compared to constant temperatures (Chang, Whyte, and Ghoshal, 2011). Others found that a single, short-term increase in temperature led to more complete degradation (Bonten et al., 1999). In many contexts, near-surface NAPL storage would ensure temperature fluctuations, maximizing  $\dot{m}_{outLOSSES}$ .

### 2.8.4 Retention Time

As biodegradation is a time-dependent process, increasing the time NAPL is stored in an aerobic zone increases  $\int_{t_1}^{t_2} (\dot{m}_{outLOSSSES})$ . The important aspect of increasing retention time is not just increasing the time stored in the REV, but the time stored where oxygen availability is maximized. Storing the NAPL as close to the surface water or atmosphere as possible maximizes oxygen availability. For example, at the site mentioned in Section 2.6, storage would ideally occur in the 2.5m closest to the streambed, where attenuation is at its maximum.

### 2.8.5 Oleophilic Material

The choice of sorptive material is essential to the design of an OBB. One important trait of an OBB sorbent is that the contaminant must be bioavailable for biodegradation. Materials commonly used in sorptive barriers rely on a mechanism of irreversible chemisorption, yielding many of the traditional sorbents ineffective for use in an OBB.

For this research, the Tendrain II – 1010 (Syntec Corp) geocomposite was used. A geonet and two layers of geotextile are thermally fused to create a geocomposite. The geonet is a rigid 3D grid made of High-Density PolyEthylene (**HDPE**), illustrated in Figure 8. It is hydraulically transmissive in two of three directions. The geotextile is a 10 oz/yd<sup>2</sup> nonwoven polypropylene fabric that is thermally fused onto each side of the geonet. Although the HDPE geonet is also oleophilic, the large surface area of the geotextile makes it the primary NAPL-sorbing element. Grids and textiles made of other polymers could be combined to create a contaminant-specific sorbent.

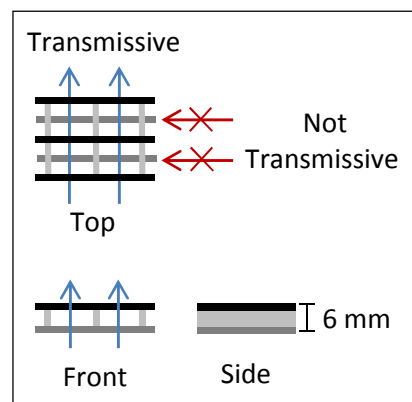


Figure 8: Geonet core structure

The term “oleophilic” is used to describe a material’s interfacial force interactions with NAPL. NAPL has high adhesive forces with oleophilic materials, which

cause it to preferentially wet the material instead of water. Oleophilic wetting could also be thought of as a multi-layer sorption, where there are enough sorbate layers to form a bulk phase. This mechanism can be understood through interactions on the molecular level. A PolyPropylene (**PP**) geotextile is used in this study. The chemical structure of PP can be found in Figure 9. Made up of a backbone of C-C bonds, the polymer is composed entirely of apolar constituents (Swarzenbach, 2005). The monomer cannot donate or accept hydrogens, and cannot ionize in environmental conditions. The apolar constituents cause van der Waals forces to dominate intermolecular interactions. In a system with NAPL, water, and PP, the apolar hydrocarbons will be at a lower energy state when in contact with the PP than with water. Similarly, water is at a lower energy state when in contact with itself than with PP. Therefore, the configuration that maximizes contact between PP and hydrocarbons has the lowest energy state. In essence, the oleophilic properties of the PP derive from the van der Waals interactions between the NAPL and PP.

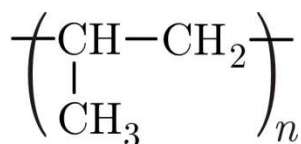


Figure 9: Chemical structure of polypropylene

### **3 Lab Studies**

Laboratory-scale studies were performed to better understand the oleophilic nature of the geocomposite material and to establish a proof-of-concept for its use as a component of a sheen remedy. Lab studies included the following: 1) resolving sorption capacity of the geocomposite material, 2) sand tank experiments testing sheen mitigation potential using a simulated subsurface NAPL release, and 3) a flow-through column experiment testing the geocomposite's ability to deplete contaminants dissolved in water.

#### **3.1 Oleophilic Capacity Tests**

##### **3.1.1 Objectives**

One of the most important factors governing the success of the geocomposite material as a sorbent is its capacity to hold NAPL. Determining general constraints on capacity allows for a better understanding of the storage capacity of an OBB. Three basic laboratory tests were performed to measure how much NAPL the geocomposite could retain under a range of conditions.

##### **3.1.2 Methods**

Laboratory and subsequent field studies used the Tendrain II – 1010 (Syntec Corp) geocomposite. A detailed description of the material is provided in Section 2.8.5. Diesel fuel from a retail gas station (Fort Collins, CO) was used as the NAPL for all lab studies. Diesel was selected for its immiscibility, low volatility, and tendency to spread at air-water interfaces.

The first test was a simple “dip test”. A 17.8 cm x 13.3cm rectangular geocomposite sample of known mass was oriented parallel to the ground, placed into a bath of diesel and allowed to saturate for 20 minutes. It was then removed from the bath and held horizontally, allowing the NAPL to drain. When NAPL no longer drained from the geocomposite, the mass of the saturated sample was measured.

For the second test, a 10.2 cm diameter geocomposite disc of known mass was placed in a bath of NAPL and allowed to saturate for 20 minutes. When NAPL ceased draining from the sample, forceps were used to hold the disc by the geotextile at its center-point. The forceps were then taped to the drill bit of an 18V cordless drill (Black and Decker). The drill was oriented to keep the sample horizontal, and turned to its highest speed for 10 seconds, draining the geocomposite. The manufacturer specifications state that the maximum rpm of the drill is 650 rpm. Sample mass was then measured.

The third test was designed to test the geocomposite under water-wet conditions. A disc of geocomposite was cut to fit inside a 4" diameter PVC column. The disc was placed perpendicular to the central axis of the column and sealed in place with o-ring gaskets to eliminate flow along the column edge, as shown in Figure 10. The column was filled with water. Subsequently, NAPL

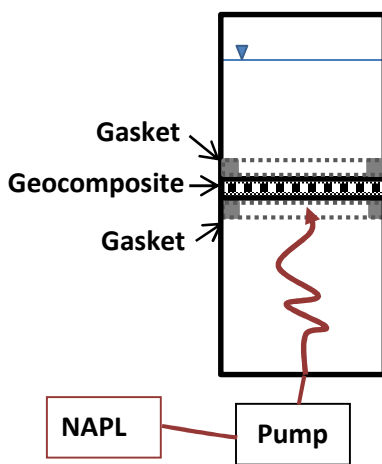


Figure 10: Geocomposite capacity test configuration

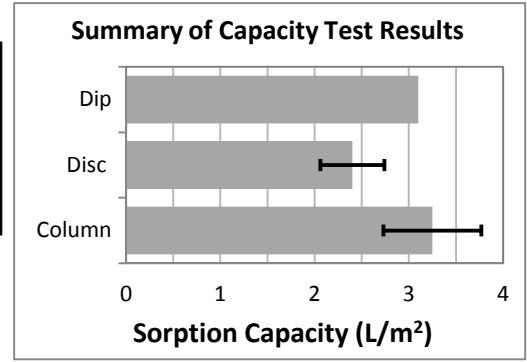
was pumped into the bottom of the column until a sheen was observed. Time to sheen appearance was recorded. The total NAPL introduced to the column was calculated by multiplying time to sheen by the calibrated pump flow rate. NAPL was introduced to the column using a compact peristaltic pump (REGLO model, ISMATEC) via 1/16" ID Fluorinated Ethylene Propylene (FEP) tubing (Cole Parmer). This experiment was run a total of four times, at three different loading rates: 0.06, 0.2, and 1.0 mL/min.

### 3.1.3 Results

Mean geocomposite NAPL retention capacities ( $L/m^2$ ) for each test type are summarized in Table 2 and Figure 11. Tests showed that the geocomposite has the ability to retain 3 L of NAPL per  $m^2$  of geocomposite. The results serve as a general value that can be used to estimate the sheen retention capacity of the geocomposite in an OBB.

**Table 2: Summary of Capacity Test Results**

Test	Mean Capacity (mg/kg)	Mean Capacity (L/m <sup>2</sup> )	Standard Error (L/m <sup>2</sup> )	n
Dip	523000	3.1		1
Disc	452000	2.4	0.34	6
Column	528000	3.25	0.52	4



**Figure 11: Summary of Capacity Test Results**

The relationship between the volume of NAPL stored on a geocomposite and the number of sheens associated with the stored NAPL can be expressed as

$$n_{capacity} = \frac{V_{capacity}}{V_{sheen}} = \frac{V_{capacity}}{\left(\frac{\pi d^2}{4} * b\right)}$$

where,

$n_{capacity}$  is the number of sheens the geocomposite can hold

$V_{capacity}$  is the volume of NAPL the geocompoiste can hold

$V_{sheen}$  is the volume of NAPL associated with one sheen

$d$  is the diameter of a sheen

$b$  is the thickness of a sheen

Using a conservative sheen diameter of 1.5m, based on field observations dicussed in Section 4.1 , and sheen thickness of 0.3 microns, a NAPL capacity of 3L/m<sup>2</sup> is equivalent to 5660 sheens/m<sup>2</sup>. Given a loading rate of 1 sheen/m<sup>2</sup>/day, and no losses of retained NAPL, calculations indicate that the geocomposite could absorb sheens for 15 years without reaching capacity.

## 3.2 Sand Tank Experiments

### 3.2.1 Objectives

Laboratory sand tank studies were designed to test the ability of a geocomposite to mitigate sheens at a GSI with periodic water level fluctuations. The objectives of these experiments were to a) determine whether a geocomposite material could be used to delay sheen formation, b) test two designs for an OBB, and c) visualize the processes involved in sheen mitigation to gain insights into how an OBB may function. Dyes that fluoresce under ultraviolet (**UV**) light were used to enhance the visibility of NAPL as it migrated across a sand tank and interacted with the geocomposite material. More detail is provided in the following subsections. It is important to note that although microbial degradation is an essential function of an OBB, degradation was not addressed in this study.

### 3.2.2 Materials

#### 3.2.2.1 Sand Tank

The custom-made aluminum-framed sand tank, shown in Figure 12, had front and rear glass panels and an open top. The tank had an internal width, height and depth of 180 cm, 38.5 cm, and 5.3 cm, respectively. A screen was installed 3 cm from the right side of the tank, creating a sediment-free

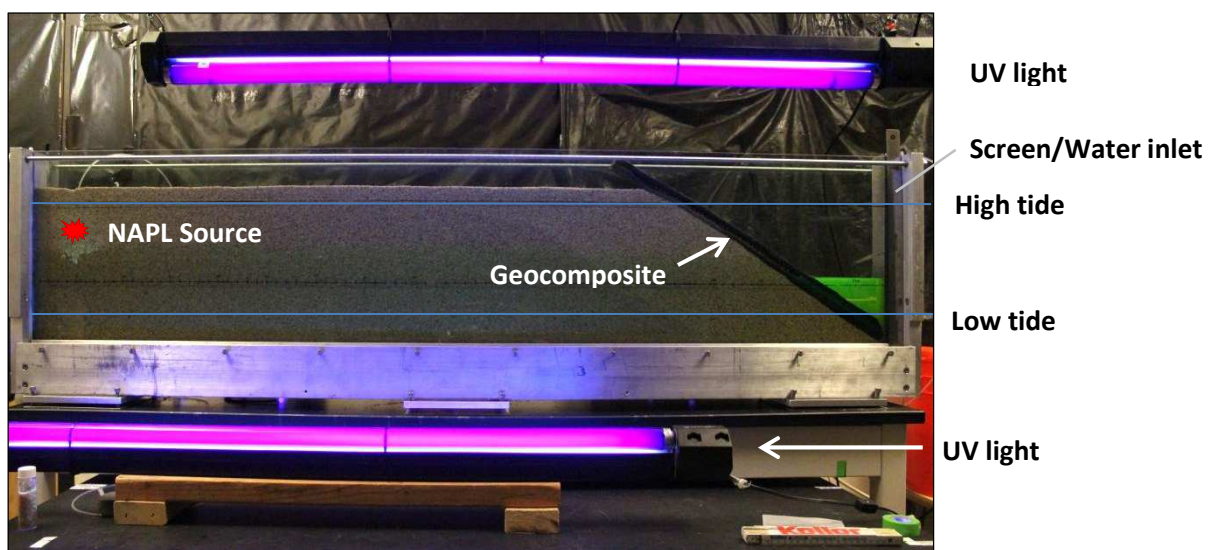


Figure 12: Sand tank setup with geocomposite

column, used to control the water table. The screen was constructed from a round-hole perforated stainless steel sheet of length 38.5 cm, bent into a C-shaped channel of depth 2.5 cm and width 5.3 cm. It was then wrapped with a 304 stainless steel, 50 x 50 wire mesh (McMaster-Carr).

#### *3.2.2.2 Porous Media*

A medium-grained sand (10-20) (Colorado Silica Sand) was used as the porous media in this experiment. The sand was rinsed to remove fines and dried prior to use. The geocomposite used in this study was the Tendrain II – 1010 (Syntec Corp).

#### *3.2.2.3 Pumps and Tubing*

Compact peristaltic pumps (REGLO model, ISMATEC) were used to introduce NAPL and water to the tank via 1/16" ID FEP tubing (Cole Parmer). The water pump was controlled by a laptop running LabVIEW software (National Instruments).

#### *3.2.2.4 Liquids and Dyes*

To employ photographic analysis and enhance NAPL visibility in the tank, fluorescent dyes and UV lights were utilized. Diesel fuel obtained from a gas station in Fort Collins, CO was used as the NAPL in both experiments.

Based on research by Ryan Taylor, as presented in Sale et al., 2007, the fluorescent dye Stay-Brite (BSL 715, Brite Solutions) was selected to dye the NAPL. Staybrite was added to the NAPL to a concentration of 0.01% by volume.

The water used in all experiments was Fort Collins tap water, deaired at -24 in Hg for three hours. Following work by Lee Ann Doner, as presented in Chapman et al., 2012, Fluorescein (Science Lab) was selected to dye the water. Fluorescein was added to the water to a concentration of .0025% by volume.



#### *3.2.2.5 Lighting*

Two 40W, T12 black lights (Ace Hardware, Fort Collins, CO) were used to induce fluorescence. The black lights were 120 cm long. UV light placement can be seen in Figure 12. One UV light was hung facing down, 25 cm above the tank, aligned to the right side of the tank. The other UV light was placed facing up, 17 cm below the tank, aligned with left side of the tank. Both lights were 10 cm from the front of the tank.

The source of visible light consisted of two 10W compact fluorescent single-bulb stand mounted portable lights (Ace Hardware, Fort Collins, CO). The lights were placed 2 m from the front of the tank and 1 m to each side. The lights were mounted 50 cm higher than the tank, and pointed up to prevent reflection from the glass.

#### *3.2.2.6 Cameras*

Two DSLR cameras, a Rebel T3i and a Rebel T2i (Canon U.S.A., Inc.) were used to photograph the experiment. They were mounted on tripods, manually focused and set to a no-flash auto setting. Windows laptops operating Camera Window software (Canon U.S.A., Inc.), were used to automate photography.

### **3.2.3 Methods**

Sand was rained into the top of the tank through a funnel. The funnel was moved back and forth across the length of the tank to distribute the sand evenly and prevent preferential flow paths from forming. Sand was filled to a level surface of height of 33 cm (Figure 12). The sand was filled to the left wall of the tank. On the right side of the tank, a surface was created that sloped to the bottom of the tank at the sand's natural angle of repose, roughly 45°. A strip of geocomposite the width of the tank was placed on the angled surface and extended from the bottom to the top of the tank. Next, the Fluorescein-dyed water was pumped into the screened area at the right of the tank until the water level

reached the high level of tidal fluctuation (30 cm). The water was then drained to the low tide level, and the NAPL “source” tubing was placed at a depth of 10 cm, 10 cm from the left end of the tank.

A LabVIEW program was generated to pump water in and out of the tank to the upper and lower tidal levels (8 cm, 30 cm) on a 12-hour cycle, simulating tidal fluctuations. NAPL was pumped into the tank at a constant rate of 6.3 mL/hour. Two cameras were set up on tripods and set to take photos at regular intervals. The T3i was zoomed in on the NAPL front and was panned along the tank as the experiment progressed. The T3i took photographs every 7.5 minutes. The T2i was centered on the tank, zoomed to the width of the tank, and took photos every 15 minutes. The experiment ran until NAPL reached the water surface beyond the geocomposite, forming a sheen. The photos were then compiled to create a video using Premier Elements 9 (Adobe). Photos taken immediately prior to failure were individually analyzed to understand the conditions that led to failure.

After completion of the first experiment, the water was pumped out of the tank. Then, the NAPL pumped out of the tank until no NAPL could freely drain. The geocomposite strip was removed and replaced with a new geocomposite strip. A 1.5 cm layer of 40-60 sand (Colorado Silica Sand) was installed on top of the geocomposite strip, as seen in Figure 15b. The tank was filled with dyed water to the high water mark, then drained to the low water mark. The pumps were then started, and the experiment was run identically to the first iteration.

### **3.2.4 Results**

Results of the tank studies include qualitative analysis of oleophilic properties (Section 3.2.4.1), quantification of the delay in sheen formation for each design (Section 3.2.4.2), and quantification of relative NAPL capacity for each design (Section 3.2.4.2). Videos of the experiments can be found online at <http://projects-web.engr.colostate.edu/CCH>.

#### 3.2.4.1 Sorption and Wicking

In the first tank study, the geocomposite material delayed sheen release by adsorbing NAPL. The geocomposite began to retain NAPL at first contact. NAPL spread along the geocomposite not only through tidal smearing, but by wicking. Figure 14 shows NAPL wicking up the outer layer of geotextile over the span of 30 minutes. NAPL advanced 3 cm in height, as compared to the 0.5 cm advance of water. Figure 13 shows that NAPL stayed sorbed to the geocomposite even when in direct contact with the water surface, demonstrating the geocomposite's ability to prevent sheens.

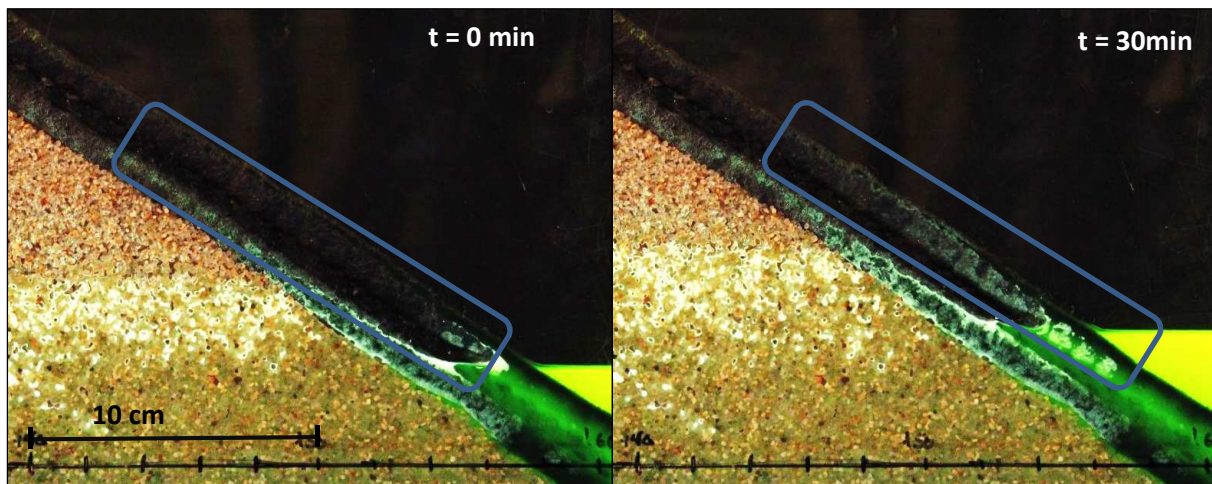


Figure 14: NAPL wicking up geocomposite during a rising tide over 30 min

#### 3.2.4.2 NAPL Retention and Delay of Sheen Formation

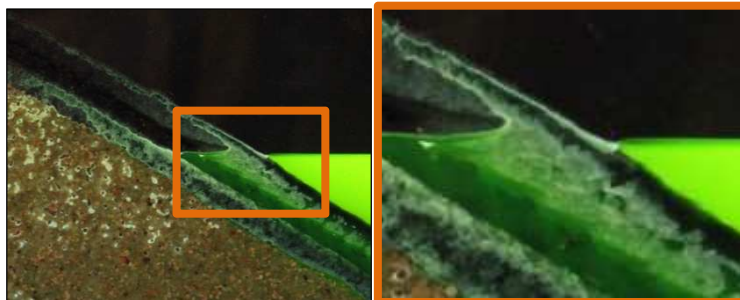


Figure 13: Closeup of Geocomposite retaining NAPL in contact with water

Results presented below include a comparison of NAPL thicknesses and time to failure for systems with and without a top sand layer. Figure 15 shows the photo taken in each experiment immediately prior to sheen formation. These images were used to measure the height of NAPL in the geocomposite for each, and time when failure occurred to the nearest 0.125 hr.

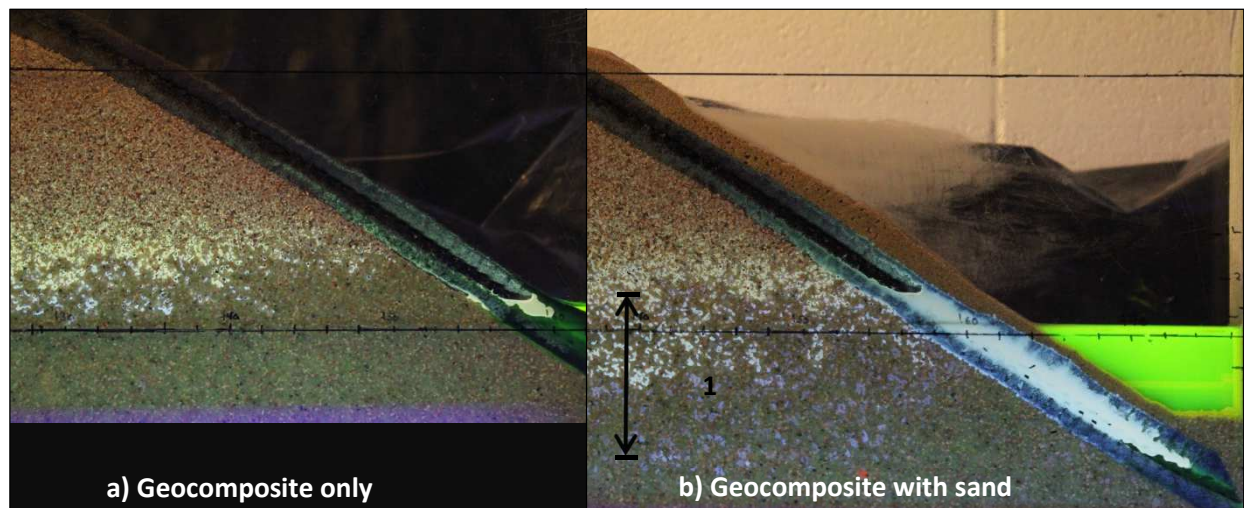


Figure 15: Comparison of OBB tank experiments prior to failure

Results from the experiment with no sand showed that the NAPL took roughly 32 hours, nearly three tidal cycles, to breach the geocomposite. NAPL crossed equivalent thicknesses of sand in as little as 7.5 minutes. Over 32 hours, a thickness of 2.0 cm of NAPL accumulated in the geocomposite. This result is not intended to be directly applied to any field setting, given the dependence on the physical configuration of the shore, tidal levels, and geocomposite. The continuous release of NAPL in this study led to subsurface NAPL saturations high enough to create a continuous phase of NAPL, as seen in Figure 15a. Many sites experiencing sheen formation are late-stage sites, as evidenced by the survey discussed in Section 2.3.5. At these sites, there is often no active release, and saturations can be much lower. In addition, degradation processes absent in this experiment are an essential mechanism for preventing saturation and subsequent failure of an OBB, as discussed in Section 2.4. This study, although not

quantitatively applicable to a field application, does illustrate the potential for a geocomposite to be used to control sheen release to surface water by retaining NAPL.

Table 3 provides a comparison of results between the experiments with and without a sand layer. Time to sheening was increased by 48 hours or 147%. Over this time, the geocomposite with sand accumulated 10.6 cm of NAPL, an increase of 430%. Again, these numbers are specific to the geometric configuration of the simulated bank and OBB constructed in the tank and should not be applied to field estimates. This result does, however, demonstrate the increased potential for sheen prevention when a layer of sand is installed over the geocomposite.

**Table 3: Summary of sand tank experiment results**

<b>Experiment</b>	<b>Time to sheen (hours)</b>	<b>Vertical thickness of NAPL in geocomposite (cm)</b>
Without Sand	32.7	2.0
With Sand	80.7	10.6
Improvement	147%	430%

### **3.3 Aqueous Sorption Experiment**

While the geocomposite is presented as a tool for preventing NAPL transport, it may also have an impact on dissolved phase hydrocarbons. Being a product manufactured from petroleum, freshly manufactured geocomposite material may contain manufacturing residuals that could leach into water. Contrarily, the oleophilic properties described in Section 2.8.5 suggest that dissolved phased hydrocarbons sorb to it.

#### **3.3.1 Objectives**

The objective of this experiment was to investigate the effect of geocomposite on sorbed phase hydrocarbons by determining whether the geocomposite a) sorbs dissolved hydrocarbons and/or b) leaches hydrocarbons into water.

### 3.3.2 Methods

The basic design of this experiment was to pump water containing dissolved hydrocarbons through a control column and a column treated with geocomposite and compare effluent hydrocarbon concentrations. The experimental setup is shown in Figure 16. Both columns were 2" ID, glass columns, 36" in length. Long, narrow strips of geocomposite material with an area totaling 68 in<sup>2</sup> were placed into the first column. Next, 40-60 sand (Colorado Silica Sand) was rained into the column, filling it to the top. The second column was filled only with 40-60 sand. Rubber stoppers with holes for influent and effluent tubing plugged the ends of each column. A solvent-free silicone sealant (Dow Corning) was applied to seal the stopper to the glass column. Since hydrocarbon mass may partition into pore gas, pore gas entrapped upon filling with water had to be minimized. Three pore volumes of CO<sub>2</sub> were pumped through the columns prior to filling with water. This way, the entrapped pore gas (CO<sub>2</sub>) could dissolve into the water, ensuring that the pore space was filled with water. The columns were also filled at a low flow rate, over the span of an hour. The solution of hydrocarbons was stored in a glass carboy with a nitrogen headspace to prevent degradation or oxidation. A compact peristaltic pump (REGLO model, ISMATEC) was used to pump the solution into the columns simultaneously, via 1/8" diameter FEP tubing (Cole Parmer). Effluent samples were collected into glass 10 mL crimp-top vials using flow-through vial fillers seen in Figure 17.

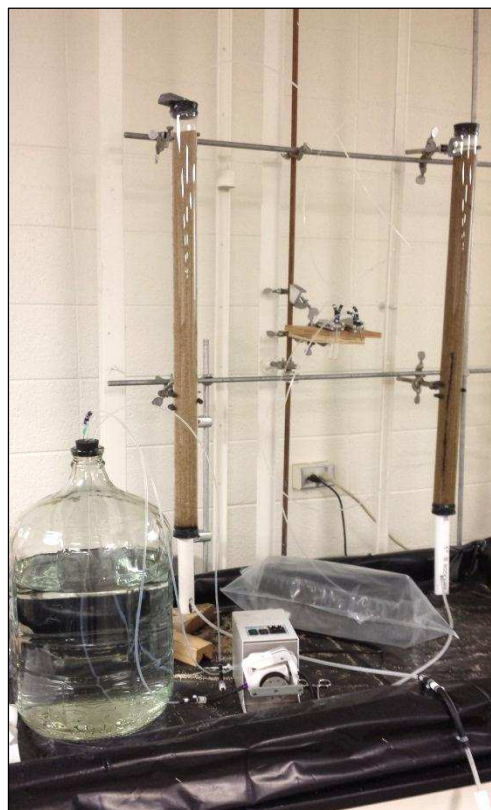


Figure 16: Column setup for sorption experiment



The solution of aqueous phase contaminants made use of four hydrocarbons commonly found in the aqueous phase at petroleum contaminated sites: Benzene, Toluene, Ethylbenzene and Xylenes (**BTEX**). 10 mL of each NAPL was mixed with 4 gal of tap water in a glass carboy. The carboy was shaken vigorously for 5 minutes at 1 hour intervals for 5 hours, and left 12 hours to equilibrate. The water was then transferred to a carboy filled with nitrogen, and the remaining NAPL was discarded. The solution was pumped into each column at a rate of 6.9 mL/min. Effluent samples were taken at 12 minute intervals, corresponding to 0.1 pore volumes of flow through the control column. After 2 pore volumes of flushing, the sampling interval was increased to 24 minutes, or 0.2 pore volumes. Effluent samples were extracted at a 1:1 volume ratio using dichloromethane, and analyzed on a 6890 Gas Chromatograph (**GC**) equipped with a 5973 Mass Selective Detector (**MS**) (Agilent) and a Rx-624Sil, 30.0 m x 250  $\mu$ m x 1.4 $\mu$ m column (Restek).



Figure 17: Flow-through sampling

Influent samples were taken before the experiment began. Effluent peak areas were compared to the initial influent peak areas, creating a ratio of effluent to influent concentrations,  $C/C_0$ .

### 3.3.3 Results

The results presented in this section show the difference in effluent hydrocarbon concentrations between the treated and untreated columns as a fraction of influent concentrations. Figure 18 shows  $C/C_0$  through time for one representative compound, o-xylene. All other compounds followed a similar pattern of behavior. Breakthrough curves of all detected compounds for the treated and untreated columns can be found in Appendix B. No dissolved compounds other than those intentionally

introduced to the columns were detected, leading to the conclusion that the geocomposite did not release detectable quantities of dissolved hydrocarbons.

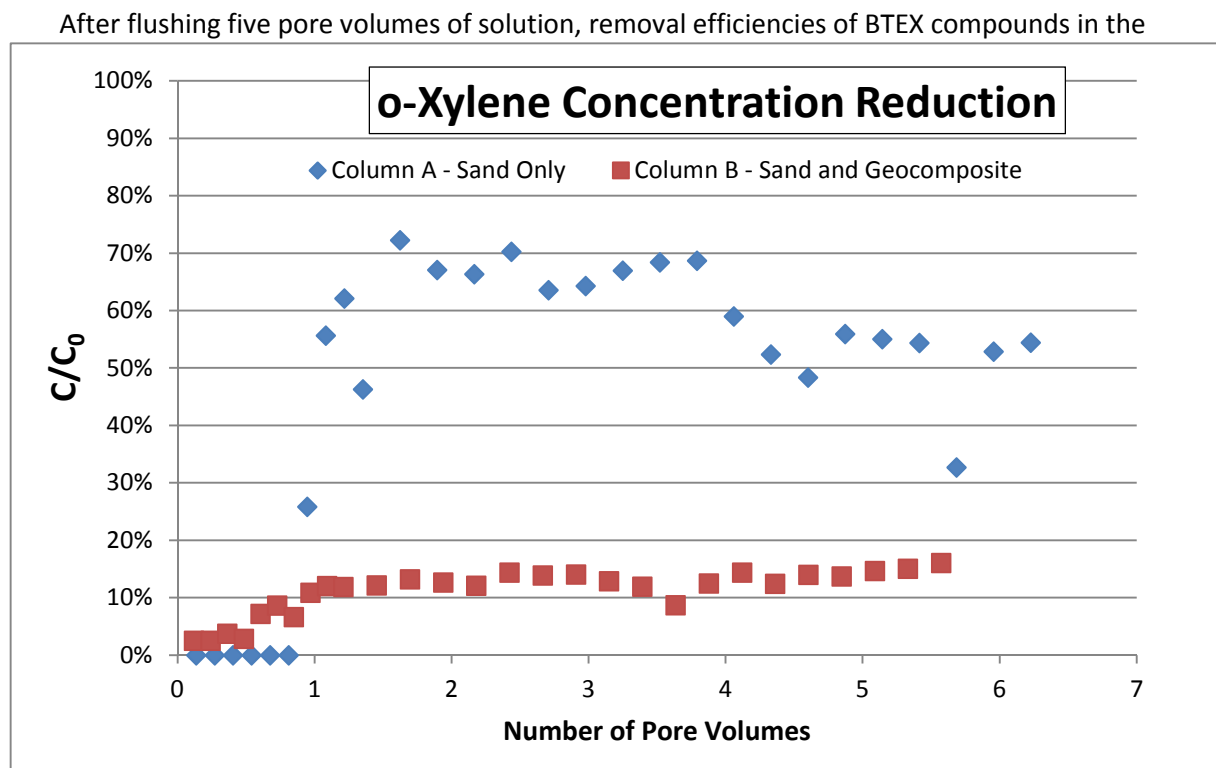


Figure 18: o-xylene effluent concentrations for a control column and a column treated with geocomposite

treatment column compared to the control ranged from 77% for ethylbenzene to 34% for benzene, as shown in Table 4. The effect of sorbate alkyl groups on sorption to the geocomposite can be seen by the grouping of removal efficiencies. The more alkylated the benzene ring, the more of contaminant was removed. Dominance of van der Waals interactions, and therefore sorption affinity, increases with size and alkylation of sorbate (Schwartzbach et al., 2005; Choi, Cho and Luthy, 2013). Large and/or alkylated compounds make up a large portion of hydrocarbons found in diesel fuel, fuel oil, crude oil and other petroleum products. As such, the geocomposite material can be expected to sorb dissolved phase hydrocarbons coming from these sources more efficiently than BTEX compounds.



This experiment demonstrates the geocomposite's potential to reduce hydrocarbon concentrations

**Table 4: Hydrocarbon concentration reduction due to geocomposite treatment**

<b>Hydrocarbon</b>	<b>Number of alkyl carbons</b>	<b>Avg <math>C_{\text{eff}}/C_{\text{inf}}</math> Control</b>	<b>Avg <math>C_{\text{eff}}/C_{\text{inf}}</math> Treatment</b>	<b>Reduction by Treatment</b>
Benzene	0	65%	42%	34%
Toluene	1	56%	24%	57%
Ethylbenzene	2	53%	12%	77%
o-Xylene	2	55%	13%	77%
p-Xylene	2	55%	16%	70%

in a system with dissolved hydrocarbons. It also shows that no detectable hydrocarbons sourcing from freshly manufactured geocomposite dissolve into water.

## 4 Preliminary OBB Field Study

The potential of an OBB as a sheen management tool was tested in two sequential field implementations described in this chapter (4) and the following chapter (5). In both cases, work was conducted by ARCADIS, with CSU providing technical support. Field studies were conducted to better understand construction methods and effectiveness of an OBB at small and large scales in a field setting. Insights into governing processes, design considerations, and monitoring methods were gained from these studies. This chapter contains a description of the field site followed by the objectives, methods, and results of the small-scale OBB field study.

### 4.1 Site Description

A petroleum liquids storage facility located on a large, tidal, freshwater river was identified as an appropriate field site to study the OBB's potential to manage sheens. The facility will be referred to herein as “the site”. The site is managed by ARCADIS US, and background information about the site has been provided by ARCADIS. The site's sporadic sheens, well characterized source, and low NAPL flux at a GSI made it an appropriate choice to test an OBB.

The Site includes 120 m of river bank and is situated among other petroleum facilities. The

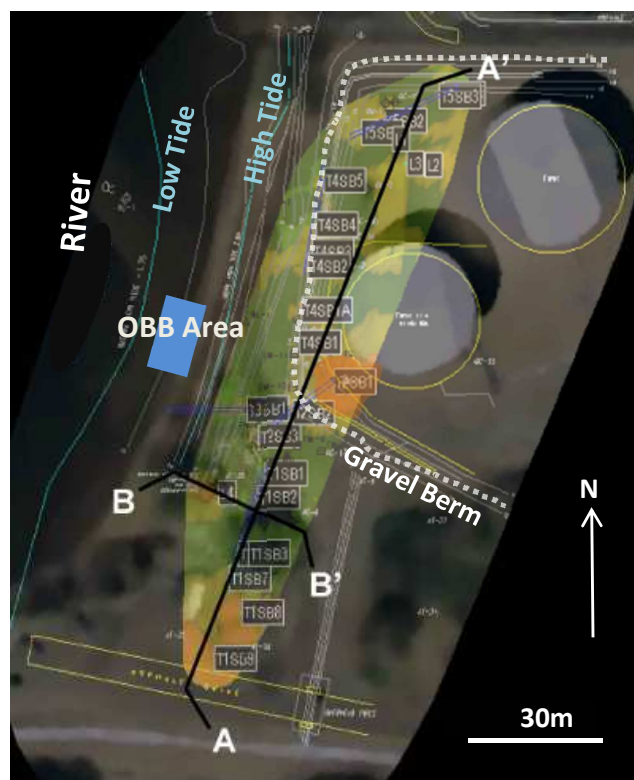


Figure 19: Site layout and hydrocarbon heat map (ARCADIS)

Site houses several 30 m diameter aboveground storage tanks that are separated from the river bank by

a gravel berm, as shown in Figure 19 and Figure 20. The shoreline is made up of two main sediment layers: a sand/gravel layer that extends from the high water mark roughly halfway into the intertidal zone, and an underlying layer of fine-grained sediments that extends into the river beyond the low water mark, as illustrated in Figure 20.

Sheen observations and upland site characterization support the conceptual model shown in Figure 20. A laser-induced fluorescence survey was used to create the hydrocarbon heat map shown in Figure 19. Sediment hydrocarbon analyses, as well as monitoring well NAPL thicknesses, confirm the presence of a high-saturation zone of NAPL in the

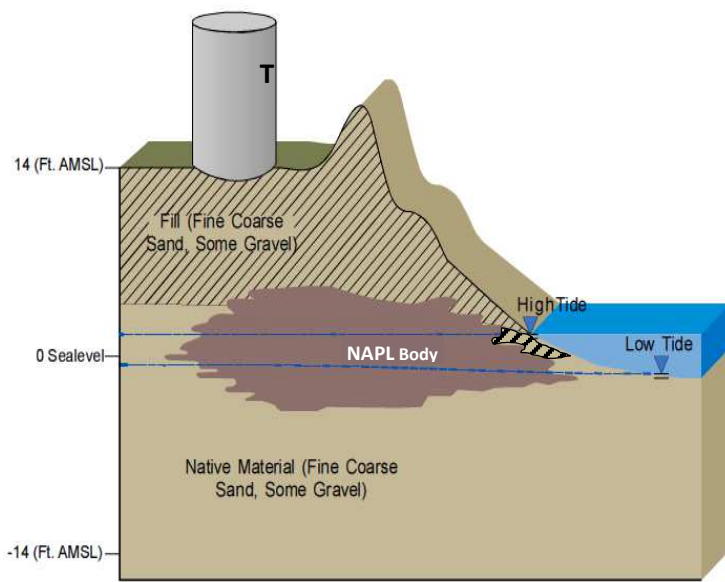


Figure 20: Conceptual Model of the site (ARCADIS)

southwest corner of the containment berm that extends towards the river. The net hydraulic gradient at the site has been calculated as .0012 towards the river. NAPL saturations in the intertidal sediments range from 1.2 to 7.9.

Since 2010, small sheens have formed sporadically on the shoreline, observed an average of 3 times out of 22 observations per year. The majority of these sheens were reported on the scale of inches, though some have been as large as 2 m across. Sheens have been observed mostly as seeps sourcing from the fine-grained sediments at the edge of the gravel layer. Ebullition sheens have been observed sourcing from the fine-grained sediments. Sheens caused by ice scour have also been suspected. The unpredictable timing of sheen formation, well understood source, and low NAPL flux made this an appropriate site to test an OBB.

## **4.2 Preliminary Field Study Objectives**

The objectives of the preliminary OBB field study were to 1) develop anchoring and monitoring equipment appropriate for an OBB in a tidal setting 2) characterize geochemistry and temperatures of an OBB, and 3) study sheen prevention via NAPL sorption to the geocomposite. The OBB was installed in March 2013 and monitored until August 2013, when it was decommissioned. Installation and monitoring were performed in collaboration with ARCADIS.

Insights into anchoring and monitoring infrastructure were gained through visual observations that took place biweekly (every two weeks) and upon decommissioning. Biweekly sheen observations, a UV fluorescence survey of the geocomposite, and analytical hydrocarbon analysis of the sediment, geocomposite, and water were performed to observe sheen prevention and NAPL sorption. Temperature and geochemical data were collected to understand environmental conditions relevant to biodegradation. Geochemical conditions were characterized by the analysis of river water and sediment pore water for pH, Oxidation Reduction Potential (**ORP**), cations, and anions.

## **4.3 Preliminary OBB Installation and Monitoring Equipment**

The following section describes the methods used to construct the OBBs and related performance monitoring equipment. The preliminary OBB system consisted of four square geocomposite mats anchored with cinderblocks and fitted with FEP tubing for water sampling. Thermocouples were installed under the geocomposite mats. Tubing and thermocouple wires ran from under the geocomposite up a post to a waterproof box where temperature dataloggers and sampling ports were housed. The trial-scale OBBs were constructed as follows, and installed on March 19, 2013.

#### 4.3.1 Geocomposite and Sampling Tubes

Four 1 x 1 m squares of Tendrain II 91010 (Syntec LLC) geocomposite were used as the oleophilic sorbent. Five 1/16" ID FEP tubes (Cole Parmer) were fastened to the bottom of each square using a high-temperature hot glue (Ace Hardware), configured as shown in Figure 21. Note that the numbering is ordered right to left when viewing from the bottom. The port numbers increase left to right in a plan view. 153 micron nylon filter cloth was sewn onto the end of each tube using Teflon thread.

#### 4.3.2 Monitoring System

Because the OBBs would be located in a tidal zone, a waterproof case was employed to enclose temperature dataloggers and water sampling ports. A Drybox 3000 (Otterbox) was fitted with watertight brass fittings (Swagelok) to receive FEP tubing and thermocouple wires, as shown in Figure 22. The fittings were sealed with solvent-free silicone sealant (Dow Corning). The box was mounted to a 1.5 m tall U-channel fence post (Figure 23). The FEP tubing and thermocouple wires were run through a 1" PVC conduit that extended from the waterproof case, down the post, to the edge of the geocomposite.

#### 4.3.3 Thermocouples

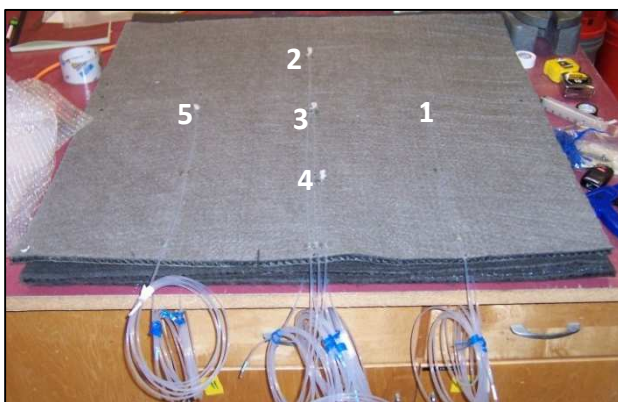


Figure 21: Sampling tube configuration. The white dots are sampling tube ends wrapped with filter cloth.

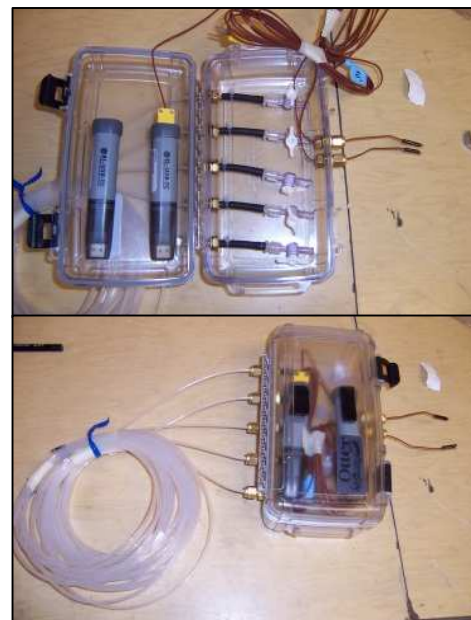


Figure 22: Waterproof housing for data loggers and sampling ports

K-type thermocouples were installed under the geocomposite were placed at the center of each mat to collect temperature data. One was installed at grade, immediately below the geocomposite, and the other was installed 45 cm below the ground surface. The thermocouples were connected to battery-operated, waterproof EL-USB-1 dataloggers (Lascar Electronics), which were housed in the waterproof case.

#### **4.3.4 Placement and Anchoring**

The geocomposite squares were located where sheens had previously been observed, in the “OBB area” in Figure 19. They were placed side-by-side, each centered on the contact between coarse and fine-grained sediments, as shown in Figure 23. They were lettered from south to north A, B, C, and D. The mats were

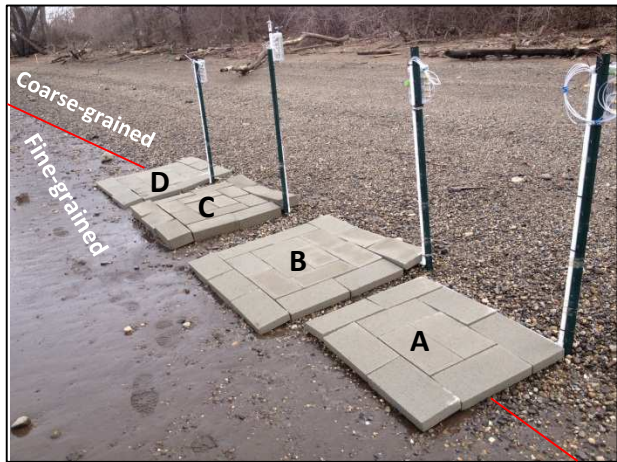


Figure 23: Small-scale OBBs

held in place by four plastic garden stakes, one at each corner of the mat. Two inch thick paving cinderblocks were used to anchor the geocomposite, creating a continuous pattern that extended over the edge of each geocomposite by 15 cm on each side. An as-built drawing of an OBB is provided in Appendix C.

#### **4.4 Data Collection and Analysis**

Methods used for monitoring, sampling, and analysis are described herein. The four OBBs were monitored from March 19 to August 14, 2013. On August 13 and 14, the OBBs were sampled and decommissioned. Sheen monitoring lasted throughout the study (149 days), and water quality samples and data were collected on April 29 and August 13. All other analyses and sample collection occurred

only on August 14, at the time of decommissioning. Table 5 provides a summary of all monitoring and sampling activities.

**Table 5: Preliminary study monitoring and sampling plan**

<b>Goal</b>	<b>Means</b>	<b>Time</b>	<b>Monitoring/ Sampling Media</b>
Evaluate Construction/ Design	Visual condition observation	Biweekly	Cinderblocks and monitoring equipment
Evaluate NAPL transport and sorption to geocomposite	Visual sheen observation	Biweekly	OBBs and shoreline
	UV survey	Final sampling	Underside of geocomposite
	Hydrocarbon analysis	Final sampling	Geocomposite, sediments, water
Evaluate environmental conditions relevant to microbial degradation	Temperature monitoring	Every 30 minutes	Immediately beneath geocomposite, 45 cm under geocomposite
	Measure ORP, pH and Ion concentrations	April 29, August 13	Water

#### **4.4.1 Sheen Monitoring**

Visual observations were made for signs of NAPL. Observations were made for NAPL staining on the cinderblocks, sheens sourcing from the OBBs or adjacent shoreline, and condition of the monitoring system. A total of 13 biweekly observations were made over 149 days.

#### **4.4.2 Water Quality**

Water quality data collected include ORP, pH, dissolved phase hydrocarbons and major ion concentrations. Data and samples were collected on April 29 and August 13. ORP and pH data were



taken using a custom low-volume flow-thru cell, Symphony probes (VWR), and Ultrabasic Portable Meters (Denver Instruments). ORP values were measured using a Ag-AgCl probe and were converted to and reported in the Standard Hydrogen Electrode (SHE) reference frame. Water samples were taken for hydrocarbon analysis, cation

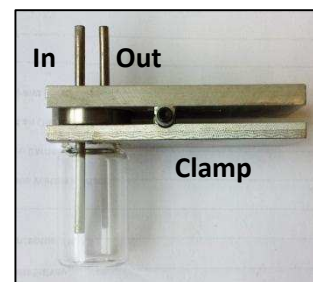


Figure 24: Flow-thru vial filler

analysis, and anion analysis. Samples for cation and hydrocarbon analysis were taken into glass 10 mL, crimp-top vials (Wheaton) and sealed using foil caps with PTFE-lined septa (Thermo Scientific). Custom stainless steel flow-thru vial

fillers were used to collect samples (Figure 24). Flow-thru sampling allows for minimized air contact with the sample. Minimizing air contact can prevent hydrocarbon gas phase partitioning and/or reduce oxygen contact with ion samples. Samples were taken using a custom peristaltic pump driven by an 18V cordless drill (Black & Decker) (Figure 25). Anion samples were collected into 10 mL glass



Figure 25: Custom peristaltic pump driven by a cordless drill

serum vials (Wheaton) prepared with a nitrogen headspace to ensure that no oxygen contacted the sample, and sample redox conditions were preserved. The vials were capped with crimp-top foil caps and butyl rubber septa. The vials were capped in an anaerobic chamber, causing them to be filled with nitrogen. Anion samples were collected into the prepared vials, using a 2", 18G needle (Becton Dickinson) to pierce the septa. Both anion and cation samples were taken through a 0.45 micron Acrodisc filter (Pall Life Sciences). All water samples were stored on ice and shipped to Colorado State University (CSU), where they were refrigerated until being analyzed. During the August sampling event, stainless steel porewater samplers (M.H.E. Products) were used to sample porewater at 30 cm and 90 cm below ground surface, 15cm south of OBB A. A product information sheet for the porewater samplers can be found in Appendix H.



Water samples were analyzed by the Colorado State University Soil, Water and Plant Testing Laboratory for the following analytes: Fe, Mn, Na, K, Ca, Mg, B (EPA 200.7);  $\text{SO}_4^{2-}$ ,  $\text{Cl}^-$  (EPA 300.0)  $\text{NO}_3^-$  (EPA 353.2),  $\text{CO}_3^{2-}$ ,  $\text{HCO}_3^-$  (EPA 310.1) Hardness (Standard Methods 2340B, calculation), Alkalinity (Standard Methods 2320B, titration) and TDS (Modified Standard methods 2540C).

#### **4.4.3 UV Fluorescence Survey**

UV fluorescence was used to detect NAPL on the geocomposite before sample collection. After water sampling was complete, the cinderblock anchoring was removed from each mat. A camping tent covered in black plastic sheeting was used to create a dark environment. Each geocomposite square was turned upside down and moved into the tent for inspection under a 21 LED 395 nm UV flashlight (Simple Solution). Photographs were taken under visible and UV light using a Rebel T2i DSLR camera (Canon). Locations of fluorescence were recorded on the “OBB UV Survey and Sampling form” attached in Appendix D.

#### **4.4.4 Hydrocarbon Analysis**

Sediment, geocomposite, and water samples were collected for hydrocarbon analysis. Samples were collected and extracted as described in the following sections. Extracts were analyzed on a 5890 Series II GC (Hewlett Packard) equipped with a Flame-Ionization Detector (**FID**) and an Rtx-5 30m x .32 mm ID x .25  $\mu\text{m}$  column (Restek), according to a modified EPA method 8015c. Results were reported as concentrations of Total Petroleum Hydrocarbons (**TPH**).

##### **4.4.4.1 Geocomposite Samples**

Geocomposite samples were taken from three locations that fluoresced. One background sample was taken from a location with no fluorescence, no visible microbial growth, no visible hydrocarbons and no hydrocarbon odor. The samples were cut from the geocomposite using heavy-duty snips (Wiss).

Geocomposite samples were collected into 40 mL glass jars with PTFE-lined caps (VWR). Samples were stored and shipped on ice to CSU.

To extract hydrocarbons, the jars were filled with known quantities of dichloromethane (ACS grade, Fisher Scientific) and shaken vigorously on a multi-tube vortexer (SMI) for 20 min. The samples were then immersed in an ultrasonic bath (Aqua Wave 9376, Barnstead) and sonicated for 20 minutes. A 2 mL sample of the dichloromethane was then taken into a 2 mL glass GC vial (VWR) and stored at -20°C until it was analyzed on the GC.

Extracted samples were then analyzed on a GC/FID according to a modified EPA method 8015c. A blank extracted from a pristine sample of geocomposite showed higher levels of hydrocarbons than any field samples, due to the geocomposite's petroleum-derived components. A field blank contained a similar geocomposite fingerprint, but with peak areas similar to field samples. Total chromatogram area from the field blank was subtracted from other geocomposite field samples.

#### *4.4.4.2 Sediment Samples*

Sediment samples were taken from locations in direct contact with fluorescing geocomposite samples. Background sediment samples were taken from locations corresponding to no fluorescence as well as 15cm to the north of the OBB D footprint. Note that the absence of fluorescence in OBBs C and D (Section 4.5.3) justify the background sample location to the north. Sediment samples were taken into 10 mL HDPE centrifuge tubes (Becton Dickinson) and shipped on dry ice to CSU, where they were stored at -20°C. The samples were originally intended for use as DNA samples, but were ultimately used for hydrocarbon analysis.

The sediment was transferred onto 15 mL of dichloromethane in a 40mL glass vial with a fluoropolymer resin-lined screw top cap (VWR). The centrifuge tube was then rinsed with 10 mL dichloromethane, and the rinsate was added to the vial with the sample. Sediment samples underwent

shaking and sonication under the same process as geocomposite samples (Section 4.4.4.1). 2mL of the dichloromethane was then pipetted into a 2mL glass GC vial (VWR) and stored at -20°C until GC analysis.

Extracts were analyzed on a GC/FID, according to a modified EPA method 8015c. Because the HDPE tubes were rinsed with dichloromethane, strong noise resulted in sample chromatograms. Calibrations were performed using sections of the chromatogram not contaminated by the HDPE signal. More detail on this method can be found in Appendix E.

#### 4.4.4.3 Water Samples

Water samples taken for hydrocarbon analysis in April 2013 were collected as described in Section 4.4.2. Samples were prepared by liquid-liquid hexane extraction according to a modified EPA method 3520. A 4 ml sub-sample was pipetted onto 400 µL of n-hexane (ACS grade, Sigma Aldrich) in a 4 mL glass vial. The vials were shaken vigorously on a multi-tube vortexer (SMI) for 20 min. 300 µL of the hexane was pipetted into a 2mL glass GC vial with a 400 µL insert and stored at -20°C until being analyzed on the GC.

Extracts were analyzed on a GC/FID according to a modified EPA method 8015c. Since these results yielded no hydrocarbons, a new method with higher sensitivity was adopted.

Water samples taken for hydrocarbon analysis in August 2013 were collected directly into 20mL crimp-top headspace vials. Using the flow-thru vial filler, vials were filled to a consistent level, as illustrated in Figure 26. As the water is pumped into the vial, it fills to the level of the outlet. Samples were introduced to a GC/FID using a headspace autosampler and analyzed according to a modified EPA method 8015c.

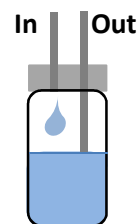


Figure 26:  
Consistent  
headspace  
sampling

#### **4.4.5 Temperatures**

The EL-1 USB temperature data loggers were programmed to record thermocouple temperatures at 30 min intervals. The dataloggers were collected and data were downloaded on August 14.

### **4.5 Results**

Results presented herein yielded important information regarding the design and efficacy of an OBB. Knowledge gained includes sheen prevention potential, microbial degradation feasibility, and design insights. Data presented in this section include the following:

- condition assessment of anchoring and structure
- geochemical characterization
- temperature data
- sheen observations
- geocomposite UV survey and hydrocarbon analysis

#### **4.5.1 Inspection of Anchoring and Structure**

All geocomposite mats stayed in position throughout the study. Cinderblock coverings shifted only slightly around the edges. Observation on June 25 showed that the OBB C monitoring port post had been bent (Figure 27). Damage was assumed to have been caused by a large log that had washed up nearby. Although the post was bent, the functionality of the monitoring system was maintained, and the damage did not affect data collection. However, evidence of damage to this system during the less harsh summer season did raise concerns about winter conditions where ice is present. A



**Figure 27: Monitoring equipment damaged by river debris**

monitoring system that protruded above the ground surface was at risk of substantial damage by river ice during winter months.

Qualitative inspection of the geocomposite showed that where wetted with hydrocarbons, no loss of material integrity occurred. The geogrid core remained rigid and resistant to deformation, while the textile stayed intact and fused to the geogrid. Integrity of the geocomposite was apparent when cutting samples from the geocomposite. Geocomposite remained a challenge to cut with snips, showing no signs of softening or weakening.

Inspection of the geocomposite showed that cinderblock anchoring may have inhibited microbial growth on the geocomposite. Figure 28 shows that microbial communities on the geocomposite developed in areas near the joints between blocks. Growth occurring near block joints could be due to increased oxygen delivery or water flow. An anchor minimizing direct contact with the geocomposite and maximizing transmissivity may improve circulation and oxygen delivery, thereby promoting microbial growth. Sedimentation and microbial growth, shown in Figure 28, show that permeability reduction may be an issue during long-term applications.



Figure 28: Microbial growth patterning on top of geocomposite from OBB A

#### 4.5.2 Geochemistry and Temperatures

Temperature data for the 149 day study are shown in Figure 29. Temperatures immediately beneath the geocomposite fluctuated more than temperatures 45 cm below ground surface. During the summer months, temperatures fluctuated as high as 12.5°C at grade, 11.5°C higher than temperatures fluctuated at 45 cm depth. From July 4 to July 20, temperatures were an average of 4.1°C higher at the ground surface. Installing the geocomposite at the depth with higher temperatures and temperature fluctuations could lead to higher degradation rates, as discussed in Section 2.6 .

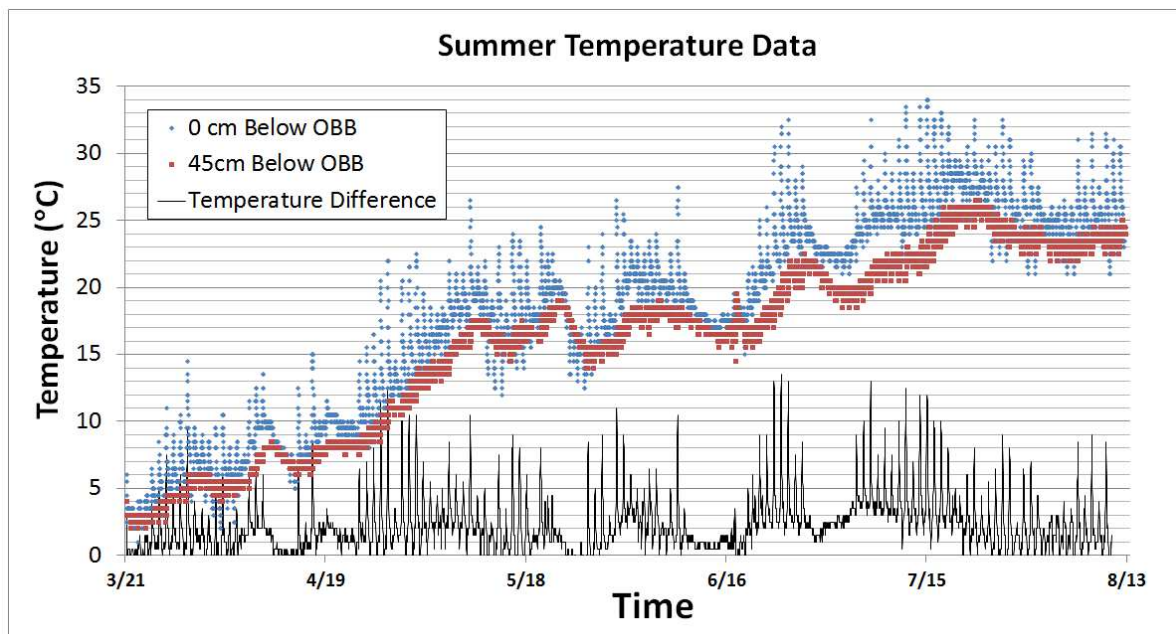


Figure 29: OBB Temperatures from March 21 to August 13

Water quality data are presented in Table 6 and Figure 30. Table 6 shows all ORP and pH data collected in the study. ORP data shows that water from OBB sampling ports had similar ORP and pH values to the river water. August data shows that redox potential decreases with depth. Lower redox potentials in deeper sediments are consistent with the conceptual model that aerobic surface sediments are underlain by anaerobic sediments. The similarity between OBB and river water supports the idea that an OBB installed at the ground surface is exposed to oxygenated river water.

Figure 30 shows ion concentrations for April and August. The river and pore water can be characterized as a moderately hard water with moderate alkalinity and normal pH. Electron acceptors present include iron and sulfate.

Ion concentrations were similar among all OBB ports. Mean OBB port concentrations are compared to concentrations from 30 cm and 90 cm depth in

Figure 30. Although absolute concentrations were higher in August, the same ion profiles can be observed. 8 of 15 analytes increased between 27 and 57% from April to August. All others followed an increasing trend. The uniformly higher concentrations in August could be explained by dilution. Dilution may be caused by variable baseflow or streamflows.

**Table 6: ORP and pH values**

<b>Port</b>	<b>ORP (SHE, mv)</b>	<b>pH</b>
<b>April 2013</b>		
A3	315	6.87
B3	355	6.83
C3	325	7.02
D3	302	7.11
River	351	6.92
<b>August 2013</b>		
A3	423	7.12
Porewater 12"	303	7.41
Porewater 36"	62	6.7
River	339	7.08

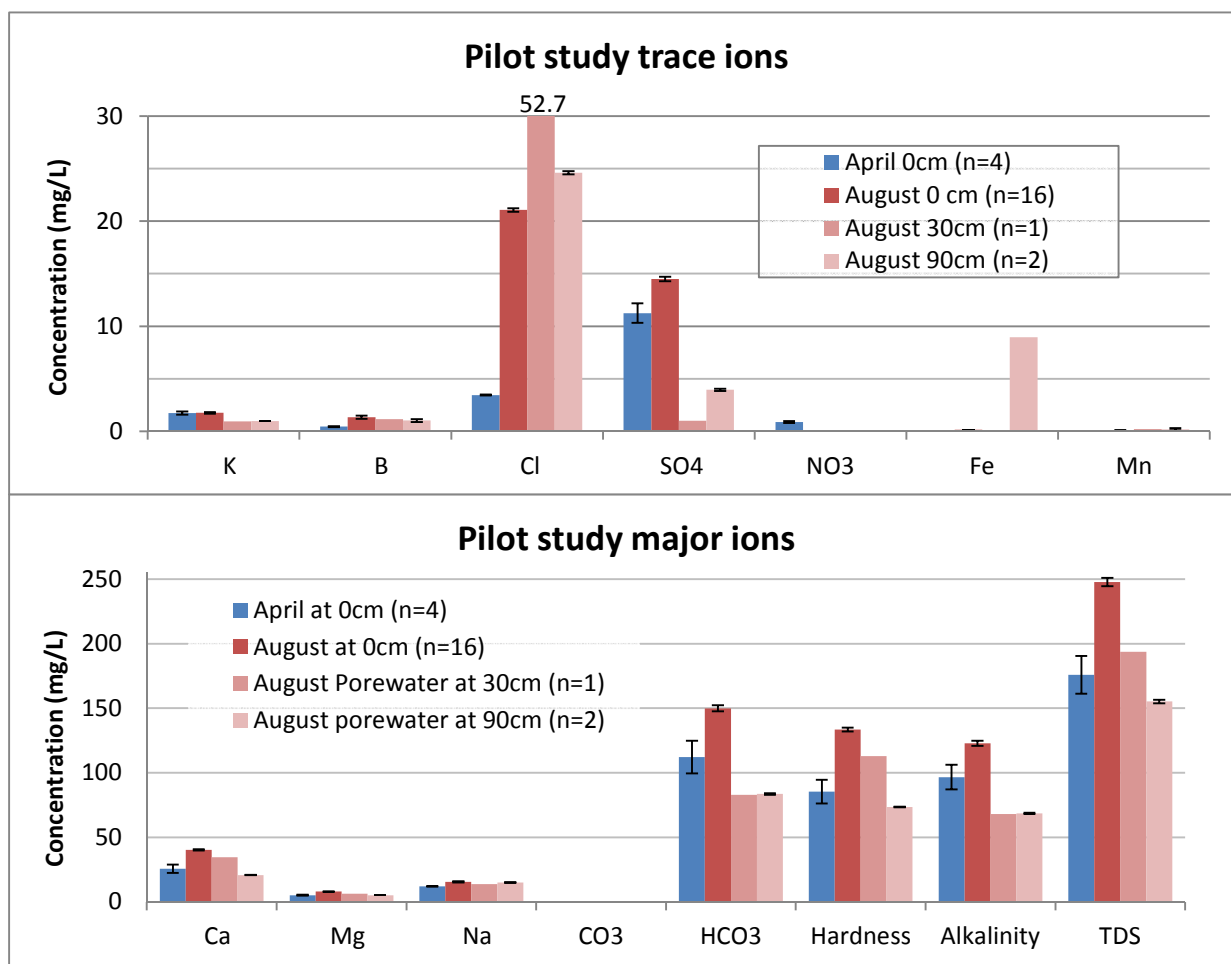


Figure 30: Mean and standard error of ion concentrations from the preliminary study. August 30cm Cl column is truncated.

The depth-discrete August data shows vertical concentration gradients. B, K, Ca, Mg, and TDS all decrease with depth. Alkalinity and SO<sub>4</sub> are higher at the surface than at 90 cm. 30 cm depth samples do not follow a decreasing trend, but this could be due to random error, given that n=1 for the 30 cm depth. The presence of iron at a concentration of 8.9 mg/L in water from 90cm depth suggests that iron at this depth is in the reduced form Fe<sup>2+</sup>. The presence of dissolved Fe corroborates the reduced redox potential at 90cm.

Overall, gradients in redox potential and temperature suggest that surface conditions are most favorable for aerobic degradation. Iron and sulfate are also present as electron acceptors used in microbial hydrocarbon degradation. Although microbes can oxidize hydrocarbons via sulfate or iron



reduction, slow degradation rates make these processes less favorable than aerobic degradation. Geochemical and temperature data show that an OBB optimizing aerobic biological hydrocarbon degradation should be installed at or near the sediment surface.

#### 4.5.3 Sheen Prevention via NAPL Sorption

Zero of 13 observations for sheens yielded observations of sheens sourcing from the OBBs or from surrounding sediments.

OBBs A and B displayed fluorescence covering roughly 20% and 35% of their areas respectively, while C and D showed only traces of fluorescence. Figure 31 shows areas of OBB A and B under visible and UV light. A summary of UV survey results can be found in Figure 32.

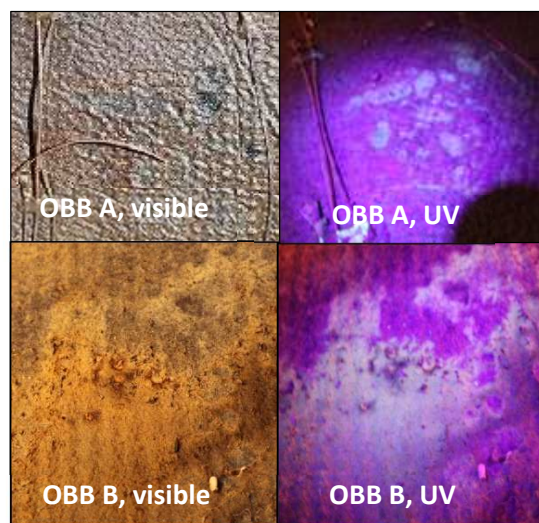


Figure 31: Fluorescing geocomposite

Table 7 summarizes sediment and

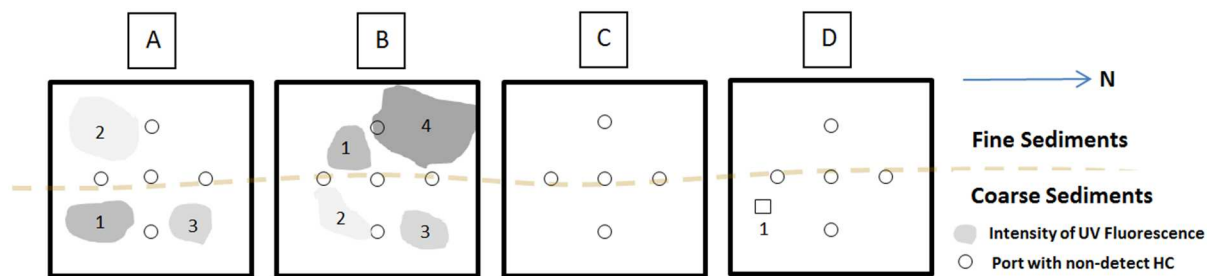







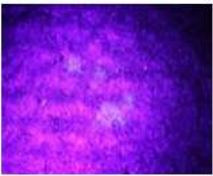
Figure 32: Plan view UV fluorescence and sampling location key. Numbered regions used to ID samples.

geocomposite hydrocarbon analyses. The two most saturated samples (B2 and B3) showed that hydrocarbon mass made up 28% and 25% of the samples, corresponding to a saturation of about 1.6 L/m<sup>2</sup>. This saturation is within the range of lab-measured capacities (average of 53% of the sample or 3.3 L/m<sup>2</sup>), as discussed in Section 3.1.3. Sample D1 displayed no visual indicators (visible or fluorescent)

of hydrocarbons, and These data suggest that the geocomposite successfully sorbed NAPL sourcing from the sediments, thereby preventing sheen formation.

No aqueous hydrocarbons were found in April or August. This result supports the theory that water from OBB ports consisted of river water. Porewater samples collected in August from 30 and 90 cm depth contained visible sheens, and were not analyzed for dissolved phase hydrocarbons. The presence of NAPL at 30 cm depth suggests that degradation processes occurring below 30 cm are insufficient to attenuate NAPL fluxes into surface sediments, supporting the conceptual model of reducing conditions and slow degradation in underlying sediments.

**Table 7: Selected OBB fluorescence photos and concentrations**

Location/ OBB Mat	sub-area	Visual Light Pic	UV Fluorescence	Sediment Conc. (mg/kg)	OBB Conc. (mg/kg)
B	2		yes	171	280000
B	3		yes	349	250000
B	4			3	ND
D	1	 (No visible NAPL)	 (No fluorescence)	no sample	ND
Adjacent Sediments	north of D	N/A	N/A	18, 30	no sample

## **5 Full-Scale OBB Field Demonstration**

This section describes the construction and performance monitoring of a full-scale OBB module. First, objectives of the study are presented. Next, details on the OBB construction process and monitoring methods are described. Methods are followed by results from performance monitoring. Conclusions and recommendations for future OBB implementations and research conclude this chapter.

### **5.1 Objectives**

The objectives of this study were to construct and evaluate a full-scale OBB. Design and implementation occurred with three potential outcomes in mind for the OBB: removal, continuation, or upscaling. The OBB would be evaluated based on performance monitoring data collected over a year-long span. The OBB was evaluated with respect to sheen prevention via NAPL sorption, biological activity, and mechanical stability. Monitoring methods and OBB design were also evaluated to aid in the design and monitoring of future OBBs.

Performance monitoring for the evaluation of the OBB had three main focuses: prevention of NAPL release to surface water, biological activity, and mechanical stability of the OBB. Prevention of NAPL release was studied using 1) UV fluorescence 2) geocomposite and sediment hydrocarbon analyses and 3) visual observations of the OBB and shoreline for hydrocarbon sheens. Biological degradation was studied using a weight of evidence approach, incorporating a variety of data to support the assertion that degradation had occurred. These data included 1) hydrocarbon composition changes, 2) temperature, 3) water quality, 4) microbial DNA, and 5) water level fluctuations. OBB condition was monitored via visual observation. A more detailed description of monitoring objectives and activities is provided in Section 5.3 .

## **5.2 OBB Construction Methods and Monitoring Equipment**

This section describes the methods used to construct a full-scale OBB module. The full-scale OBB was designed in collaboration with ARCADIS US. A utility patent was filed with the US patent office for the OBB concept and design in September of 2014, with inventors from CSU, ARCADIS and Chevron (Zimbron et al., 2014). ARCADIS oversaw construction of the OBB in November 2013, at the Site described in Section 4.1. Sampling and monitoring efforts were coordinated and supported by ARCADIS staff. Because design and construction were performed in imperial units, imperial units are used in this section for the sake of simplicity. The full-scale OBB consisted of a 36' x 18' footprint with a layered design including oleophilic geocomposite, sand, and reno mattress anchoring. More details on the design and construction of the OBB are provided in Section 5.2.1 and Section 5.2.3. A monitoring port system was designed to facilitate sampling and was constructed with the OBB. Details on the design and construction of the monitoring port are provided in Section 5.2.2.

### ***5.2.1 Full-Scale OBB Design***

This section describes the placement and layered design of the OBB, including reno mattress, sand, and geotextile layers.

The full-scale OBB was designed to cover the area of shoreline experiencing the heaviest and most frequent sheens. The target area was a 6 ft wide zone, straddling the coarse-fine sediment contact described in Section 4.1. The geocomposite material is distributed as a 12.5 ft wide roll. Given the well-matched dimensions of the target zone and geocomposite, one natural design was to unroll the geocomposite to the desired length over the target zone. The final OBB footprint dimensions were based on reno mattress dimensions, and came out to 36 ft x 18 ft. Figure 33 shows an as-built drawing of the OBB. Note that the OBB is centered north-south over the two preliminary OBBs that contained NAPL. The original as-built drawings with detailed dimensions are provided in Appendix F.

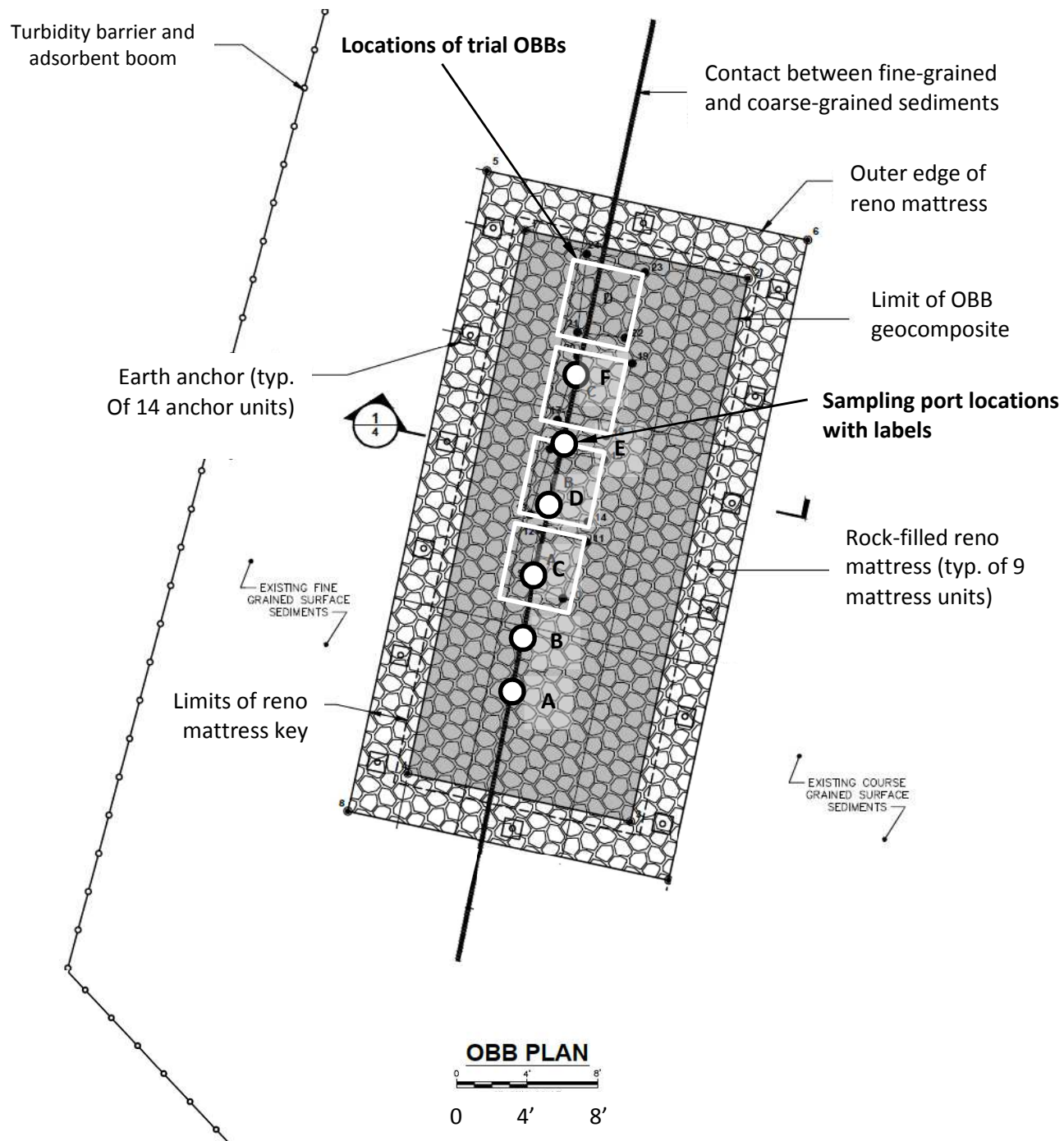


Figure 33: Full-scale OBB construction drawing (modified from ARCADIS)

Reno mattresses were installed to help the OBB withstand abrasion and forces from river ice. During the winter, sheets of ice form on surface and shoreline of the river, as shown in Figure 34. Tidal fluctuations induce vertical forces on the ice, breaking it into plates. River flows induce lateral forces that drag the ice across the shoreline like a plow. This effect, known as ice scour, can disturb impacted sediments and cause sheens. Any structure built on the shoreline could also become frozen into the ice sheets and subject to the same forces and motion as the ice. To anchor the OBB and protect it from ice scour, reno mattresses were installed. Reno mattresses are mattress-shaped wire baskets filled with large rock, commonly used to protect shorelines from erosion and ice scour. The edges of the reno mattress extended past the geocomposite. The edges of the reno mattress were installed into a trench-like key, forming a smooth, continuous surface with the adjacent sediments. A detailed section drawing of the OBB is provided in Appendix F.



Figure 34: Full-scale OBB covered in ice, January 2015

A layer of sand and a layer of geotextile were included in the full-scale OBB to prevent sedimentation and improve storage capacity. A schematic of the layered design is shown in Figure 35. A sand layer is commonly used in conjunction with a geocomposite in geotechnical applications. The sand is meant to protect the geocomposite from being damaged by upper layers (the reno mattress) during construction and to create a filter layer to manage sedimentation. To prevent the sand from washing out and/or redistributing, a geotextile layer was placed between the sand and the reno mattress. The lab study described in

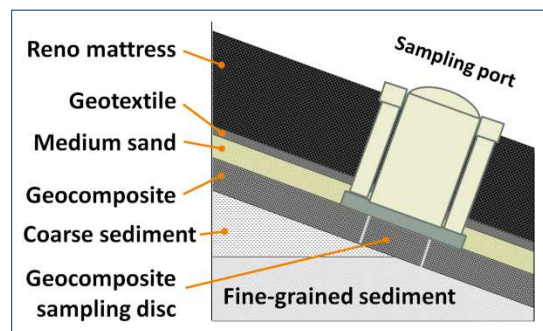


Figure 35: Schematic of OBB layers and sampling



Section 3.2.4.2 showed that a sand layer could also increase the OBB's capacity for NAPL. The additional layer of geotextile could also increase sorption capacity of the system and add a redundant layer of protection.

### **5.2.2 Sampling Port Design**

A sampling port was designed to allow access to environmental media under the reno mattress and to protect sampling equipment. The port extends through the upper layers of the OBB to facilitate access to porewater, sediments, and geocomposite. Protective housings for temperature and pressure dataloggers are attached to the sides of the port. The monitoring port system was designed and assembled at CSU. A detailed set of assembly instructions and complete parts list can be found in Appendix H.

The port's main structure consists of a 6 inch diameter schedule 40 PVC pipe anchored to the geocomposite layer by a PVC flange (Figure 36). The 6 inch pipe provides access directly to the geocomposite layer, while minimizing impact to upper layers. To facilitate geocomposite sampling, a 6 inch hole saw (Milwaukee Tool) was used to pre-cut discs out of the geocomposite layer, as shown in Figure 37a. Discs were cut from the geocomposite prior to installation, creating a hole for each sampling port location. Ports were installed over the holes. Each disc cut from the geocomposite was left in its hole (Figure 37b), to be collected and replaced as a sacrificial sample during each sampling event.



Figure 36: Flange with 6 inch PVC pipe



Figure 37: a) geocomposite disc cut with hole saw b) disc placed back in hole

Four 1 ¼ inch diameter schedule 40 PVC pipes were mounted to the outside of the main pipe, as shown in Figure 35 and Figure 38a. The 1 ¼ inch pipes house water sampling ports and data loggers. Stainless steel porewater samplers (Pushpoint, MHE Products) were installed at each port. A length of FEP tubing (Cole Parmer) was run from each sampler into a 1 ¼ inch PVC housing to allow porewater access from the surface of the OBB. Samplers at 1, 2, and 3 foot depths were installed at each port and occupied three of the four 1 ¼ inch housings. BaroLogger (Solinst) pressure dataloggers were connected to the 3 foot samplers to measure pressure at the 3 foot depth. The fourth 1 ¼ inch pipe housed temperature dataloggers connected to thermocouples at 0 and 24 inch depths below the geocomposite.

Each monitoring port contained an insert used to keep debris out of the 6 inch pipe and mimic OBB conditions outside the sampling port. The insert is made of a 5 inch diameter PVC pipe with a wire mesh installed on the bottom, as seen in Figure 38. The mesh was lined with geotextile, and the insert was filled with gravel to match reno mattress transmissivity.



Figure 38: a) OBB sampling port b) sampling port insert



### **5.2.3 OBB Construction**

This section describes the materials used to construct the full-scale OBB module. Construction drawings and a set of photos documenting the OBB construction process can be found in Appendix H.

The following materials were used in the construction of the full-scale field demonstration. Photos and/or product data sheets for materials marked with an asterisk (\*) are included in Appendix H.

Thicknesses of layers associated with layer materials are noted.

- Geocomposite – Tendrain II 91010 (Syntec) – 0.55 in
- Geotextile – non-woven 10 oz polyester geotextile – 0.16 in
- Sand – well graded sand – Coarse (#8) to fine (#100)\* – 2-3 in
- Reno mattresses (Diamond Wire Netting and Finished Products)\* – 12 in
- Duckbill Earth Anchors (Model 138-DB1, MPS Civil Products)\*
- Reno mattress fill – cobbles
- PushPoint samplers (M.H.E. Products)\*

The OBB was constructed by the following process:

- Site Preparation
  - Established staging area and access
  - Constructed access road to shoreline
  - Installed silt curtain and booms to protect river water quality
  - Staked out/surveyed extents of OBB based on known seeps
  - Unrolled geocomposite and pre-cut access holes at locations corresponding to sampling port locations
- Installation
  - Set anchors

- Dug key
- Smoothed ground surface to ensure good geocomposite/ground contact
- Placed geocomposite by unrolling
- Anchored 6 inch PVC flanges to geocomposite and fastened 1 ¼ inch tubes on to main pipe as described in Appendix H
- Installed sand layer over geocomposite
- Placed geotextile over sand
- Cut holes in geotextile for monitoring ports
- Placed wire reno mattress baskets and cut holes for ports
- Filled reno mattresses, and fastened wire tops according to specification
- Installed anchor plates onto anchor cables, and tightened plates against reno mattresses

### **5.3 Performance Monitoring Plan and Schedule**

Three sampling events occurred in the first year of deployment. Sampling was originally planned to occur quarterly, however, ice cover and high river stages prevented sampling from occurring until May, 2014. Sampling events also occurred in August 2014 and November 2014, in keeping with a quarterly schedule. A summary of monitoring activities, goals, and methods is shown in Table 8.

Table 8: Full-Scale OBB performance monitoring plan

Goal	Means	Monitoring Method	Frequency	Monitoring/Sampling Location	Timeframe	Monitoring/Sampling Media
<b>Evaluate Construction/Design</b>	Document integrity of OBB construction materials in long-term application	Visual observation	Biweekly	OBB components	November 13 on	OBB system components and adjacent areas
<b>Evaluate NAPL transport/sorption to geocomposite</b>	Observe shoreline and OBB for sheens	Visual observation	Biweekly	Intertidal zone	November 13 on	Intertidal zone, including OBB footprint
	Quantify hydrocarbons in media	Sampling and GCMS analysis at CSU	varied	A, B, E	Aug-14	OBB Geocomposite
				Sampling ports C, D, F, SW corner	Nov-14	
			Initial	Sampling ports (A-F)	May-14	Surface sediment
			Seasonal	Sampling ports (A-F)	May-14	Porewater
					Aug-14	
					Nov-14	
	Document UV fluorescence	Hand-held ultraviolet light	Seasonal	Sampling ports (A-F)	May-14	OBB geocomposite
					Aug-14	
					Nov-14	
<b>Evaluate sorption and transformation</b>	Document presence of hydrocarbons and changes in composition	Sampling and PAH biomarkers GC/MS Full Scan at Zymax Labs	Seasonal	Sampling ports (A-F)	May-14	Geocomposite roll (blank), OBB geocomposite, surface sediment
				Sampling Port A,B & E	Aug-14	OBB geocomposite, surface sediment
				Sampling Port A,B & E, SW Corner	Nov-14	OBB geocomposite, surface sediment
	Document presence of hydrocarbons and changes in composition	Sampling and PAH biomarkers GC/MS Full Scan at Zymax Labs	Seasonal	Sampling Ports B, E	May-14	Porewater
				Sampling Ports A, B, E	Aug-14	
<b>Evaluate factors relevant to microbial degradation</b>	Evaluate water quality parameters (pH, ORP)	Hand-held meter	Seasonal	Sampling ports (A-F)	May-14	Porewater
					Aug-14	
					Nov-14	
	Characterize geochemistry and observe changes	Cation and anion analysis	Seasonal	Sampling ports (A-F)	May-14	Porewater
					Aug-14	
					Nov-14	
	Quantify microbes on media	Sampling and qPCR analysis	Biannually	Sampling ports (A, B, E), sediment adjacent to OBB, SW Corner	May-14	OBB geocomposite and surface sediment
					Nov-14	
	Characterize microbial diversity	Sampling and 454 pyrosequencing	Once	Sampling ports (A, B, E)	May-14	

### 5.3.1 Selection of Ports for Continued Analysis

Limited sampling media and high cost of DNA and hydrocarbon forensics analyses led to the selection and sampling of a reduced number of sampling ports for analysis after the May sampling event.

The amount of geocomposite and sediment available for sampling was limited. Only one geocomposite disc was housed in each port. Each disc is large enough for roughly four samples (40-50 g). To track changes in hydrocarbon composition through time, one half of each disc would be left for future analysis. Sediment sampling material was also limited. The cumulative effect of sediment collection created a cavity beneath each port sampled, as shown in Figure 39. To prevent washout and the collection of samples not representative of surface sediments, sediment sampling was reduced. Because of the limited amount of sample material available during each sampling event, the monitoring plan adapted through time based on each event's results.

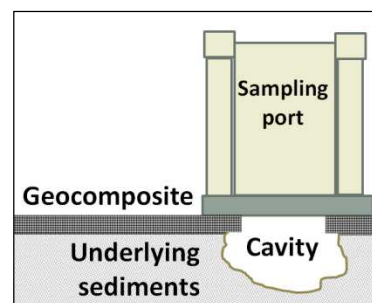


Figure 39: Cavity formed by sediment sampling

To manage costs associated with hydrocarbon and DNA analyses, three of the six sampling ports were selected for ongoing analysis. Port selection was based on May data. In May, geocomposite and sediment samples from all six ports underwent hydrocarbon analysis. Ports which had the most hydrocarbon and the highest quality of forensics data were chosen. Ports A, B, and E were selected for microbial diversity analysis and ongoing hydrocarbon forensics.

The sampling schedule resulting from limited sample material and selective forensics and DNA analyses is summarized in Table 9.

Table 9: Sampling Schedule Summary. Letters represent ports sampled. SW refers to sample collection described in Section 5.3.2

Media	Monitoring method	May	August	November
Shoreline/OBB	Visual Monitoring	Biweekly		
Water	Ion analyses	A-F	A-F	A-F
	ORP/pH	A-F	A-F	-
	HC Qty	A-F	A-F	A-F
	HC Forensics	B, E	A, B, E	-
Sediment	HC Qty	A-F	-	C,D,F, SW
	HC Forensics	A-F	A, B, E	A, B, E
	Microbes Qty	A-F	-	A, B, E
	Microbes Characterize	A, B, E	-	-
Geocomposite	UV Survey	A-F	A-F	A-F
	HC Qty	-	A, B, E	C,D,F, SW
	HC Forensics	A-F	A, B, E	A, B, E
	Microbes Qty	A-F	-	A, B, E
	Microbes Characterize	A, B, E	-	-

### 5.3.2 Southwest Corner Sampling

Sedimentation in sampling ports and the appearance of a sheen adjacent to the OBB in August prompted the investigation of OBB conditions outside of sampling ports. In November 2014, samples noted in Table 9 were collected from the southwest corner of the OBB, adjacent to the location of the sheen observed in August. The samples were collected to investigate whether the geocomposite was saturated, causing NAPL to seep from under the OBB. Another possible explanation is that digging the key for reno mattress integration into sediments created a preferential flow path. The sheen is located directly above the edge of the sediment disturbed by key digging.



Figure 40: Sheen observed in August, adjacent to SW corner of OBB

To collect samples, the reno mattress lid was opened, stones from inside were removed, and a hole was cut in the bottom of the wire mattress. The underlying geotextile was cut open, and sand was

cleared from atop the geocomposite. The geocomposite was visually inspected for sedimentation. Two geocomposite and two sediment samples were collected for hydrocarbon analysis, as in Section 5.4.7. One sample of each type was sent to CSU and to Zymax. After sample collection, new geocomposite was placed overlapping the edges of the hole, and overlying materials were replaced before the reno mattress was refilled and closed. Samples collected from the southwest corner are represented by a “SW” in tables and figures.

## **5.4 Performance Monitoring Methods**

The methods for observation, sample collection, and sample analysis utilized during the full-scale OBB study are described in this section.

### **5.4.1 Visual Observations**

Visual observations for sheens and OBB condition occurred biweekly, for a total of 26 observations. During each observation, the shoreline was inspected for sheens. The monitoring ports and surface of the OBB were inspected for sheens and hydrocarbon staining during each observation. The reno mattresses were inspected for damage to wire baskets, anchor plates and/or anchor cables. The OBB were also inspected for any major sediment deposition, settlement, erosion, and movement of reno mattress fill. Sampling ports were also inspected for damage.

### **5.4.2 Sedimentation**

Geocomposite samples collected in November were measured and weighed to quantify sedimentation. Geocomposite samples collected from sampling ports C, D, F, and the southwest corner were photographed. Next, any layer of accumulated sediment on the surface of the geocomposite was scraped off using a metal spoon in order to capture only the weight of the intruded sediment. The samples were measured and weighed. Mass per area of geocomposite was calculated as a measure of sediment intrusion into each sample.

### **5.4.3 Temperature Data**

Temperature data was taken for the entirety of the study. From November 2013 to May 2014, temperatures were collected from 2 feet below the ground surface, at the ground surface below the OBB, and in the reno mattress. Temperatures at the 0 and 2 foot depths were logged using Lascar EL-1 thermocouple dataloggers housed in 1¼-inch PVC tubing. From May through November, only temperatures in the reno mattress were recorded. Reno mattress temperatures were logged using BaroLoggers (Solinst). Laboratory tests confirmed that temperatures logged by the two devices stayed within 1°C over a 24-hour period.

### **5.4.4 Pore Pressure Data**

Two pressure loggers (BaroLogger, Solinst) were housed in a rigid, low-volume enclosures connected to porewater samplers of 3 foot depth. The low volume and rigidity of the enclosure were designed to allow pore pressure at the 3 foot depth to be accurately transmitted to the logger. Details on the design of the pressure enclosures are provided in Appendix H. The loggers were programmed to record pressure at 30 minute intervals. Logged data were compared to river stage data collected from a nearby, upstream USGS station (USGS, 2015).

### **5.4.5 Water Quality Analysis**

Water quality data collected include ORP, pH, cation, anion, and hydrocarbon analyses. ORP and pH data were collected according to the methods described in Section 4.4.2. In November, equipment malfunction prevented the collection of ORP and pH data. Water samples were collected from porewater sampler ports using the pump and tubing described in Section 4.4.2. All water samples were collected and shipped on ice to CSU, where they were stored at 4°C.

Cation samples were taken through a 0.45 micron nylon filter (Acrodisc, Pall Life Sciences) into 8 mL glass vials with aluminum, screw-top caps. The vials were pre-filled with 100 µL nitric acid as a

preservative. The vials were prepared by Pace Analytical. Cation samples were analyzed by the CSU Soil, Water and Plant Testing Lab, according to the methods described in Section 4.4.2. Target analytes included  $\text{Ca}^{2+}$ ,  $\text{Mg}^+$ ,  $\text{Na}^+$ ,  $\text{Cl}^-$ , Fe, and Mn.

Anion samples were collected through a 0.45 micron nylon filter (Acrodisc, Pall Life Sciences) into anaerobically prepared serum vials, as described in Section 4.4.2. Anion analysis was performed on an 861 Advanced Compact Ion Chromatograph (Metrohm USA Inc.) according to a modified EPA Method 300.2.

#### **5.4.6 UV Survey**

A UV survey observation was conducted for geocomposite samples in each port during each sampling event. Each geocomposite sample was removed from its port and placed in a glass dish. The top and bottom of each sample was observed under UV and visible light. A covering made from black plastic sheeting was used to block out natural ambient visible light. A hand-held, 395 nm UV LED flashlight (Simple Solution) was used to induce fluorescence. A Rebel T2i DSLR camera (Canon) was used to photograph geocomposite samples. During the May sampling event, all samples were photographed in visible and UV light. In subsequent events, only fluorescing samples were photographed.

#### **5.4.7 Geocomposite and Sediment Sampling**

After the UV survey, portions of each disc were allotted to hydrocarbon and DNA analyses.

In May, geocomposite samples from all six ports were divided up in the same way. Heavy-duty snips (Wiss) were used to cut the disc in half. One half was placed back into the north side of the sampling port to be collected at the following event. A new half-disc was placed in the south side. One quarter of the disc was allotted to DNA analysis, the other quarter to hydrocarbon forensics. In August and November, half of the “old” half was sampled from ports A, B, and E and replaced with a new half.



In August, a sample was taken for hydrocarbon forensics. In November, samples were taken for hydrocarbon forensics and DNA analyses.

Geocomposite DNA samples were collected into 1-quart Ziploc® bags, then stored and shipped on dry ice to CSU. Sediment DNA samples were collected into 15 mL centrifuge tubes (Becton Dickinson) before being stored and shipped on dry ice to CSU. All DNA samples were stored at -20°C until processing.

Geocomposite and sediment hydrocarbon samples were collected into 120 mL glass jars with PTFE-lined caps. Samples were stored and shipped on ice to CSU. Samples were stored at 4°C until being extracted.

#### **5.4.8 Hydrocarbon Analysis**

Water, sediment, and geocomposite samples were collected and analyzed for hydrocarbons. Samples were collected for two types of analysis: quantification and forensics. The objective of quantification was to determine the concentration of hydrocarbons present in each sample with the goal of understanding NAPL transport in the sediment and OBB. The objective of forensics analysis was to track changes in hydrocarbon composition associated with biological degradation. As discussed in Section 5.3, geocomposite and sediment sampling media was limited. Since data from forensics analysis are associated with biological activity, ports undergoing microbial characterization also underwent continued forensics analysis. Samples from ports A, B, and E were chosen for continued analysis based on results of the May hydrocarbon quantification and forensics analyses, as discussed in Section 5.3.

##### **5.4.8.1 Quantification Analysis**

Hydrocarbons were extracted from sediment, geocomposite, and water samples were extracted using dichloromethane. Jars containing geocomposite samples were used for extraction. Since

sediment jars were full, half of the sample was moved to a second 120 mL jar for extraction. The sediment and geocomposite jars were filled with known quantities of dichloromethane (ACS grade, Fisher Scientific) and shaken vigorously on a multi-tube vortexer (SMI) for 20 minutes. The samples were then immersed in an ultrasonic bath (Aqua Wave 9376, Barnstead) and sonicated for 20 minutes. A 2 mL sample of the dichloromethane was then taken from each jar and stored at -20°C until GC analysis. Hydrocarbons were extracted from water samples by a 3:1 liquid-liquid dichloromethane extraction according to a modified EPA method 3520. All sample extracts were stored at -20°C until being analyzed. All hydrocarbon extracts were analyzed on a 6890 GC equipped with a 5973 Mass Selective Detector (Agilent) and an Rx-624Sil, 30.0 m x 250 µm x 1.4 µm column (Restek).

#### *5.4.8.2 Forensics Analysis*

The objective of hydrocarbon forensics analysis was to track changes in the composition of NAPL that could correspond to degradation. Sediment, water, and geocomposite samples were analyzed by Zymax, the forensics division of Pace Analytical. The analysis performed was a GC/MS Full Scan Polycyclic Aromatic Hydrocarbon (**PAH**) Biomarker analysis. Results of the scan were used to generate a “fingerprint” of the hydrocarbons in the sample, using the relative abundances of 52 Aromatic Hydrocarbons (**AHs**). Fingerprints of media in each port were compared through time to understand how NAPL composition changed. Forensics analysis was aided by Matt Schnobrich and Julie Sueker of ARCADIS, Inc.

The AH families found in each sample were qualitatively analyzed for three criteria regarding sorption and degradation. Figure 41 shows fingerprints representative of each source analyzed. Each fingerprint consists of relative quantities of AHs from 12 different families found in each sample. Each family consists of a parent compound and its alkylated homologs containing up to six extra carbons. An example would be the second group from left on each fingerprint, the “NAPH” group. The NAPH group is made up of naphthalene, methylnaphthalene (C1 naphthalene), ethyl- and dimethylnaphthalene (C2 naphthalenes), C3, and C4 naphthalenes. A key defining all abbreviations and analytes is provided in Appendix J.

First, each fingerprint was examined for the abundance of petrogenic (petroleum-derived) AHs relative to pyrogenic (combustion product) AHs. The petrogenic compounds of interest can

be seen in abundance in the two NAPL samples in Figure 41a and Figure 41b. They include alkylbenzenes (**AB**), NAPH, fluorenes (**FL**), biphenyls (**BP**), phenanthrenes (**PHEN**), benzothiophenes (**BT**), dibenzothiophenes (**DBT**), and naphthobenzothiophenes (**NBT**). Pyrogenic AHs are typified by the background sediment sample shown in Figure 41c. Pyrogenic AHs are found in all sediment and geocomposite samples due to the Site’s highly industrial neighboring environment. Pyrogenic AHs include the lower-carbon homologs (C0, C1, C2) of pyrenes (PY), chrysenes (CHR), and PHEN. Samples

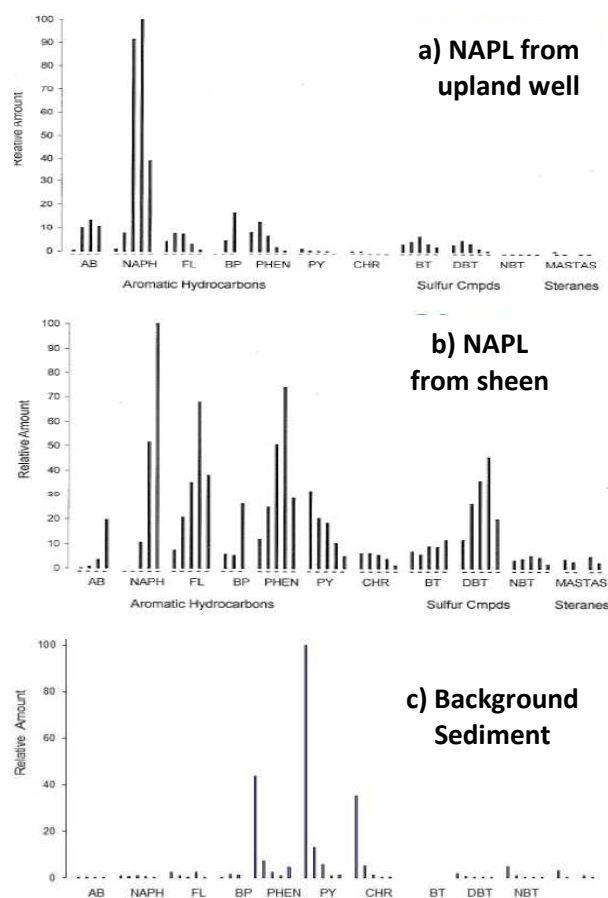


Figure 41: PAH biomarker fingerprints

with petrogenic AHs above background were rated either “high,” “medium,” or “low,” based on petrogenic abundances relative to pyrogenic abundances.

Next, fingerprints were examined for signs of weathering. Analysis for weathering involved the comparison of the abundance of soluble petrogenics to less soluble petrogenics. Abundances of AB and NAPH were compared to abundances of PHEN and DBT and rated “high,” “medium,” or “low.” A low rating corresponds to ratios similar to those found in upland monitoring well NAPL, while a high rating corresponds to ratios found in the sheen sample.

Last, each fingerprint was evaluated based on degradation patterns. Less alkylated AHs degrade more quickly than their high-homolog relatives. Petrogenic groups of each fingerprint were analyzed for their enrichment of high-homolog AHs. Groups with “downwards” patterns, exemplified by the monitoring well PHEN group, were given a low rating for biodegradation. Groups with “upwards” patterns exemplified by the NAPH group of the sheen sample were given a high rating.

The combination of petrogenic, weathered, and biodegraded ratings were then used to interpret hydrocarbons found in the sample and make conclusions about transport and/or degradation. Highly petrogenic samples were interpreted as having more NAPL than less petrogenic samples. Highly weathered samples were interpreted as having a high residence time in an aqueous environment. Highly biodegraded samples were interpreted as experiencing more biodegradation, possibly due to a longer residence time in a biologically active environment.

#### ***5.4.9 Characterization of Microbial Ecology***

Laboratory work to characterize microbial ecology was performed by Maria Irianni-Renno, and the work performed followed methods from Irianni Renno (2013), as described below.

The samples collected for microbial characterization were stored at -20 °C until they were processed for DNA extraction. In preparation for DNA extraction, the samples were pretreated to remove hydrocarbons and other compounds such as humic substances that were shown to affect the yield reproducibility of the DNA extraction procedure; a washing pretreatment step was adapted from a previously published method (Whitby & Lund, 2009). In detail, 5 g of material were placed in 15-mL centrifuge tubes. Next, 80 ng of dehydrated skimmed milk (VWR) and 10 µg of polydeoxinocinic-deoxycytidilic-acid (pdIdC) (Sigma-Aldrich) were added to each sample, and the mixtures were vortexed with a Gennie-II vortex (Mo Bio) for one minute. The samples were then washed three times. For the first wash step, 10 mL of DNA-free, sterile, DI water was added to the mixture followed by the addition of: 500 µl of 50 mM tris-HCl (pH=8.3)(Sigma-Aldrich), 400 µl of 200 mM NaCl (VWR), 100 µL of 5 mM Na<sub>2</sub>EDTA (Sigma-Aldrich) and 5 µL of Triton X-100 (5% V/V)(Sigma-Aldrich). The sample solutions were vortexed vigorously for 3 minutes and centrifuged at 13,000 rpm in a Sorval Legend XTR™ centrifuge (Thermoscientific) for 5 minutes to pellet materials and biomass, and the supernatant was discarded. For the second wash step, 10 mL of DNA-free water were added followed by the addition of: 500 µl of 50 mM tris-HCl (pH=8.3), 400 µL of 200 mM NaCl, and 100 µL of 5 mM Na<sub>2</sub>EDTA. The sample solution again was vortexed and centrifuged, and the supernatant was discarded. A final washing solution containing 10 mL of DNA-free water, 500 µL of 50 mM tris-HCl (pH=8.3) and 100 µl of 5 mM Na<sub>2</sub>EDTA was added to the sample solution prior to vortexing, centrifuging the sample, and discarding the supernatant for a final time.

DNA was extracted from the pretreated samples with the Powerlyser™ Powersoil® DNA Isolation Kit (MoBio) according to the manufacturer's instructions with modifications to maximize DNA yield. Approximately 0.5 g of material were used for each extraction, instead of 0.25 g as recommended by the manufacturer. Additionally, duplicate DNA extractions for each sample were pooled and processed with a single Powersoil® spin filter. Finally, the samples were eluted with 50 to 60 µL of elution buffer, instead

of 100  $\mu$ L. DNA concentrations were quantified via optical density at 260 nm with a Gen5<sup>TM</sup> Biotek microplate reader, using a Take 3<sup>TM</sup> microplate (Biotek). DNA was extracted in triplicate from each core subsample. DNA was stored at -20 °C prior to quantitative PCR (qPCR) and pyrosequencing analysis.

Quantitative PCR (qPCR) was performed to quantify the number of 16s gene copies in each sample. Genes were quantified using SYBRgreen<sup>TM</sup> assays (Life technologies, Grand Island, NY) and an ABI 7300 real-time PCR system (Applied Biosystems, Foster City, CA). The 25- $\mu$ L qPCR reaction consisted of Power SYBR green<sup>TM</sup>, forward and reverse primers (2.4  $\mu$ M), magnesium acetate (10 $\mu$ M), PCR grade water, and 1 ng of DNA template. Calibrations were performed using genomic DNA. The detection limit of the qPCR analysis was 100 copies per reaction well. Thermocycling conditions were as follows: 95°C for 10 min, followed by 40 cycles of 95°C for 45 s, 56°C for 30 s, and 60°C for 30 s; fluorescence data was collected at the end of the elongation phase for every cycle. Dissociation curve analysis was conducted to confirm amplicon specificity.

454 pyrosequencing was used to characterize the species of microbes present in the OBB and sediments. DNA samples from the OBB and sediments were taken in May and November of 2014. The microbial community composition of each sample was determined by 454 pyrosequencing of both eubacterial and archaeal 16S rRNA genes. Sample triplicates were pooled and submitted to Research and Testing Laboratory, LLC (Lubbock, TX) for analysis. Primers 939f and 1492r were used for the eubacterial 16s rRNA gene-targeted assay, and primers 341f and 958r were used for the archaeal assay. The sequencing platform used was the Genome Sequencer FLX plus 454<sup>TM</sup> Pyrosequencer (Roche). The data analysis methodology provided by Research and Testing Laboratory can be found in Appendix I.

## 5.5 Results

### 5.5.1 Visual Sheen Observations

Sheen observations made throughout the course of the study are summarized in Figure 42. Sheens were observed on the shoreline during three of 26 observations. No sheens were ever observed sourcing from under the OBB, in the OBB, or in waters above the OBB as tides fell and rose. On August

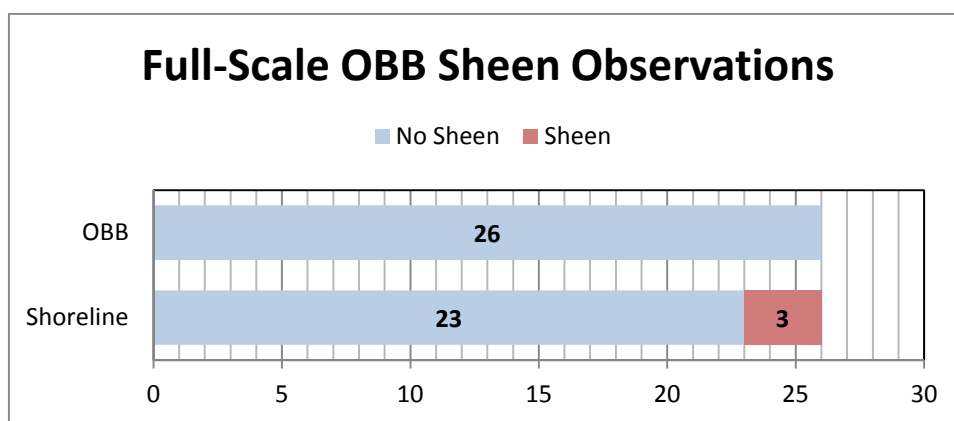


Figure 42: Summary of sheen observations, Dec 2013 to Jan 2015

13, 2014, the second day of the August sampling event, nine sheens were observed on the shoreline. A record of the observation is provided in Appendix J. Four sheens were observed directly south of the OBB and five sheens were observed directly north of the OBB, but no sheens were observed sourcing from the OBB.

### 5.5.2 Temperature

Temperature data collected from November to May are shown in Figure 43. Temperature data collected from May to November are displayed in Figure 44. The optimal temperature range for hydrocarbon degradation kinetics in fresh water is dependent on many factors, but has been generalized as 20-30°C (Das and Chandran, 2010). For the purposes of this discussion, a temperature of 15°C will be used as the benchmark for sufficiently fast degradation.

Temperatures in and under the geocomposite remained below 15°C until mid-May. These lower temperatures could correspond to a period of low degradation rates and accumulation of NAPL. From mid-May to mid-October, temperatures ranged from 15 to 42°C in the reno mattress. Temperatures were not measured under the OBB after May 11 due to failure of the dataloggers. However, based on spring data and preliminary OBB data, temperatures under the geocomposite likely remained between 15 and 28°C through mid-October.

Temperatures directly under the geocomposite fluctuated more during the preliminary study than the full-scale study, suggesting that the reno mattress served as a better insulator during the summer months than the cinderblocks. In terms of maximizing temperature fluctuations and short term temperature increases, as discussed in Section 2.8.3, the reno mattress was suboptimal.

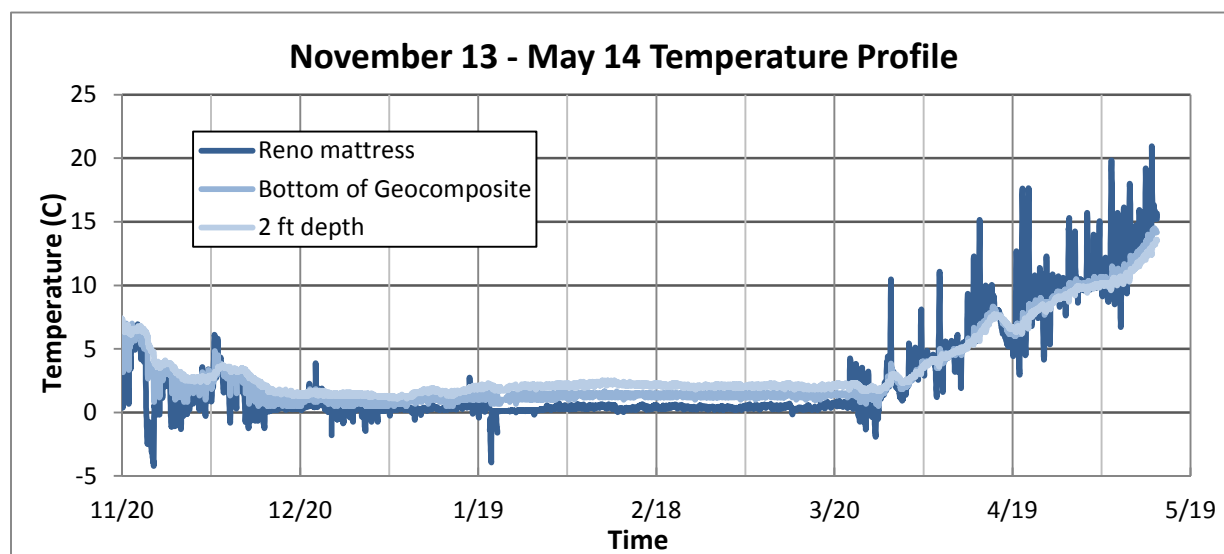


Figure 43: November 2013 – May 2014 temperature profile



Given the dependence of degradation kinetics on temperature, monitoring temperature is vital to understanding an OBB. Slower degradation associated with cooler climates could result in an overall lower NAPL attenuation capacity. Therefore, OBBs in warmer climates may be able to handle larger yearly fluxes than OBBs in cool climates. When considering whether an OBB is an appropriate choice, a site's climate should be considered.

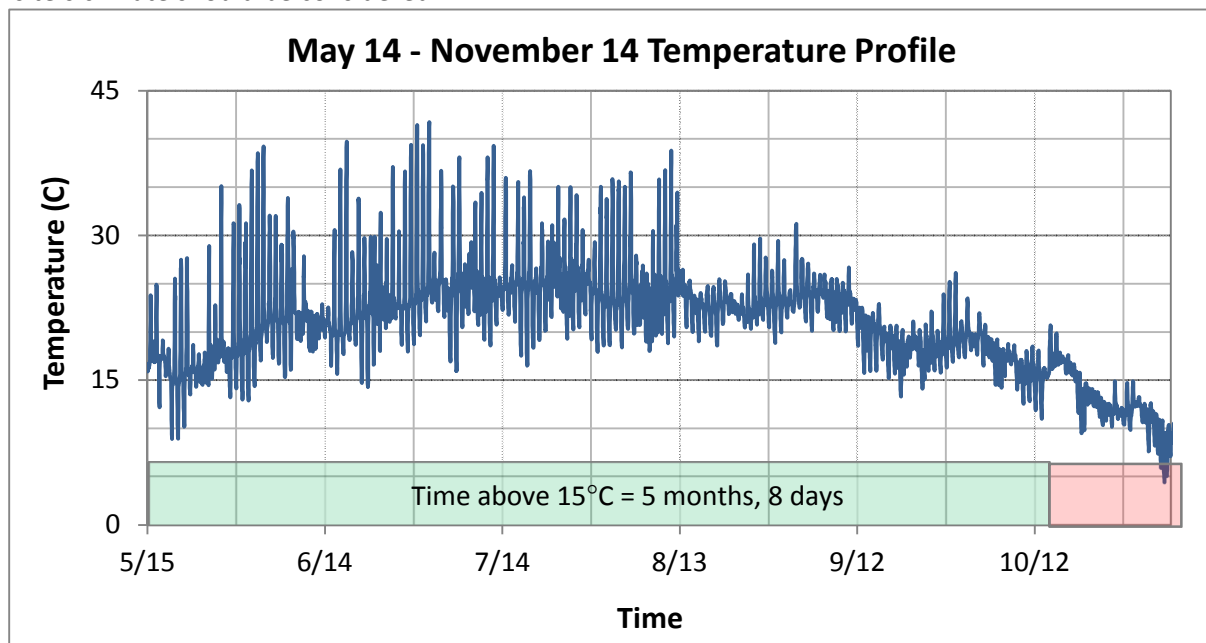


Figure 44: Summer 2014 temperature profile

### 5.5.3 Structural Integrity and Anchoring

A table containing observations and photos from condition inspections is provided in Appendix J. Overall, the reno mattress successfully protected lower layers of the OBB, requiring minimal maintenance. Wire mesh of the reno mattresses was bent up in several places, as shown in Figure 45. No noticeable amount of fill had migrated out of the wire baskets. The OBB did not appear to have shifted and was still effectively anchored to the ground. The lid panels that had become disconnected from baskets were fastened back into place in November 2014, requiring about one person-hour of work to repair.

The monitoring system sustained notable damage. The overall structure of the ports remained in place, and access to underlying sediments was maintained. The basket inserts effectively prevented major debris from entering the ports. The waterproof housings for temperature dataloggers did not retain waterproofness, and although they had lasted from November 2013 to May 2014, all of the EI-1 dataloggers sustained irrecoverable water damage by August 2014.



Figure 45: Reno mattress with bent panel

Temperatures below the geocomposite and in the sediments were not collected, but temperatures within the reno mattress were still collected by the levelloggers for the extent of the study.

Performance of the pushpoint samplers suggests that some of them may have either corroded and cracked, or sampling ports had become disconnected from the samplers. While pumping water from ports D3 and F2 in August, air bubbles came up with water. While this may have been due to a well-drained pocket of coarse sediment emptying during a low tide, the same ports along with others displayed this problem months later, in November. In November, 7 of 17 ports produced only air when pumped. Further investigation prior to sampling in Spring 2015 is required to elucidate the mechanism of failure resulting in ineffective sampling ports.

Collected samples yielded insights into sedimentation processes in the OBB. Many geocomposite samples collected from the ports were coated in a layer of fine sediments up to 2 cm thick, as shown in Figure 46. The deposited sediments appeared to contain organic material such as leaves and/or algae. Particles ranged in size from clay-sized to sand-sized. Fines had also visibly intruded into the geotextile and geonet components of the geocomposite samples within sampling ports. Samples examined in May contained visibly less sediment than those examined in August or November. Ice cover may have prevented sedimentation over the winter months. Geocomposite was also observed for sedimentation



Figure 46: Tops of geocomposite samples displaying different levels of sedimentation: a) E port, May b) E port, November and c) Southwest corner, November

away from the sampling ports. Geocomposite in the southwest corner of the OBB was accessed and sampled as described in Section 5.3.2. The geocomposite collected outside of sampling ports did not display visible layers of accumulated fines or intrusion of fines into the geonet, as shown in Figure 46. Samples collected from sampling ports had an average mass/area 37% higher than the sample collected from the southwest corner. The low sedimentation observed outside of sampling ports suggests that the geotextile and sand filter layers successfully prevent the intrusion of fine sediments into the geocomposite layer. Highly sedimented geocomposite samples from sampling ports suggest that sampling ports cause sedimentation in the summer and fall months.

Table 10: Mass/area of geocomposite samples

Sample	Mass/Area ( $\text{g}/\text{cm}^2$ )
SW	0.91
F	1.37
D	1.32
C	1.07

#### 5.5.4 UV Survey

Of the 19 samples that were surveyed, one fluoresced. In November 2014, geocomposite material from Port B showed a 1.5 cm diameter area of fluorescence, as shown in Figure 47. Forensics hydrocarbon analysis of this sample confirmed the presence of NAPL. The lack of fluorescence in hydrocarbon-containing samples could be due to sediment buildup on the geocomposite material in sampling ports. The fine-grained sediment could have blocked light from reaching the geocomposite material, preventing fluorescence.



Figure 47: Fluorescence observed on November geocomposite sample B

### 5.5.5 Hydrocarbon Quantification

Results for the quantification of hydrocarbons in water, sediment, and geocomposite samples are summarized in Table 11.

No hydrocarbons were detected in any of the water samples collected throughout the study. This result is consistent with the results of the preliminary study. Periodic flushing of river water into the sediments likely caused concentrations to be lower than method detection limits.

Table 11: Full-scale OBB hydrocarbon concentrations

Sample Type	Event	Samples	C (ppm)
Water	May, Aug, Nov	All (A-F, 1-3)	ND
Sediment	May	A	74.7
Sediment	May	B	<10
Sediment	May	E	<10
Sediment	May	C, D, F	ND
Sediment	Nov	C, D, F, SW	ND
Geocomposite	Aug	A, B, E	ND
Geocomposite	Nov	C, D, F	ND

Sediment samples collected in May from ports A, B, and E showed detectable hydrocarbons. The presence of hydrocarbons in these samples led to the selection of ports A, B, and E for DNA analyses and continued hydrocarbon forensics. No hydrocarbons were detected in samples from C, D, and F in May or November.

No hydrocarbons were detected in any of the geocomposite samples analyzed for quantification. A lack of detectable hydrocarbons was corroborated by the UV fluorescence survey. The absence of hydrocarbons on geocomposite samples could be due to the sedimentation observed in sampling ports. With the geotextile layers saturated in fines and covered in a layer of fine sediments, NAPL would not be able to wet the geocomposite.

Geocomposite and sediment samples collected outside of sampling ports also contained no detectable hydrocarbons. These samples were collected from a location adjacent to a small sheen observed just outside the footprint of the OBB. A lack of hydrocarbons in the samples support the theory that the sheen did not source from under the OBB.

### 5.5.6 Hydrocarbon Forensics

Results for the analysis of hydrocarbon forensics fingerprints are presented in Table 12.

Table 12: Results summary of hydrocarbon forensics

Port	Time	Geocomposite			Sediment			Water		
		Petros?	Weathered?	Degraded?	Petros?	Weathered?	Degraded?	Petros?	Weathered?	Degraded?
C	May	no	-	-	no	-	-			
D	May	no	-	-	no	-	-			
F	May	low	high	high	low	med	low			
SW	Nov	no	-	-	no	-	-			
A	May	Med	low	low	low	high	high			
	Aug	low	high	high	low	high	high	low	high	high
	Nov	no	-	-	High	high	high			
B	May	low	low	med	no	-	-	high	low	low
	Aug	low	high	low	med	high	high	med	med	high
	Nov	med	high	high	low	high	high			
E	May	low	high	low	low	high	high	med	med	low
	Aug	low	high	high	low	high	low	low	med	high
	Nov	no	-	-	high	low	med			

The presence of petrogenic AHs in A, B, and E samples in May informed the decision to continue forensics analysis of samples from these ports in future sampling events. Quantitative hydrocarbon analysis confirmed the presence of hydrocarbons in ports A, B, and E.

Water samples were interpreted separately from geocomposite and hydrocarbon results. Since porewater was shown to fill and drain from sediments on a daily basis, the water sampled at a given time is not necessarily representative of a specific depth or location. However, trends in water hydrocarbon composition can be interpreted on a seasonal level. Samples B and E showed similar trends through time. In May, samples contained high levels of petrogenic compounds that were not degraded. In August, B and E samples showed decreases in AB and NAPH. An enrichment of the higher-homolog AHs supports the theory that decreases in AB and NAPH could be due to biological degradation. The correlation of this trend with temperature profiles also supports the theory of seasonal microbial degradation dynamics. The May samples were collected at the end of the cold winter. Low temperatures may have inhibited degradation, causing porewater concentrations to

increase. August samples collected after a warm summer displayed lower concentrations of dissolved AHs, enriched in higher-homologs. Water hydrocarbon forensics analysis supports the theory that microbial degradation kinetics is seasonally influenced.

Sediment and geocomposite samples were interpreted as related, and were analyzed for patterns through time. Due to the highly spatially variable nature of NAPL fluxes observed at the Site, each port was analyzed individually. Samples with low amounts of highly degraded and weathered AHs were considered background for the contaminated ports, given that with a long enough residence time, NAPLs would become depleted by weathering and degradation processes.

Geocomposite in port A contained unweathered, non-degraded NAPL in May. The presence of soluble compounds suggests that the NAPL did not have time to dissolve into the water, and may have been transported quickly. Low degradation could be due to low residence time or transport to the surface during a microbially inactive winter season. Sediment samples contained low amounts of highly weathered and degraded hydrocarbons until winter, when a new flux of NAPL was detected. The difference in levels of petrogenics between sediment and geocomposite samples may be caused by a lag in arrival. NAPL that moved through the sediment over the winter sorbed to the geocomposite in May. Similarly, NAPL arriving in November had not yet reached the geocomposite.

May geocomposite from port B was characterized by a similar pattern of unweathered NAPL experiencing limited degradation. The presence of this “fresh” NAPL after the winter season may be an indicator of seasonally influenced degradation processes. The geocomposite NAPL subsequently shows a degraded signal in August. August sediment samples showed weathered, degraded NAPL, which in turn shows up on the geocomposite in November, following the pattern of a delayed arrival.

Geocomposite from port E showed a small amount of undegraded NAPL in May, followed by degraded NAPL in August, and no NAPL in November. Sediment from E showed a highly petrogenic

fingerprint with unweathered, undegraded NAPL characteristic of freshly transported NAPL. The appearance of NAPL in November A and E sediment samples may be an artifact of the sampling method. As described in Section 5.3.1, the collection of sediment samples led to the creation of a cavity beneath sampling ports and subsequent sampling of deeper and deeper sediment material. In addition, the heavy sedimentation seen on the November E sample (Figure 46b) may have prevented the geocomposite from sorbing NAPL in November.

Overall, geocomposite samples from all three ports showed increasing levels of high-homolog enrichment consistent with biological degradation. Furthermore, NAPL in these samples also displayed increasing levels of weathering consistent with the long residence time expected of retained NAPL. NAPL appearing on the geocomposite in May is consistent with the seasonally limited degradation observed in water samples.

#### 5.5.7 Pressure Data

A selection of river stage (USGS, 2014) and BaroLogger pressures at the 3 foot depth are shown in Figure 48. Data for the week of June 12, 2014 demonstrates a pattern seen throughout the year. When low tides receded below mean sea level, sediments 3 feet below the OBB were exposed to atmospheric pressures. The fluctuation between atmospheric pressure and high tide levels demonstrates water

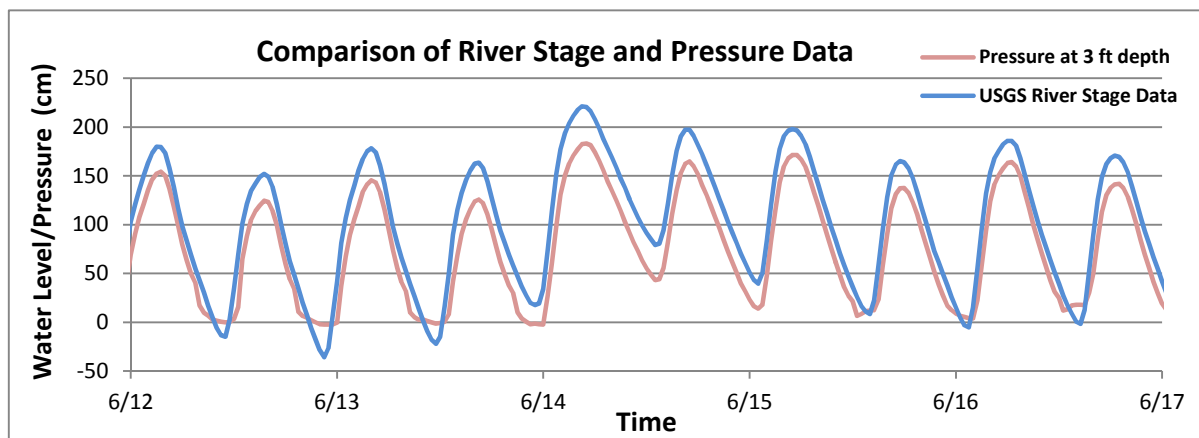


Figure 48: June 2014 river stage and pore pressure fluctuations

levels rising and falling in the sediments. These tidal fluctuations pump atmospheric air and oxygenated river water in and out of the sediments twice daily.

Moderate precipitation in the river's watershed occurred on June 13 (CBS6albany.com, 2014), leading to runoff that elevated river levels above mean sea level on June 14, preventing sediments from draining. This pattern was typical of spring data. After the influence of spring precipitation had receded, sediments drained daily. From July 5 through the November sampling event, sediments at 3' depth reached atmospheric pressure on every tidal cycle.

#### **5.5.8 Water Quality**

Water quality data presented in this section include depth-discrete porewater ORP, pH and ion concentrations for three sampling events.

ORP and pH data are presented in Figure 49. Although ORP data were spatially variable, all values reported are considered aerobic for the pH range measured (6.56 – 7.99). Average ORP decreased from 255 to 191 mV (SHE) between May and August. This decrease may have been caused by an increase in the oxygen demand of the microbial community as temperatures rose. The decrease in ORP correlates to the hydrocarbon degradation observed in geocomposite, sediment, and water samples.



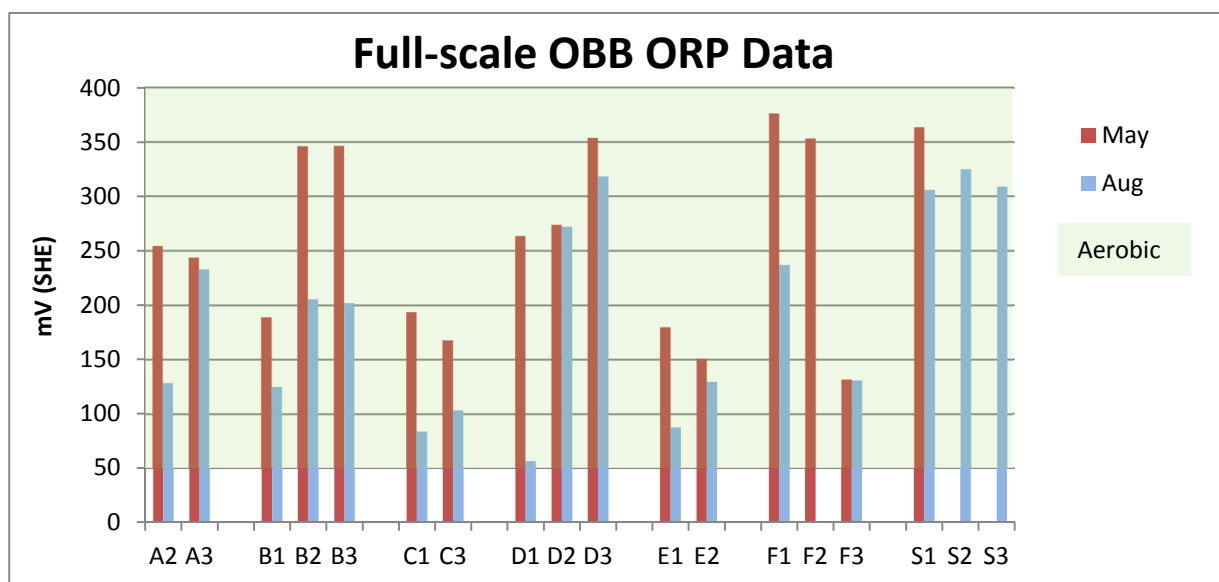


Figure 49: ORP data for each sampling port. Readings are labeled by port and depth in feet.

Iron, Sulfate, and Manganese data from May, August, and November are shown in Figure 51 and Figure 50. The data showed that sulfate, iron, and manganese are present as electron acceptors in the sediments, with sulfate in the highest concentrations. Figure 51 shows that sulfate concentrations decrease with depth, but increase with time. Figure 50 shows that metals concentrations generally increase with depth, but peak at 2ft depth. The opposing gradients suggest that sulfate originates from the river, while the metals originate from the subsurface. Although May and August display similar concentration versus depth trends, concentration magnitudes changed. Sulfate concentrations increased while metal concentrations decreased. Again, opposing trends suggest different sources. Heavy rainfall, causing high river stages and fast-flowing water prior to the August sampling event, may have caused increased porewater-surface water mixing. Increased sediment sulfate concentrations can also be explained by increased mixing. Metal concentrations may have decreased due to dilution from increased mixing. High water stage may have suppressed groundwater flow via a reduced hydraulic gradient toward the river.

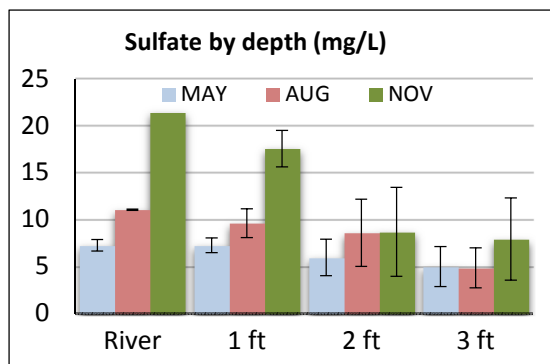


Figure 51: Sulfate mean values and standard errors

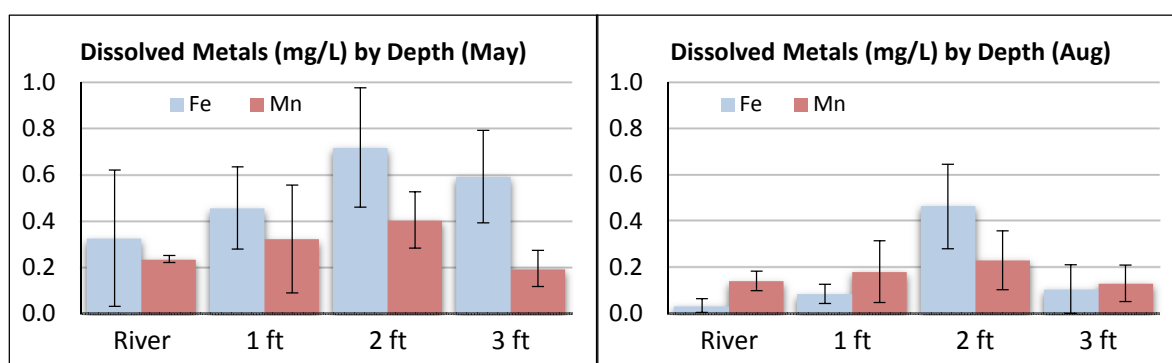


Figure 50: Dissolved metals mean values and standard errors

### 5.5.9 Microbial Characterization

qPCR data quantifying bacteria and archaea gene counts is summarized in Figure 52. Results of 454 pyrosequencing analysis used to characterize microbial diversity in and around the OBB are shown in Figure 53 and Figure 54.

Similar quantities of microbial genes were found on the geocomposite and surrounding sediments. All bacterial gene count averages with  $n \geq 3$  were within one order of magnitude of each other. All archaeal gene counts with  $n \geq 3$  were also within one order of magnitude of each other. These data support the theory that a geocomposite can be used as a microbial substrate in the design of an OBB.

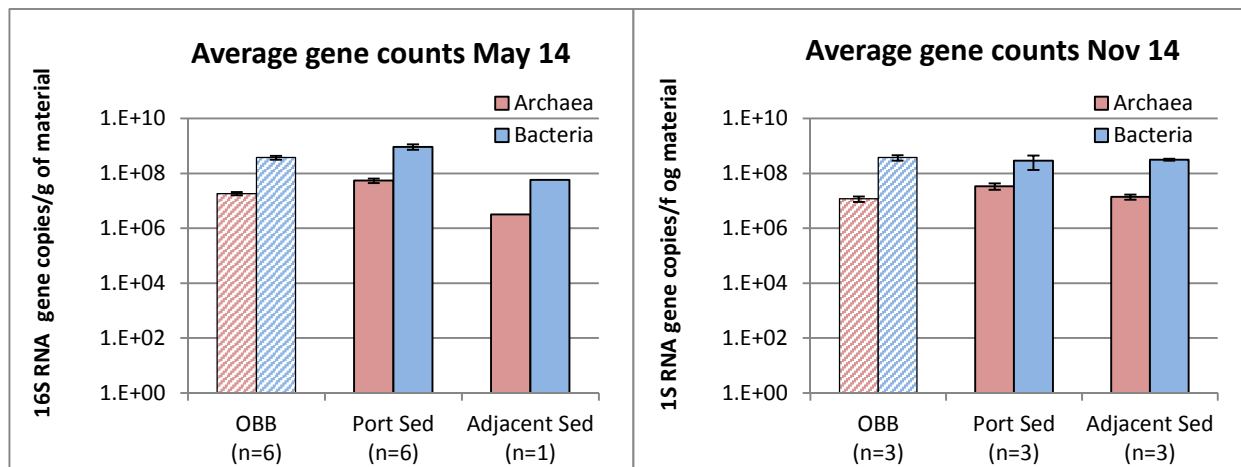


Figure 52: Summary of average bacteria and archaea gene counts and standard errors

454 pyrosequencing of DNA was used to characterize the diversity of the microbial community found in and around the OBB. An average of 41% of the bacterial and 55% of the archaeal DNA could be identified. Relative amounts of genes from identified genera are displayed in Figure 53 and Figure 54. Table 13 lists the microbes found in order of frequency and provides a description of each. Raw data from 454 pyrosequencing are provided in Appendix J. The data show that a diverse set of microbes lives in the system. Microbial communities on the geocomposite were comprised of a similar set of species to that of surrounding sediments. The similarity between communities shows that the geocomposite is a suitable substrate for naturally occurring microbes to grow on. The microbial community contained aerobic, anaerobic, and facultative microbes, showing that oxygen is present in the OBB. The presence of anaerobic, methanogenic archaea suggests that conditions in the system are heterogeneous, containing anaerobic pockets. The presence of methanotrophic bacteria suggests that methane is present in the system. Increasingly reduced conditions with depth, shown by ORP and ion data, support the conceptual model that methane is being produced in anaerobic sediments below the OBB. Methane produced below the OBB can then transport to the surface, giving rise to the methane oxidizers seen in and around the OBB. Historical observations of ebullition originating from the lower, fine sediment layer are consistent with the theory of methane gas transport to the surface.

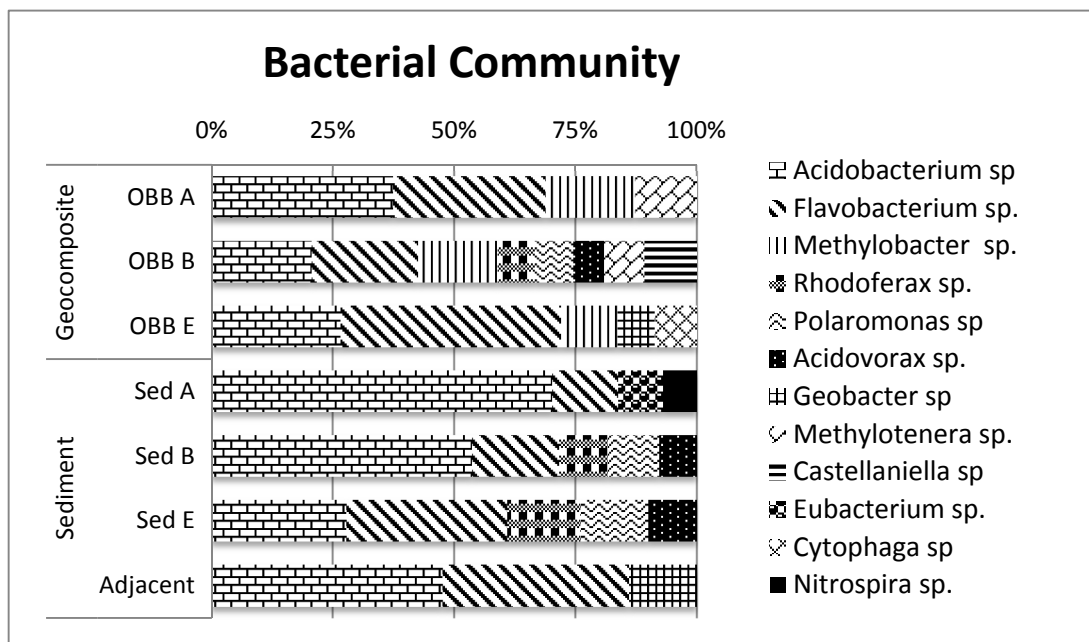


Figure 53: Composition of identified bacterial community for each sample taken in May 2014

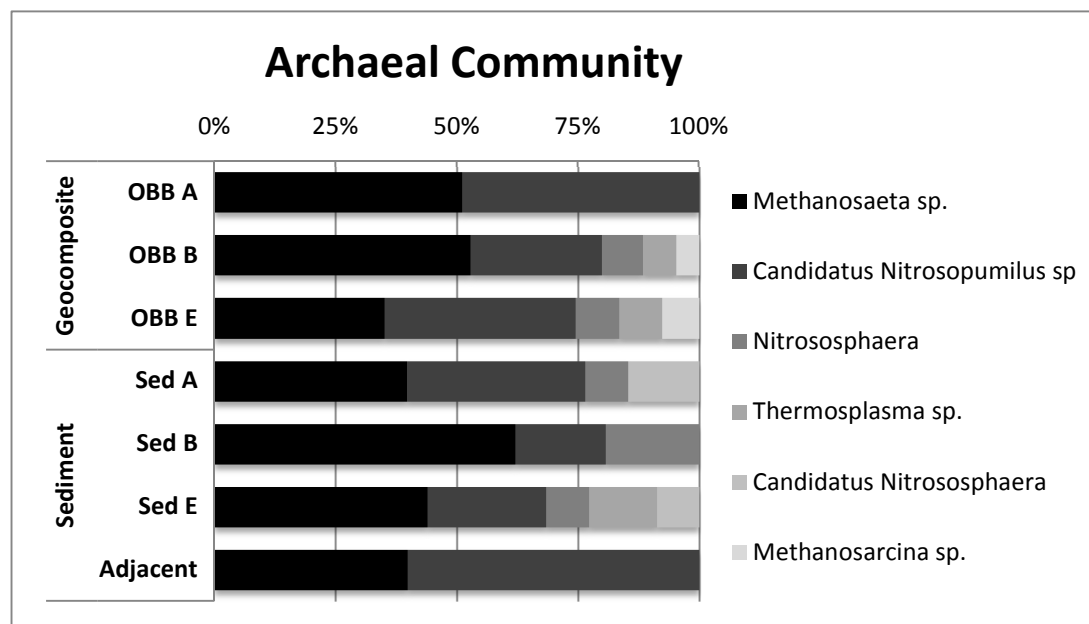


Figure 54: Composition of identified archaeal community for each sample taken in May 2014

Table 13: Descriptions of microbes found in site samples

	Associated with hydrocarbon degradaton?	Description
<b>Bacteria</b>		
<i>Acidobacterium sp</i>	<i>Some. Benzene</i>	Found in soils. Facultative Fe reducer. (Coates, 1999), (Xie, Sun and Luo, 2010)
<i>Flavobacterium sp.</i>	<i>Yes. PAHs</i>	(Okpokwasili et al., 1984)
<i>Methylobacter sp.</i>	<i>Methane Oxidizer</i>	Aerobic methane oxidizer. (Bowman et al., 1993)
<i>Rhodoferrax sp.</i>	<i>Some. Alkylbenzenes</i>	Facultative anaerobe Fe reducer. (Prince, Gramain and McGenity, 2010)
<i>Polaromonas sp</i>	<i>Yes. BTEX, PAHs</i>	Benzene degrader cont. soils (Xie, sun, luo 2010)
<i>Acidovorax sp.</i>	<i>Yes. Benzene, PAHs</i>	Aerobic. (Meyer et al., 1999) (Fahey et al., 2009), (Svenja et al., 1999)
<i>Geobacter sp</i>	<i>Yes. Monoaromatics</i>	Anaerobic Fe reducer. (Chakraborty and Coates, 2004) (Zhang, et al., 2013)
<i>Methylothermus sp.</i>	<i>Methane Oxidizer</i>	Aerobic methane oxidizer. (Kalyuzhnaya et al., 2006)
<i>Castellaniella sp</i>	No	Facultatively anaerobic, denitrifier. (Liu et al., 2008)
<i>Eubacterium sp.</i>	No	Anaerobic. Found on human tissues. (Moore, Cato and Holdeman, 1969)
<i>Cytophaga sp</i>	Some	Primarily aerobic, some facultative. (Reichenbach, 2006)
<i>Nitrospira sp.</i>	No	Nitrite Oxidizer common in wwtp and labs. (Hovanec, et al., 1998)
<b>Archaea</b>		
<i>Methanosaeta sp.</i>	<i>Yes. PAHs</i>	Methanogenic. (Berdugo-Clavijo et al., 2012)
<i>Candidatus Nitrosopumilus sp</i>	No	Aerobic Ammonia oxidizer. (Naoki et al., 2011)
<i>Nitrososphaera</i>	No	Aerobic Ammonia oxidizer found in soils. (Tournay, 2011)
<i>Thermoplasma sp.</i>	No	Facultative anaerobe. Acidophile, thermophile. (Darland et al., 1970)
<i>Candidatus Nitrososphaera</i>	No	Aerobic, thermophilic ammonia oxidizer. (Hatzenpichler et al., 2008)
<i>Methanosarcina sp.</i>	<i>Yes. PAHs</i>	Methanogenic. (Wook, Um and Holoman, 2006)

Microbes associated with hydrocarbon degradation are among the most common in both media. Both the geocomposite and underlying sediments contained more genera associated with hydrocarbon degradation than did adjacent sediments. The geocomposite contained seven genera associated with hydrocarbon degradation. Underlying sediments contained five genera associated with hydrocarbon degradation. Adjacent sediments contained only two genera associated with hydrocarbon degradation. The only genera not found in geocomposite samples were nitrate and ammonia oxidizers not associated with hydrocarbon degradation. Since microbial diversity has been positively correlated to hydrocarbon degradation efficiency (Dell'Anno, 2012), more efficient degradation may be occurring in the OBB.

DNA data showed that the installation of an OBB did not negatively impact the amount or diversity of microbes found in native sediments. Geocomposite samples from the OBB showed the highest diversity of hydrocarbon degraders and microbes in quantities similar to those of surrounding sediments. These data show that an OBB constructed with an oleophilic geocomposite has the capacity to enhance hydrocarbon degradation by enhancing the diversity of the microbial community.

## 6 Construction Cost Estimate for a Full-Scale OBB

A basic analysis of construction costs allow OBBs to be compared to current sheen solutions on a cost basis. OBB construction costs are estimated in this section based on similar, commonly executed projects.

Costs from the full-scale demonstration are not included, as they do not accurately capture the costs associated with OBB construction. Extenuating factors led costs to be higher than anticipated. Work in a tidal zone, delays in materials procurement, and limited shoreline access incurred additional costs not representative of standard conditions. In addition, mobilization costs were disproportionately high because only a single module was constructed.

OBB construction costs were estimated based on sediment cap construction costs. Sediment caps were used as a basis because of their similarity to OBBs in design and construction methods. Much research has been done on sediment caps, the design and construction of which are well understood (Palermo, 1998; US EPA, 2013). Cap designs often consist of layers of geotextile and sand, topped with a layer of armoring stone. As such, cap construction costs should be an accurate proxy for OBB construction costs. The main difference between these designs is that OBBs consist of less material and thinner layers to promote oxygen diffusion into contaminated sediments. Because thinner layers require less construction effort and material costs, sediment cap costs serve as a conservative cost estimate of OBB costs. The following cost estimates have been made for sediment caps similar to an OBB:

Sand/Armor caps – \$100,000-400,000/acre (Mohan et al., 2011)

Sand/Geocomposite caps – \$94,863-179,563/acre (NJDEP, 2014)

Sand/Sediment cap – \$179,080/acre (Reible, 2004)

For comparison, an estimate of sheet pile costs is provided. Using estimates based on the North American Steel Sheet Piling Association’s 2009 report titled “Comparison of Retaining Wall Design and Cost Study: Sheet Pile vs. Various Walls,” the online tool isheetpile.com estimates various barrier construction costs (NASSPA, 2009; isheetpile.com, 2015). For a 21 ft tall, 1000 ft long sheet pile barrier, the cost estimate totals \$1,001,490. An OBB of width 40 ft (double that of the full-scale OBB module) and length 1000 ft has an area of 0.92 acres, and corresponding cost of roughly \$100,000.

Construction costs for an organoclay barrier could be estimated similarly to sediment cap and OBB costs. Organoclay barriers are built similarly to sediment caps. The only additional cost would be the cost of the organoclay material, at \$2.50 per ft<sup>2</sup> (EPA, 2013). For 0.92 acres, the material cost of organoclay comes out to \$100,188. Adding the cost of organoclay to the \$100,000 in construction costs, the total is roughly \$200,000.

Table 14 provides a cost comparison of three equivalent sheen remedies. As shown in the table, the cost of an OBB is an order of magnitude lower than a sheet pile wall and half as expensive as an organoclay cap.

**Table 14: Sheen Remedy Cost Comparison**

<b>Remedy</b>	<b>Length (ft)</b>	<b>width (ft)</b>	<b>height (ft)</b>	<b>Total Cost (\$)</b>
OBB	1000	40		<b>\$100,000</b>
Organoclay	1000	40		<b>\$200,000</b>
Sheet Pile	1000		21	<b>\$1,001,490</b>



## **7 Conclusions and Recommendations**

### **7.1 Basic Concepts and Approach**

Petroleum production, transmission, refining and storage facilities are commonly located adjacent to surface water bodies. Accidental releases of petroleum at these facilities often result in the migration of NAPLs through subsurface media to groundwater-surface water interfaces. Active attenuation of NAPLs, via aerobic and anaerobic processes, plays an important role in limiting discharge of NAPLs to surface water. When attenuation processes at GSIs are insufficient, petroleum sheens are commonly observed in surface water. The occurrence of sheens can result in Clean Water Act violations.

Sheen remedies need to address releases via seeps, ebullition, and shoreline erosion. Common remedies are predicated on physical barriers and/or sequestration of NAPL by sorbent materials. Disadvantages of physical barriers include NAPL bypass associated with modified flow paths and finite storage capacities. Furthermore, construction and maintenance of physical barriers can be costly and detrimental to sensitive environments. Sorbent materials also have a finite storage capacity and can be short-circuited by NAPL flow. Both methods can inhibit natural biological degradation of NAPL by creating anaerobic zones where degradation is limited. The shortcomings of these methods motivated the investigation of an inexpensive, more sustainable solution, referred to as an OBB.

The concept of an OBB is that of a permeable reactive barrier installed at a GSI, which 1) employs an oleophilic geocomposite to sorb and store NAPL, 2) enhances biological degradation via delivery of oxygen and increased retention time, and 3) employs structural cover to limit erosion. OBBs are different from current remedies because their active NAPL depletion via biological degradation can delay or prevent failure associated with exceedance of finite capacities. Furthermore, OBBs appear to be a more affordable

option and more compatible with broader environmental goals. Key limitations to an OBB include an inability to address large NAPL fluxes and limited field applications to date.

Work described in this thesis includes proof-of-concept laboratory studies followed by a preliminary field study and large-scale field demonstration. The primary conclusion is that OBBs are a viable technology. This conclusion is supported by ongoing consideration of expanding the large-scale OBB and active consideration of an OBB remedy at other sites. Additionally, a full US patent application on the OBB was submitted in September 2014 (Zimbron et al., 2014).

## **7.2 Laboratory Studies**

Laboratory studies investigated the geocomposite's 1) NAPL sorption capacity, 2) sheen prevention potential, and 3) aqueous hydrocarbon sorption. Tests showed that the geocomposite was able to retain between 2.4 to 3.3 L of NAPL per m<sup>2</sup>. With this capacity, one square meter of geocomposite could theoretically store thousands of sheens worth of NAPL. Sand tank experiments simulating subsurface releases showed that the geocomposite had the ability to delay sheen formation under constant loading. Installing a layer of sand on top of the geocomposite more than doubled the geocomposite's NAPL capacity and ability to delay sheen formation. The geocomposite was also shown to sorb dissolved phase hydrocarbons, reducing concentrations by up to 77%. Consistent performance in a variety of lab tests provided proof-of-concept that the geocomposite could prevent sheens by sorbing and retaining hydrocarbons.

## **7.3 Preliminary Field Study**

The preliminary field study investigated 1) sheen prevention via NAPL sorption to the geocomposite 2) environmental conditions in the OBB relevant to biological degradation, and 3) OBB design and

performance monitoring methods. Four 1 m<sup>2</sup> OBBs were deployed and evaluated from March to August of 2013.

Over 13 sheen observations, zero sheens were observed sourcing from the OBBs. UV fluorescence confirmed that NAPL had sorbed to 20% and 35% of the surfaces of two OBBs. Analytical chemistry confirmed that samples of the geocomposite showed saturations of up to 1.6 L of NAPL per m<sup>2</sup> geocomposite, well within the lab-measured capacities.

All water collected from OBB sampling ports was aerobic, with redox potentials ranging from 302 to 423 mV. Sulfate was also present as an electron acceptor in the OBB sampling ports, with average concentrations of 11.3 mg/L and 14.5 mg/L in April and August respectively. 9.0 mg/L of iron was found at a depth of 90 cm. Dissolved iron and a redox potential of 62 mV are indicative of anaerobic conditions at 90cm depth. Aerobic conditions and abundant sulfate suggest that the surface is better suited for biodegradation than sediments at 90cm depth. Temperatures in the OBB were 4.1°C warmer than sediments at 45cm depth on average during the warmest 15 day period.

The preliminary study also yielded insights into the design of the OBB system. The geocomposite material appeared to be chemically compatible with petroleum NAPL, showing no signs of deterioration. Visual observations showed that cinderblock anchoring was sufficient to protect and anchor the OBB during the summer. Damage to a monitoring system post showed that a more robust monitoring system design would be required for semi-permanent monitoring. The UV fluorescence survey allowed for the location of hydrocarbons sorbed to the geocomposite. However, UV inspection of a full-scale OBB would prove challenging, necessitating the design of removable geocomposite subsamples.

## 7.4 Full-Scale Field Demonstration

The overarching objective of the full-scale field demonstration was to resolve performance and cost of an OBB over a one-year period starting November of 2013. The full-scale OBB has a 36 ft x 18 ft footprint, Reno mattress armoring, sand and geotextile layers for sedimentation control, and integrated sampling ports to facilitate access to geocomposite and underlying sediments. Specific objectives included 1) documentation of sheen prevention via NAPL sorption to the geocomposite, 2) investigation of biological degradation of sorbed NAPL, 3) evaluation of environmental conditions relevant to biodegradation, and 4) evaluation of structural cover efficacy.

Visual inspections showed that while sheens were observed 3 out of 26 times along the adjacent shoreline, no sheens were observed sourcing from the OBB footprint. UV inspection yielded the observation of NAPL wetting the geocomposite material. The presence of NAPL on the geocomposite was confirmed by analytical hydrocarbon analysis.

Seasonal changes in composition of hydrocarbons on the OBB showed that NAPL sorbed to the geocomposite likely degraded biologically and decreased in abundance. In addition, the OBB was shown to host a microbial community of similar abundance to and greater diversity than adjacent and underlying sediments. Aerobic, facultative, and anaerobic hydrocarbon-degrading microbes were found in the OBB and adjacent and underlying sediments. While seven genera of hydrocarbon-degrading microbes were found in the geocomposite, only five were found in underlying sediments, and three in adjacent sediments.

Tidal cycles were shown to pump aerobic water and atmospheric air into and out of sediments under the OBB twice daily. Redox potentials in porewater decreased as hydrocarbons were degraded, but remained aerobic throughout the study. Additionally, sulfate and iron were present as electron acceptors in river water and underlying sediments.

Biweekly visual inspections showed that the reno mattress prevented erosion-based sheen release. The reno mattress sustained minimal damage, requiring only one person-hour of maintenance over a one-year period. The geotextile and sand layers prevented fine-grained sediment from intruding into the OBB. The monitoring system could benefit from the modifications outlined in Section 7.6 .

## **7.5 Construction Cost Estimate**

Full-scale OBB construction costs were estimated based on sediment cap construction costs. The similarity in layered design, construction materials and working environment make sediment caps an appropriate comparison. Three recent sediment cap cost analyses placed the lower limit of construction costs at \$100,000 per acre. Costs of equivalent organoclay and sheet pile barriers were estimated to be \$200,000 and \$1,000,000 respectively, making an OBB the least costly.

## **7.6 Recommendations for Future Work**

Recommendations for future work include OBB design modifications for improved sediment control, improved environmental integration and enhanced NAPL capacity. Simplified performance monitoring, research on governing processes, methods for characterizing sheen sources, and the development of a model to support optimization of OBB design are also recommended.

Although the sand and geotextile prevented sedimentation, additional measures could be taken to ensure sediment control. Geotextile should be wrapped around the edges of the geocomposite, protecting edges from sediment intrusion. Excess geotextile along the edge of the geocomposite could be folded under the geocomposite upon installation, or additional geotextile could be wrapped around the edges of the geocomposite to achieve a similar effect.

Further integration of the OBB into native sediments could reduce visual impacts. The key designed to integrate reno mattress edges into native sediments is recommended for future designs. Integration

could be improved by matching reno mattress fill to the color of native sediments. In some applications, the wire baskets of a reno mattress could be foregone, simply using a layer of stone to armor the OBB. Burial of the OBB is not advised, as oxygen delivery, redox potential and degradation rates could be reduced.

The choice and configuration of oleophilic materials could be optimized to enhance NAPL capacity. One natural idea would be to enhance the OBB's capacity by installing multiple layers of oleophilic material. Sites also containing non-petroleum NAPLS may benefit from the addition of other sorptive materials. Other oleophilic materials could be researched to find the best balance of permeability, capacity, and cost-effectiveness.

OBB performance monitoring could benefit from more robust equipment and simpler monitoring methods. Better waterproofing is required of temperature dataloggers. To the author's knowledge, no thermocouple dataloggers with the necessary IP68 waterproofing rating (long-term, complete submersion) are commercially available. Custom waterproofing or non-thermocouple dataloggers could allow for temperature logging in intertidal sediments. Although the condition and potential failure mechanism of the porewater samplers used in the full-scale study has yet to be resolved, more robust porewater samplers are recommended for future OBB monitoring. Fluoropolymer-lined polymer samplers would allow for long-term deployment without the risk of interaction with contaminants or corrosion. Alternatively, installation and removal of standard stainless steel porewater samplers during each sampling event may also meet data collection objectives if pore pressure logging is not deemed necessary. Sampling ports constructed in the full-scale study were shown to induce sedimentation, possibly affecting geocomposite sorption. Sampling ports are not recommended for future OBB studies. Alternatively, simply removing and replacing cover materials during each sampling event could allow for

more representative geocomposite sampling while avoiding sedimentation. This approach would also resolve the limited sediment available for sampling, as discussed in Section 5.3.1.

OBB performance could be improved through further research on governing OBB processes. Although the oleophilic properties of the geocomposite were well established in lab and field experiments, the ability of an OBB to prevent ebullition-caused sheens has not been explicitly demonstrated. Preliminary work is currently underway to document ebullition-sheen prevention via sorption to the geocomposite, though further work may be required. Rates of NAPL degradation are perhaps the most important factor governing an OBB's long-term success. Lab or field studies resolving NAPL degradation kinetics and completeness are recommended. Bioavailability of sorbed contaminants is a prerequisite for microbial degradation, and factors controlling bioavailability should be researched.

Site characterization is critical to the design of any sheen remedy. Spatial distribution of sheening could be resolved by temporarily installing a sorbent geotextile or polymer sheeting followed by subsequent UV inspection of the sorbent. Tools for quantifying NAPL flux rates at GSIs should be developed, as they could be of great use in determining whether an OBB is an appropriate remedy for a given site.

Once NAPL fluxes at GSIs and OBB NAPL loss rates have been resolved, a 2-D model based on the mass-balance presented in Section 2.4 may prove useful for site managers considering OBBs. Modeling of spatially, temporally and volumetrically variable sheen loading as well as time and temperature-dependent biological degradation could allow for site-specific models, providing tailored analyses.

## 8 References

- Aburto, A., Fahy, A., Coulon, F., Lethbridge, G., Timmis, K. N., Ball, A. S., & McGenity, T. J. (2009). Mixed aerobic and anaerobic microbial communities in benzene-contaminated groundwater. *Journal of applied microbiology*, 106(1), 317-328.
- Adler, J. H. (2002). Fables of the Cuyahoga: Reconstructing a history of environmental protection. *Fordham Envtl. LJ*, 14, 89.
- Ahmad, F., Schnitker, S. P., & Newell, C. J. (2007). Remediation of RDX-and HMX-contaminated groundwater using organic mulch permeable reactive barriers. *Journal of contaminant hydrology*, 90(1), 1-20.
- American Oil & Gas Historical Society. (2014, August 24). First American Oil Well. Retrieved December 28, 2014, from <http://aoghs.org/oil-amanac/american-oil-history>
- Amos, R. T., & Mayer, K. U. (2006). Investigating ebullition in a sand column using dissolved gas analysis and reactive transport modeling. *Environmental science & technology*, 40(17), 5361-5367.
- Atlas, R. M., & Bartha, R. (1972). Biodegradation of petroleum in seawater at low temperatures. *Canadian Journal of Microbiology*, 18(12), 1851-1855.
- Atlas, R. M., & Bartha, R. (1992). Hydrocarbon biodegradation and oil spill bioremediation. In *Advances in microbial ecology* (pp. 287-338). Springer US.
- Berdugo-Clavijo, C., Dong, X., Soh, J., Sensen, C. W., & Gieg, L. M. (2012). Methanogenic biodegradation of two-ringed polycyclic aromatic hydrocarbons. *FEMS microbiology ecology*, 81(1), 124-133.



- Bonten, L. T., Grotenbuis, T. C., & Rulkens, W. H. (1999). Enhancement of PAH biodegradation in soil by physicochemical pretreatment. *Chemosphere*, 38(15), 3627-3636.
- BOWMAN, J. P., SLY, L. I., NICHOLS, P. D., & Hayward, A. C. (1993). Revised taxonomy of the methanotrophs: description of *Methylobacter* gen. nov., emendation of *Methylococcus*, validation of *Methylosinus* and *Methylocystis* species, and a proposal that the family *Methylococcaceae* includes only the group I methanotrophs. *International Journal of Systematic Bacteriology*, 43(4), 735-753.
- Chakraborty, R., & Coates, J. D. (2004). Anaerobic degradation of monoaromatic hydrocarbons. *Applied Microbiology and Biotechnology*, 64(4), 437-446.
- Chang, W., Um, Y., & Holoman, T. R. P. (2006). Polycyclic aromatic hydrocarbon (PAH) degradation coupled to methanogenesis. *Biotechnology letters*, 28(6), 425-430.
- Chang, W., Whyte, L., & Ghoshal, S. (2011). Comparison of the effects of variable site temperatures and constant incubation temperatures on the biodegradation of petroleum hydrocarbons in pilot-scale experiments with field-aged contaminated soils from a cold regions site. *Chemosphere*, 82(6), 872-878.
- Chapman, S. W., Parker, B. L., Sale, T. C., & Doner, L. A. (2012). Testing high resolution numerical models for analysis of contaminant storage and release from low permeability zones. *Journal of contaminant hydrology*, 136, 106-116.
- Choi, Y., Cho, Y. M., & Luthy, R. G. (2013). Polyethylene–water partitioning coefficients for parent-and alkylated-polycyclic aromatic hydrocarbons and polychlorinated biphenyls. *Environmental science & technology*, 47(13), 6943-6950.

Clean Water Act of 1972, 33 U.S.C. § 1251 et seq. (2002). Retrieved from

<http://epw.senate.gov/water.pdf>

Coates, J. D., Anderson, R. T., & Lovley, D. R. (1996). Oxidation of polycyclic aromatic hydrocarbons under sulfate-reducing conditions. *Applied and Environmental Microbiology*, 62(3), 1099-1101.

Conant Jr, B., Cherry, J. A., & Gillham, R. W. (2004). A PCE groundwater plume discharging to a river: influence of the streambed and near-river zone on contaminant distributions. *Journal of Contaminant Hydrology*, 73(1), 249-279.

Darland, G., Brock, T. D., Samsonoff, W., & Conti, S. F. (1970). A thermophilic, acidophilic mycoplasma isolated from a coal refuse pile. *Science*, 170(3965), 1416-1418.

Coulon, F., Brassington, K. J., Bazin, R., Linnet, P. E., Thomas, K. A., Mitchell, T. R., ... & Pollard, S. J. (2012). Effect of fertilizer formulation and bioaugmentation on biodegradation and leaching of crude oils and refined products in soils. *Environmental technology*, 33(16), 1879-1893.

Das, N., & Chandran, P. (2010). Microbial degradation of petroleum hydrocarbon contaminants: an overview. *Biotechnology research international*, 2011.

Dell'Anno, A., Beolchini, F., Rocchetti, L., Luna, G. M., & Danovaro, R. (2012). High bacterial biodiversity increases degradation performance of hydrocarbons during bioremediation of contaminated harbor marine sediments. *Environmental Pollution*, 167, 85-92.

Finneran, K. T., Johnsen, C. V., & Lovley, D. R. (2003). *Rhodoferrax ferrireducens* sp. nov., a psychrotolerant, facultatively anaerobic bacterium that oxidizes acetate with the reduction of Fe (III). *International Journal of Systematic and Evolutionary Microbiology*, 53(3), 669-673.

- Gavaskar, A., Gupta, N., Sass, B., Janosy, R., & Hicks, J. (2000). *Design guidance for application of permeable reactive barriers for groundwater remediation*. BATTELLE COLUMBUS OPERATIONS OH.
- Harayama, S., Kasai, Y., & Hara, A. (2004). Microbial communities in oil-contaminated seawater. *Current opinion in biotechnology*, 15(3), 205-214.
- Hatzenpichler, R., Lebedeva, E. V., Spieck, E., Stoecker, K., Richter, A., Daims, H., & Wagner, M. (2008). A moderately thermophilic ammonia-oxidizing crenarchaeote from a hot spring. *Proceedings of the National Academy of Sciences*, 105(6), 2134-2139.
- Hawkins, A. M. (2013). *Processes controlling the behavior of LNAPLs at groundwater surface water interfaces* (Masters Thesis, Colorado State University).
- Hemalatha, S., & Veeramanikandan, P. (2011). Characterization of Aromatic Hydrocarbon Degrading Bacteria from Petroleum Contaminated Sites. *Journal of Environmental Protection*, 2(03), 243.
- Hoffman, D. J., & Albers, P. H. (1984). Evaluation of potential embryotoxicity and teratogenicity of 42 herbicides, insecticides, and petroleum contaminants to mallard eggs. *Archives of environmental contamination and toxicology*, 13(1), 15-27.
- Hovanec, T. A., Taylor, L. T., Blakis, A., & DeLong, E. F. (1998). Nitrospira-like bacteria associated with nitrite oxidation in freshwater aquaria. *Applied and environmental microbiology*, 64(1), 258-264.
- Irianni Renno, M. (2013). *Biogeochemical characterization of a LNAPL body in support of STELA* (Masters Thesis, COLORADO STATE UNIVERSITY).
- Isheetpile.com. (2015). Steel vs Concrete Tool. Retrieved April 14, 2015, from <http://www.isheetpile.com/articles/corrosion>

- Jonker, M. T., Brils, J. M., Sinke, A. J., Murk, A. J., & Koelmans, A. A. (2006). Weathering and toxicity of marine sediments contaminated with oils and polycyclic aromatic hydrocarbons. *Environmental toxicology and chemistry*, 25(5), 1345-1353.
- Kalyuzhnaya, M. G., Bowerman, S., Lara, J. C., Lidstrom, M. E., & Chistoserdova, L. (2006). *Methylotenera mobilis* gen. nov., sp. nov., an obligately methylamine-utilizing bacterium within the family Methylophilaceae. *International journal of systematic and evolutionary microbiology*, 56(12), 2819-2823.
- Kostka, J. E., Prakash, O., Overholt, W. A., Green, S. J., Freyer, G., Canion, A., ... & Huettel, M. (2011). Hydrocarbon-degrading bacteria and the bacterial community response in Gulf of Mexico beach sands impacted by the Deepwater Horizon oil spill. *Applied and environmental microbiology*, 77(22), 7962-7974.
- Liu, Q. M., Ten, L. N., Im, W. T., & Lee, S. T. (2008). *Castellaniella caeni* sp. nov., a denitrifying bacterium isolated from sludge of a leachate treatment plant. *International journal of systematic and evolutionary microbiology*, 58(9), 2141-2146.
- Long, E. R., MacDonald, D. D., Smith, S. L., & Calder, F. D. (1995). Incidence of adverse biological effects within ranges of chemical concentrations in marine and estuarine sediments. *Environmental management*, 19(1), 81-97.
- Mackay, D. M., Roberts, P. V., & Cherry, J. A. (1985). Transport of organic contaminants in groundwater. *Environmental science & technology*, 19(5), 384-392.
- Margesin, R., & Schinner, F. (2001). Biodegradation and bioremediation of hydrocarbons in extreme environments. *Applied microbiology and biotechnology*, 56(5-6), 650-663.

- Matsutani, N., Nakagawa, T., Nakamura, K., Takahashi, R., Yoshihara, K., & Tokuyama, T. (2011). Enrichment of a novel marine ammonia-oxidizing archaeon obtained from sand of an eelgrass zone. *Microbes and environments*, 26(1), 23-29.
- Mercer, J. W., & Cohen, R. M. (1990). A review of immiscible fluids in the subsurface: properties, models, characterization and remediation. *Journal of Contaminant Hydrology*, 6(2), 107-163.
- Meyer, S., Moser, R., Neef, A., Stahl, U., & Kämpfer, P. (1999). Differential detection of key enzymes of polyaromatic-hydrocarbon-degrading bacteria using PCR and gene probes. *Microbiology*, 145(7), 1731-1741.
- Mohan, R., Palermo, M., Costello, M., Koubsky, D., Rieger, J., and Jackson, M.M. (2011). Development of an in-lieu fee for sediment remediation in the Elizabeth River. *Proceedings of the Western Dredging Association (WEDAXXXI) Technical Conference and Texas A&M University (TAMU 42) Dredging seminar, Nashville, Tennessee.*
- Moore, W. E. C., Cato, E. P., & Holdeman, L. V. (1969). Anaerobic bacteria of the gastrointestinal flora and their occurrence in clinical infections. *The Journal of infectious diseases*, 641-649.
- The New Encyclopædia Britannica. 2005. Fossil Fuels. The New Encyclopædia Britannica, 15th Edition, Chicago, IL.
- New Jersey Department of Environmental Protection. (2014). Technical Guidance on the Capping of Sites Undergoing Environmental Remediation. *Site Remediation Program.*
- North American Steel Sheet Piling Association. (2009). Comparison Retaining Wall Design and Cost Study Steel Sheet Piling vs Various Walls. *Technical Report.*

- Okpokwasili, G., Somerville, C., Grimes, D., & Colwell, R. (1984). Plasmid-associated phenanthrene degradation by Chesapeake Bay sediment bacteria. In 2. *Colloque International de Bacteriologie Marine, Brest (France)*, 1-5.
- Palermo, M. R. (1998). Design considerations for in-situ capping of contaminated sediments. *Water Science and Technology*, 37(6), 315-321.
- Pashin, Y. V., & Bakhitova, L. M. (1979). Mutagenic and carcinogenic properties of polycyclic aromatic hydrocarbons. *Environmental health perspectives*, 30, 185.
- Perelo, L. W. (2010). Review: In situ and bioremediation of organic pollutants in aquatic sediments. *Journal of hazardous materials*, 177(1), 81-89.
- Perfumo, A., Banat, I. M., Marchant, R., & Vezzulli, L. (2007). Thermally enhanced approaches for bioremediation of hydrocarbon-contaminated soils. *Chemosphere*, 66(1), 179-184.
- Prince, R. C., Gramain, A., & McGenity, T. J. (2010). Prokaryotic hydrocarbon degraders. In *Handbook of hydrocarbon and lipid microbiology* (pp. 1669-1692). Springer Berlin Heidelberg.
- Reichenbach, H. (1992). The order cytophagales. In *The prokaryotes* (pp. 3631-3675). Springer New York.
- Reible, D. (2004). Cost and feasibility of conventional and active sediment capping. In *Technology Benchmarking Workshop For Sediment and Floodplain Remediation, Ann Arbor, MI, March* (pp. 25-26).
- Sale, T., Taylor, G. R., Iltis, G., & Lyverse, M. (2007). Measurement of LNAPL Flow Using Single-Well Tracer Dilution Techniques. *Groundwater*, 45(5), 569-578.
- Sale, T., Lyverse, M. (2014). Colorado State University Report to Chevron: Petroleum Sheens Technology Transfer Memo.

- Santas, R., Korda, A., Tenente, A., Buchholz, K., & Santas, P. H. (1999). Mesocosm assays of oil spill bioremediation with oleophilic fertilizers: Inipol, F1 or both?. *Marine Pollution Bulletin*, 38(1), 44-48.
- Schroth, M. H., Istok, J. D., Selker, J. S., Oostrom, M., & White, M. D. (1998). Multifluid flow in bedded porous media: laboratory experiments and numerical simulations. *Advances in Water Resources*, 22(2), 169-183.
- Schwarzenbach, R. P., Gschwend, P. M., & Imboden, D. M. (2005). *Environmental organic chemistry*. John Wiley & Sons.
- Shahidzadeh, N., Bonn, D., Ragil, K., Broseta, D., & Meunier, J. (1998). Sequence of two wetting transitions induced by tuning the Hamaker constant. *Physical review letters*, 80(18), 3992.
- Sheppard, D. (2013, June 12). Developing World Oil Demand Surpasses Wealthy Nations. Retrieved October 24, 2014, from <http://www.reuters.com/article/2013/06/11/us-eia-stea-nonoecd-idUSBRE95A16120130611>
- Skinner, A. M. (2013). *Lnapl longevity as a function of remedial actions: Tools for evaluating lnapl remedies* (Doctoral dissertation, COLORADO STATE UNIVERSITY).
- Tratnyek, P. G., Scherer, M. M., Johnson, T. L., & Matheson, L. J. (2003). Permeable reactive barriers of iron and other zero-valent metals. *Environmental Science and Pollution Control Series*, 371-422.
- Tyagi, M., da Fonseca, M. M. R., & de Carvalho, C. C. (2011). Bioaugmentation and biostimulation strategies to improve the effectiveness of bioremediation processes. *Biodegradation*, 22(2), 231-241.

US Environmental Protection Agency. (2013). Use of Amendments for In Situ Remediation at Superfund Sediment Sites. OSWER Directive 9200.2-128FS.

U.S. Geological Survey (2015), National Water Information System data available on the World Wide Web (USGS Water Data for the Nation), accessed [February 5, 2015], at URL [<http://waterdata.usgs.gov/nwis/>].

Whitby, C., & Skovhus, T. L. (2011). *Applied Microbiology and Molecular Biology in Oilfield Systems*. Springer.

Zeman, N. R., Renno, M. I., Olson, M. R., Wilson, L. P., Sale, T. C., & Susan, K. (2014). Temperature impacts on anaerobic biotransformation of LNAPL and concurrent shifts in microbial community structure. *Biodegradation*, 25(4), 569-585.

Zimbron, J. A., Sale, T. C., Batten, P. H., Biondolillo, M. J., Chalfant, M. W., Lyverse, M. (2014). Oleophilic Bio-Barrier for Controlling NAPL Migration. US Patent Application No. 14485631, Unpublished.

Zhang, T., Tremblay, P. L., Chaurasia, A. K., Smith, J. A., Bain, T. S., & Lovley, D. R. (2013). Anaerobic benzene oxidation via phenol in *Geobacter metallireducens*. *Applied and environmental microbiology*, 79(24), 7800-7806.



## Appendix A: Confidential Sheens Survey Summary

<b>Questions</b>
1. What is the site setting?
2. What are the prevailing temperatures?
3. Do you currently, or have you had sheens present at your site?
4. What is the temporal nature of the sheens?
5. What is the spatial nature of the sheens?
6. Are sheens a regulatory issue?
7. What products cause or caused sheens at your site?
8. What is a general character of the water?
9. Have remedial actions been employed?
10. If yes, which ones?
11. Sheens are resulting from:
12. What is the primary operation at the site?
<b>Site Setting</b>
13. What is the nature of the soil/sediment associated with sheens?
14. What is the source of the sheen hydrocarbon?
15. Degree of hydrogeologic media heterogeneity (i.e., layers)
16. What is the hydraulic conductivity of the media at the soil/water interface?
17. If there is a NAPL source, what is the hydraulic conductivity of the media in the LNAPL zone?
18. Distance from NAPL edge to point of compliance (specify units, ft, yd, other)
<b>Chemical Characteristics</b>
19. What is the age of the NAPL of concern?
21. Has a comprehensive analysis of sheen components been performed?
23. Has a comprehensive analysis of NAPL been performed?
25. Has a comprehensive analysis of water with sheens been performed?
26. Has a comprehensive analysis of ground water been performed?
<b>Sheen Occurrence</b>
27. What is or was the periodicity of observed sheens?
28. Are sheens related to particular event (i.e., high precipitation, low groundwater level etc)?
29. What is a typical duration of sheens?
<b>Hydrogeology</b>
30. Main mechanism for groundwater level fluctuations
31. Groundwater level (below ground, ft)
32. Groundwater fluctuations: range, ft
33. Periodicity of groundwater fluctuations
<b>Remedies</b>
34. If remedies have been implemented, do they involve on-going O&M?
35. Are employed remedies meeting your needs?
<b>Regulatory</b>
36. What is the regulatory framework you are working under
37. Will there be additional work to address sheens?
*Note: Questions without reportable answers were not included in this summary.

Q	Range of possible answers				
1	Coastal	Estuarine	River		
2	A) Warm	B) Moderate	C) Cold		
3	A) Yes	B) No			
4	A) Historic	B) Periodic	C) Chronic		
5	A) Single point	B) Periodic	C) Sporadic	D) Continuous	
6	A) Yes	B) No			
7	A) Gasoline	B) Diesel	C) Jet Fuel	D) Fuel Oil	E) Other
8	A) Fresh	B) Brackish	C) Saline		
9	A) Y	B) N			
10	A) NAPL Recovery	B) Booms	C) Walls	D) Pumping	E) Other
11	A) Erosion	B) Sediment disturbance	C) Seeps	D) Point discharge	E) Runoff
12	A) Terminal	B) Pipeline	C) Refining	D) Marketing	E) Other
13	A) Sand	B) Silt	C) Clay	D) Other (specify)	
14	A) LNAPL pool in soil	B) Process discharge	C) Runoff	D) Other (specify)	
15	A) High	B) Medium	C) Low		
16	A) High (coarse sand)	B) Med (fine/med sand)	C) Low (clay/silt)		
17	A) High (coarse sand)	B) Med (fine/med sand)	C) Low (clay/silt)		
18	A) 10-20 ft	B) 20-50 ft	C) 50-100 ft	D) > 100 ft	
19	A) < 1 yr	B) 1-5 yrs	C) 5-10 yrs	D) 10-30 yr	E) > 30 yr
21	A) Y	B) N			
23	A) Y	B) N			
25	A) Y	B) N			
26	A) Y	B) N			
27	A) Daily	B) Seasonal	C) Other (specify)		
28	A) Y (specify)	B) N			
29	A) Hours	B) Days	C) Weeks	D) Other (specify)	
30	A) Tidal	B) Seasonal	C) River stage		
31	A) 1-5 ft	B) 5-10 ft	C) 10-15 ft	D) Other (specify)	
32	A) < 1 ft	B) 1-3 ft	C) 3-10 ft	D) > 10 ft	
33	A) Daily	B) Seasonal	C) Other (specify)		
34	A) Y	B) N			
35	A) Y	B) N			
36	(specify)				
37	A) Y	B) N			

Q	Responses				
1	1 coastal (A)	3 estuarine (B)	, 7 river (C)		
2		8 moderate	1 cold	1 warm/cold	
3	10 yes	1 no			
4	3 historic	4 periodic	4 chronic		
5	0 single point	1 periodic	7 sporadic	4 continuous front	
6	10 yes				
7	7 gasoline	9 diesel	0 jet fuel	4 fuel oil	2 (unknown, MGP)
8	3 fresh	6 brackish	1 saline		
9	10 yes				
10	8 recovery	6 booms	3 walls	2 pumping	2 other (bio, absorbant materials)
11	2 erosion	1 sediment disturbance	4 seeps	3 point disch	1 runoff
12	7 terminal	1 pipeline	1 refining	0 marketing	1 MGP
13	6 sand	6 silt	0 clay	5 (fill, sandy gravel, )	
14	7 NAPL pool in soil	0 process disch	0 runoff	4 (unknown, residual NAPL, under invest., creosote treated piles)	
15	5 high	4 med	1 low		
16	4 high	6 med	2 C		
17	5 high	5 med			
18	4 (10-20 ft)	3 (20-50 ft)	2 (50-100 ft)	0 (>100 ft)	1 (0 ft)
19	1 a (< 1 yr)	0 (1-5 yr)	0 (5-10 yr)	8 (10-30 yr)	5 (>30 yr)
21	3 (yes)	7 (No)			
23	5 (Y)	5 (No)			
25	2 (Yes)	8 (No)			
26	9 (Yes)	1 (no)			
27	3 (daily)	1 (seasonal)	6 (other- low tide, weekly, random)		
28					
29	6 (hours)	1 (days)	0 (weeks)	3 (other, minutes, continuous)	
30	7 (tidal)	4 (Seasonal)	3 (river stage)		
31	3 (1-5ft)	2 (5-10 ft)	2 (10-15 ft)	3 Other (0-10 ft, 15-20 ft)	
32	2 (<1 ft)	4 (1-3 ft)	4 (3-10 ft)	1 (>10 ft)	
33	6 (daily)	4 (Seasonal)	0		
34	9 (Yes)	1 (no)			
35	7 (Yes)	3 (no)			
36	7 state programs,	1 ,consent order	2 voluntary clean		
37	7 (yes)	2 (no)			

## Appendix B: Supplemental Lab Study Data

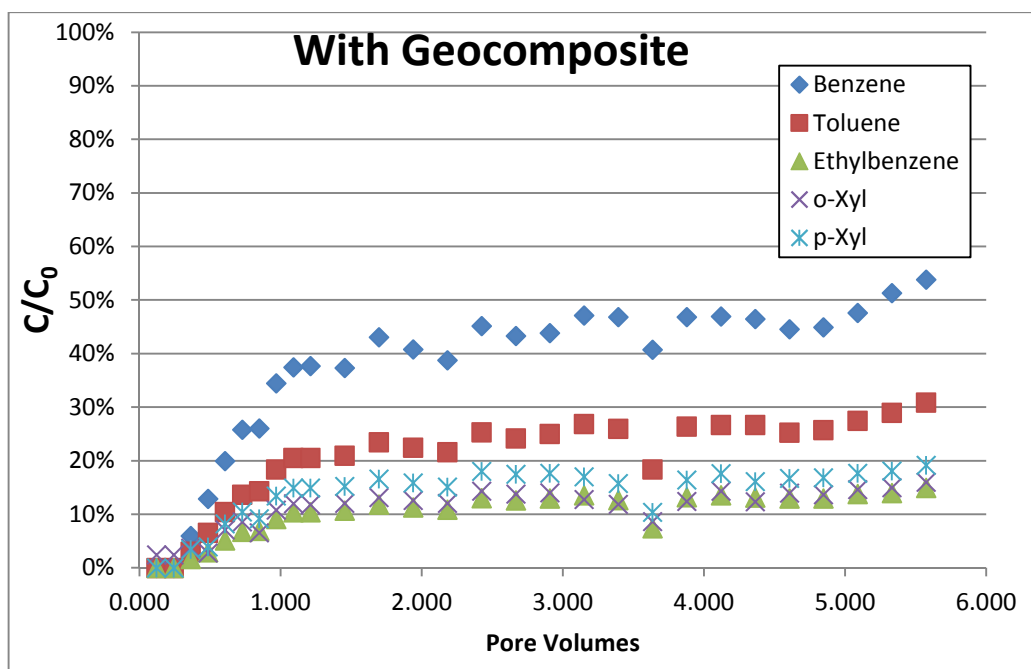


Figure 55: Aqueous sorption study treated column breakthrough curves

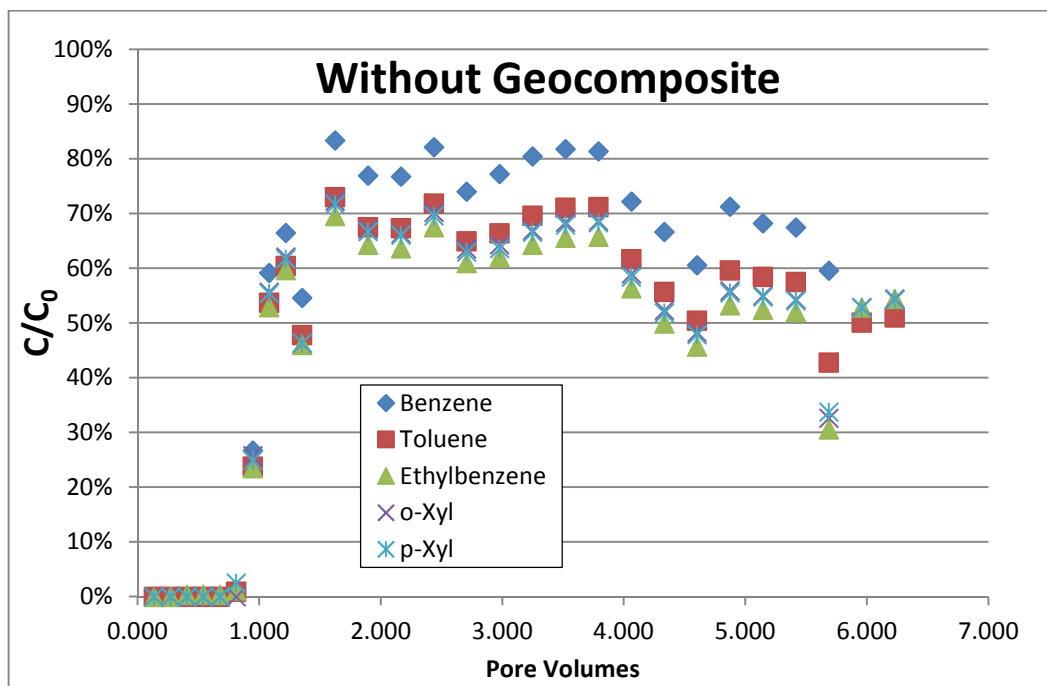


Figure 56: Aqueous sorption study untreated column breakthrough curves

## Appendix C: As-built drawing of a small-scale OBB

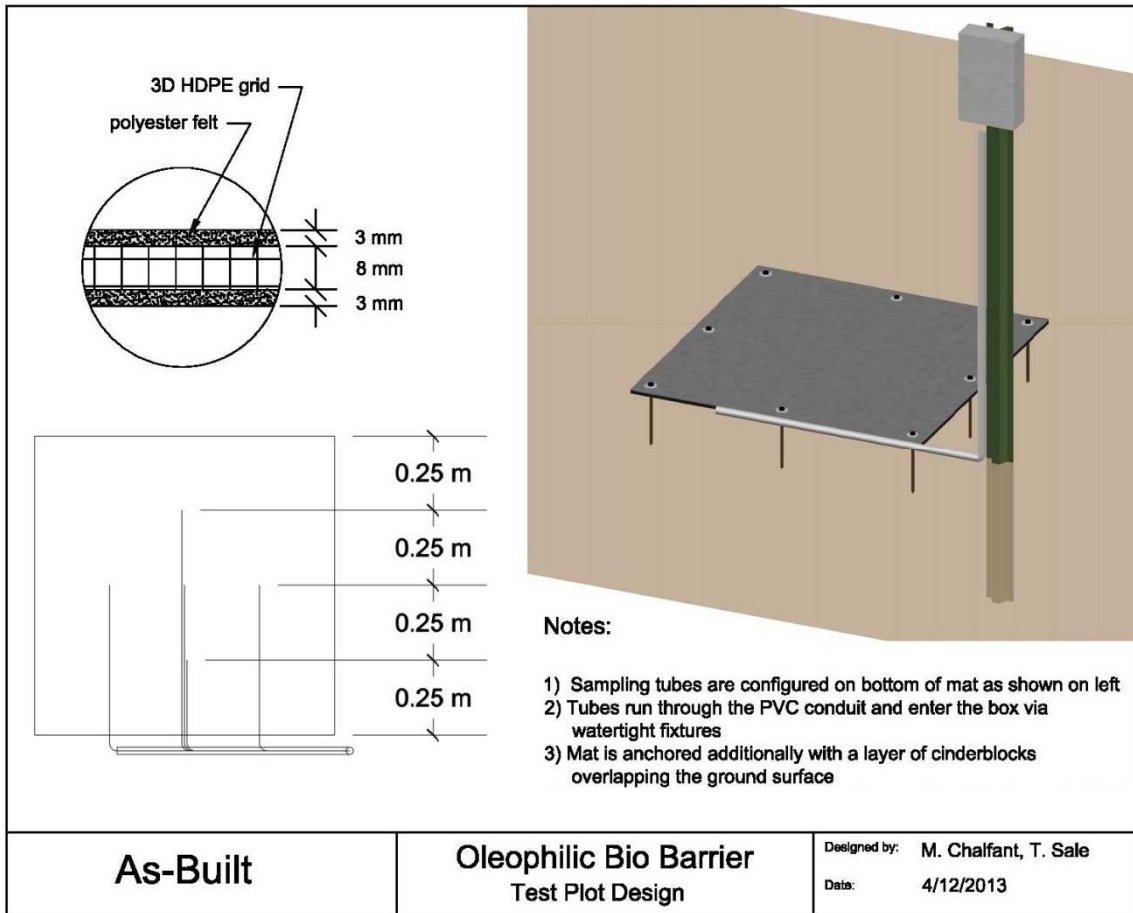


Figure 57: As-built drawing of small-scale OBB

## Appendix D: Preliminary OBB study UV survey and sampling forms

OBB UV Survey and Sampling Form																																																
<b>CSU Personnel:</b> MC, MR <b>ARCADIS Personnel:</b> JS		<b>Date:</b> 8/14 <b>OBB Mat:</b> <span style="border: 1px solid black; border-radius: 50%; padding: 2px;">A</span>	<b>Time:</b> B    C    D																																													
<b>UV Survey – Indicate areas with hydrocarbon and/or microbial growth</b>																																																
		<table border="1" style="width: 100%; border-collapse: collapse;"> <thead> <tr> <th colspan="3">Sampling Log</th> </tr> <tr> <th>Type (M,R,H)</th> <th>Location (1-9)</th> <th>Sample ID</th> </tr> </thead> <tbody> <tr><td>M</td><td>7 (A)</td><td>OBB4A</td></tr> <tr><td>D</td><td>7 (A)</td><td>DNA3</td></tr> <tr><td>M</td><td>8,9 (B)</td><td>OBB4B</td></tr> <tr><td>D</td><td>8,9 (B)</td><td>DNA4</td></tr> <tr><td> </td><td> </td><td> </td></tr> <tr><td> </td><td> </td><td> </td></tr> <tr><td> </td><td> </td><td> </td></tr> <tr><td> </td><td> </td><td> </td></tr> <tr><td> </td><td> </td><td> </td></tr> <tr><td> </td><td> </td><td> </td></tr> <tr><td> </td><td> </td><td> </td></tr> <tr><td> </td><td> </td><td> </td></tr> <tr><td> </td><td> </td><td> </td></tr> </tbody> </table>		Sampling Log			Type (M,R,H)	Location (1-9)	Sample ID	M	7 (A)	OBB4A	D	7 (A)	DNA3	M	8,9 (B)	OBB4B	D	8,9 (B)	DNA4																											
Sampling Log																																																
Type (M,R,H)	Location (1-9)	Sample ID																																														
M	7 (A)	OBB4A																																														
D	7 (A)	DNA3																																														
M	8,9 (B)	OBB4B																																														
D	8,9 (B)	DNA4																																														
<b>Description / Notes:</b> Pics 65 → * Small OBB ≈ 27" x 30" * Shaded region showed slight/minor fluorescence ↳ AND MAJOR FL - from stake ± A: Orange color w/ tundra texture → Green fluor. B: Black spots, depressed ≈ 1mm → Bluish fluor. C: Sediment surface rusty orange color ↳ in 1" Below surf. Black color - extremely local → "Chrom Sulfides?" - Maria ± Orange NAPL VISIBLE, not just sheer → Brightest fluor.		M = OBB Material Str R = OBB Respirometric H = OBB Hydrocarbon S = Soil HC D = Soil DNA *Soil samples taken from top 3 cm of sediment directly contacting indicated location																																														

Figure 58: Preliminary study final sampling log: OBB A

OBB UV Survey and Sampling Form																																												
<b>CSU Personnel:</b> MC MR  <b>ARCADIS Personnel:</b> JS	<b>Date:</b> 8/14 <b>Time:</b>  <b>OBB Mat:</b> A <u>B</u> C    D																																											
<b>UV Survey – Indicate areas with hydrocarbon and/or microbial growth</b>																																												
	<table border="1" style="width: 100%; border-collapse: collapse;"> <thead> <tr> <th colspan="3">Sampling Log</th> </tr> <tr> <th>Type (M,R,H)</th> <th>Location (1-9)</th> <th>Sample ID</th> </tr> </thead> <tbody> <tr><td>M</td><td>1,4 (A)</td><td>OBB 3A</td></tr> <tr><td>SED</td><td>1,4 (A)</td><td>TPH 1</td></tr> <tr><td>DNA</td><td>" (A)</td><td>TPH 4</td></tr> <tr><td>M</td><td>3,8 (B)</td><td>OBB 3B</td></tr> <tr><td>DNA</td><td>" (B)</td><td>DNA 5</td></tr> <tr><td>SED</td><td>" (B)</td><td>TPH 6</td></tr> <tr><td>M</td><td>3,6,8,9 (C)</td><td>OBB 3C</td></tr> <tr><td>SED</td><td>3,6 (D)</td><td>TPH 2</td></tr> <tr><td>DNA</td><td>3,6 (D)</td><td>TPH 3</td></tr> <tr><td> </td><td> </td><td> </td></tr> <tr><td> </td><td> </td><td> </td></tr> <tr><td> </td><td> </td><td> </td></tr> </tbody> </table>		Sampling Log			Type (M,R,H)	Location (1-9)	Sample ID	M	1,4 (A)	OBB 3A	SED	1,4 (A)	TPH 1	DNA	" (A)	TPH 4	M	3,8 (B)	OBB 3B	DNA	" (B)	DNA 5	SED	" (B)	TPH 6	M	3,6,8,9 (C)	OBB 3C	SED	3,6 (D)	TPH 2	DNA	3,6 (D)	TPH 3									
Sampling Log																																												
Type (M,R,H)	Location (1-9)	Sample ID																																										
M	1,4 (A)	OBB 3A																																										
SED	1,4 (A)	TPH 1																																										
DNA	" (A)	TPH 4																																										
M	3,8 (B)	OBB 3B																																										
DNA	" (B)	DNA 5																																										
SED	" (B)	TPH 6																																										
M	3,6,8,9 (C)	OBB 3C																																										
SED	3,6 (D)	TPH 2																																										
DNA	3,6 (D)	TPH 3																																										
<b>Description / Notes:</b> D is SED ONLY, MIRROR LOCATION OF A Pics 3150-53, → 64 (OBB 3C) A: Yellow-orange to rust color mat ↳ Darker orange = more fluorescence																																												
<b>Legend:</b> M = OBB Material Str R = OBB Respirometric H = OBB Hydrocarbon  S = Soil HC D = Soil DNA  *Soil samples taken from top 3 cm of sediment directly contacting indicated location																																												

Figure 59: Preliminary study final sampling log: OBB B



OBB UV Survey and Sampling Form																																																					
<p><u>CSU Personnel:</u></p> <p><u>ARCADIS Personnel:</u></p>	<p>Date: 8/14      Time:</p> <p>OBB Mat:    A      <u>B</u>      C      D</p>																																																				
<p><b>UV Survey</b> – Indicate areas with hydrocarbon and/or microbial growth</p>																																																					
	<table border="1" style="width: 100%; border-collapse: collapse;"> <thead> <tr style="background-color: #f2f2f2;"> <th colspan="3" style="text-align: center; padding: 5px;">Sampling Log</th> </tr> <tr style="background-color: #f2f2f2;"> <th style="width: 20%; padding: 5px;">Type (M,R,H)</th> <th style="width: 20%; padding: 5px;">Location (1-9)</th> <th style="width: 60%; padding: 5px;">Sample ID</th> </tr> </thead> <tbody> <tr><td style="text-align: center;">M</td><td style="text-align: center;">4, 7</td><td>OBB 2 A</td></tr> <tr><td style="text-align: center;">M</td><td style="text-align: center;">9</td><td>OBB 2 B</td></tr> <tr><td style="text-align: center;">M</td><td style="text-align: center;">6</td><td>OBB 2 C</td></tr> <tr><td> </td><td> </td><td> </td></tr> <tr><td> </td><td> </td><td> </td></tr> <tr><td> </td><td> </td><td> </td></tr> <tr><td> </td><td> </td><td> </td></tr> <tr><td> </td><td> </td><td> </td></tr> <tr><td> </td><td> </td><td> </td></tr> <tr><td> </td><td> </td><td> </td></tr> <tr><td> </td><td> </td><td> </td></tr> <tr><td> </td><td> </td><td> </td></tr> <tr><td> </td><td> </td><td> </td></tr> <tr><td> </td><td> </td><td> </td></tr> <tr><td> </td><td> </td><td> </td></tr> </tbody> </table>		Sampling Log			Type (M,R,H)	Location (1-9)	Sample ID	M	4, 7	OBB 2 A	M	9	OBB 2 B	M	6	OBB 2 C																																				
Sampling Log																																																					
Type (M,R,H)	Location (1-9)	Sample ID																																																			
M	4, 7	OBB 2 A																																																			
M	9	OBB 2 B																																																			
M	6	OBB 2 C																																																			
<p><b>Description / Notes:</b></p> <p>Pics 3134 - 3132</p> <p>3132 - HEAVY NAPL</p> <p>* OBB 2B showed visible NAPL/STAINING</p>																																																					
<div style="display: flex; justify-content: space-between;"> <div> <p>M = OBB Material Str</p> <p>R = OBB Respirometric</p> <p>H = OBB Hydrocarbon</p>   <p>S = Soil HC</p> <p>D = Soil DNA</p> </div> <div> <p>*Soil samples taken from top 3 cm of sediment directly contacting indicated location</p> </div> </div>																																																					

Figure 60: Preliminary study final sampling log: OBB C



OBB UV Survey and Sampling Form		
<b>CSU Personnel:</b> <u>MARC CHALFANT, MR</u>	<b>Date:</b> <u>8/14</u> <b>Time:</b>	
<b>ARCADIS Personnel:</b> <u>JAMES SCHIDZICK</u>	<b>OBB Mat:</b> A      B      C <u>(D)</u>	

**UV Survey – Indicate areas with hydrocarbon and/or microbial growth**

Sampling Log		
Type (M,R,H)	Location (1-9)	Sample ID
M	6	OBB1
M	6	OBB2
S	6	OBB1

**Description / Notes:**

---

---

---

---

---

---

---

---

---

---

**M = OBB Material Str**  
**R = OBB Respiriometric**  
**H = OBB Hydrocarbon**  
  
**S = Soil HC**  
**D = Soil DNA**

\*Soil samples taken from top 3 cm of sediment directly contacting indicated location

Figure 61: Preliminary study final sampling log: OBB D

## Appendix E: Notes on preliminary study sediment hydrocarbon analysis

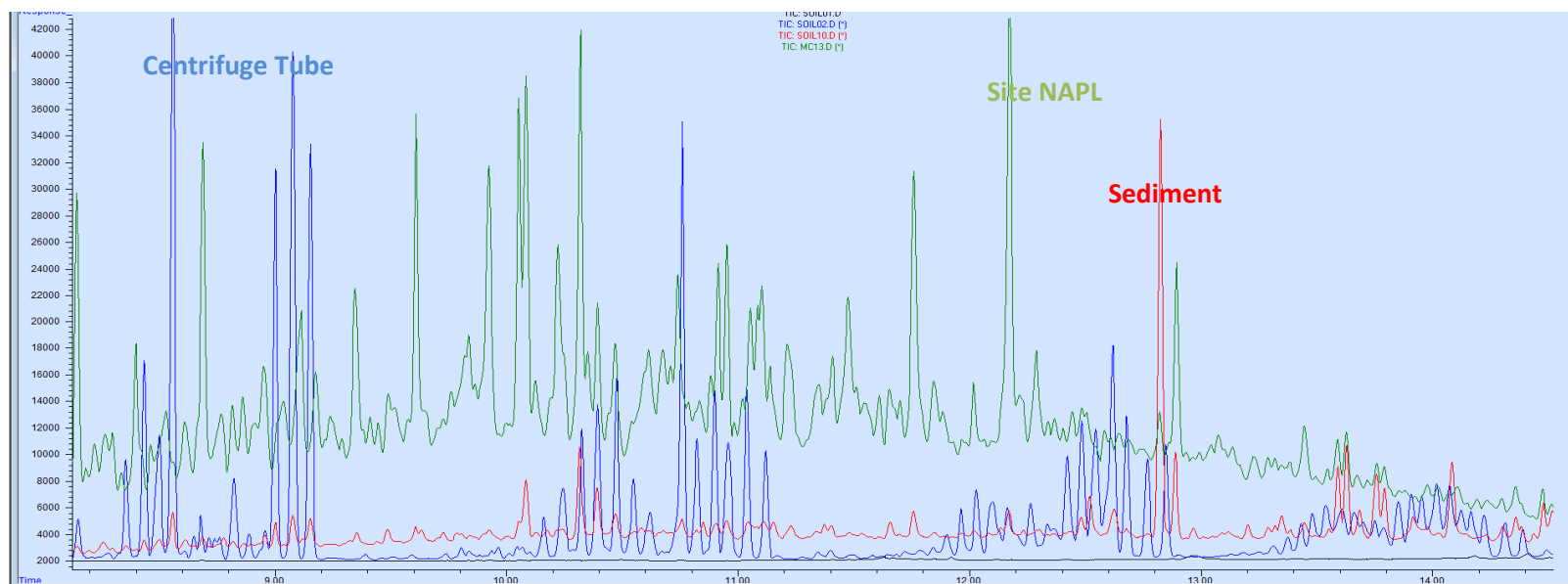


Figure 62: Sediment hydrocarbon chromatograms

The blue “Centrifuge tube blank” curve shows the chromatogram of dichloromethane shaken in an empty centrifuge tube. The red “sediment Sample” curve is a sediment sample that showed some interference from the centrifuge tube extraction process. Distinct ranges of peaks were not affected by centrifuge tube noise (9.2 to 10.12, 11.16 to 11.82 and 12.88 to 13.4). The Site NAPL chromatograms were integrated over the unaffected ranges and used to create a calibration curve. The centrifuge tube noise within this range was integrated and subtracted out of the sediment sample areas. The noise-corrected sediment chromatogram areas were then multiplied by the Site NAPL calibration slope to calculate corrected sediment concentrations.

## Appendix F: Full-scale field demonstration construction documents

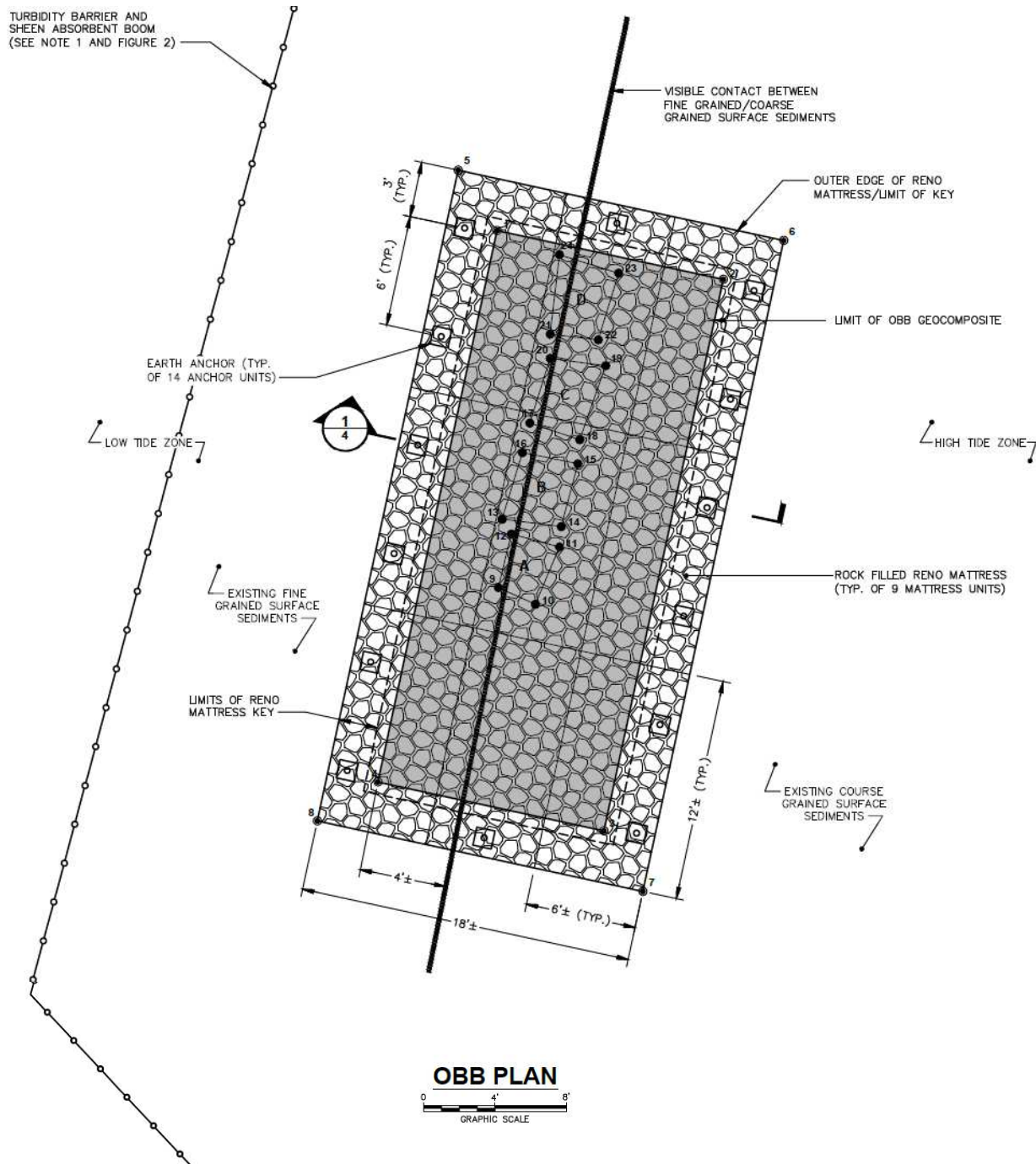


Figure 63: OBB Layout Plan



## Appendix G: Monitoring system parts list and assembly instructions

Table 15: Parts List for monitoring port system

Item	Qty per port	Item	Qty per port
<b>6" PVC Assembly</b>	<b>1</b>	<b>Pressure Assemblies</b>	<b>1</b>
6" Sch. 40 PVC (L=12")	1	60mL Luer Lock Syringe <sup>1</sup>	1
6" Flange	1	BaroLogger (Solinst)	1
6" PVC Cap	1	¾" Geotextile Disc	1
Anchor Edging Spikes (L=8")	4	Epoxy	
Anchor Washers (>1" OD)	4	<b>Pushpoint Assemblies</b>	<b>3</b>
<b>5" PVC Assembly</b>	<b>1</b>	Pushpoint porewater sampler <sup>2</sup>	3
5" Sch. 40 PVC (L=12")	1	2-Way Luer-Lok Valve <sup>3</sup>	1
Hose Clamp (D=5.5")	1	¼" Female Luer transition <sup>3</sup>	1
#4 x 3/8" countersunk screws	4	1/8" Male Luer fitting <sup>3</sup>	2
#4 washers	4	1/16" FEP tubing (18")	1
Wire Mesh Circle (D = 7")	1	1/8" Viton tube (1.5") <sup>4</sup>	2
Geotextile Circle (D= 7")	1	3/8" Vinyl tube transition (2")	1
¼" all-thread rod (L = 6")	1	4" Ziptie	5
¼" nut to match all-thread	2		
¼" washer to match all-thread	2		
<b>1.25" PVC Assemblies</b>	<b>4</b>		
1.25" PVC (L = 12")	4		
1.25" PVC Cap	4		
1.25" PVC screw-on cap w/ fitting	4		
½" cube rubber spacer	4		
Hose Clamp (12")	2		
PVC Cement			
<b>Thermocouple Assemblies</b>	<b>1</b>		
¼" Nylon Swagelock Fitting	1		
32" K-Thermocouple	1		
22" K-Thermocouple	1		
Silicon sealant (Dow Corning)			

<sup>1</sup>Made by Kimble Chase

<sup>2</sup>Made by MHE Products

<sup>3</sup>Made by BD

<sup>4</sup>Made by Masterflex

### Monitoring port assembly instructions

- 1) 6" ID PVC Flange (x1 per port x 6 ports = 6)

- a. Enlarge four flange holes with a 2" hole saw, as shown in Figure 65
- 2) 6" diameter PVC (x1 per port x 6 ports = 6)
  - a. Cut to 12" length
  - b. Drill ¼" drain holes at four evenly spaced locations on circumference, at 4" intervals along length of pipe



Figure 65: PVC flange modified to receive 1 1/4" PVC tubes. Flange is centered over hole in geocomposite. Note: edging spike is not relevant to port assembly

- 3) 5" Diameter PVC Basket Insert (x1 per port x 6 ports = 6)
  - a. Cut 5" PVC to 12" length
  - b. Drill ¼" drain holes at four evenly spaced locations on circumference, at 4" intervals along length of pipe
  - c. Install grate
    - i. Cut welded wire mesh (½" opening) to a 7" diameter circle
    - ii. Place circle over end of 5" PVC and fold excess material over edges, cutting radial slots into mesh as needed to facilitate folding
    - iii. Tighten hose clamp over mesh, 1/8" from end of pipe
    - iv. Drill #4 screw pilot holes at 4 evenly spaced locations along hose clamp
    - v. Install screws with washers through pilot holes, securing hose clamp and mesh to PVC, as shown in Figure 66
    - vi. Cut off hose clamp tightener using rotary cutter
  - d. Install Handle
    - i. Drill two ¼" holes opposite each other, ½" from open end of pipe
    - ii. Screw all-thread into one hole, so it protrudes into pipe



iii. Put washers and nuts on rod as shown in Figure 67

iv. Screw rod into hole on other side and tighten  
nuts against washers

e. Cut 6" diameter circle of geotextile and place inside  
grate, centered

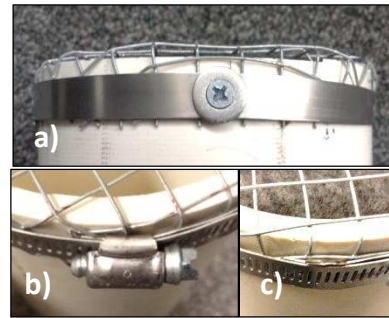


Figure 66: a) Hose clamp and screw fasten grate to pipe b) hose clamp tightener c) hose clamp tightener removed

4) Peripheral housings (x4 per port x 6 ports = 24)

a. Cut 12" length of 1.25" PVC

b. Cement screw-top cap receiver onto PVC

c. Drill 3/8" hole into PVC end-cap

d. Assemble water port housings (x3 per port x 6 ports  
= 18)



Figure 67: Handle assembly

i. Assemble water sampling ports as in Figure 68  
(x3 per port x 6 ports = 18)

ii. Push vinyl tubing on end of porewater assembly through hole in end-cap. assembly  
should be on inside of cap

iii. Note: PVC tube is not intended to be water-  
tight/waterproof

iv. Fit cap onto PVC tube with port assembly  
inside of tube



Figure 68: Water sampling port

e. Construct pressure vessel for BaroLogger (x1 per port x2 ports = 2)

i. Cut the tip off of plunger from luer-lock syringe as shown in Figure 70a

ii. Cut out center of rubber sealing from tip of plunger as shown in Figure 70b

iii. Drop 3/4" disc of geotextile into syringe body to act as a spacer

- iv. Place programmed BaroLogger into syringe, with geotextile at the tip as shown in Figure 69
- v. Epoxy modified plunger tip into place, capping open syringe end
- vi. Connect luer-lok tip of syringe to sampling port with 3' sampler, open valve
- vii. Place loaded syringe/pressure vessel into PVC tube and screw on PVC cap

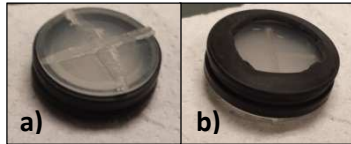


Figure 70: Modified plunger tip a) side sawed-off of plunger b) side with cut rubber



Figure 69: BaroLogger pressure vessel

- 5) Temp Datalogger Housing (x1 per port x 6 ports = 6)
- a. Cut 12" length of 1.5" OD Schedule 40 PVC pipe
  - b. Drill and thread 1.5" PVC end-cap to receive Swagelok fitting as shown in Figure 71
  - c. Install Swagelok fitting with teflon tape and seal with silicon sealant
  - d. Cement threaded cap receiver and bottom cap with Swagelok fitting onto PVC tube
  - e. Thread thermocouple wires through nylon fitting so that thermocouples are on outside, as shown in
  - f. Epoxy thermocouple wires into fitting at correct length (2" and 13" outside of tube)
  - g. Seal fitting and wires with silicone sealant
  - h. Note: tube should be waterproof to protect temperature dataloggers
  - i. Assemble thermocouple plugs onto end of thermocouple wires as shown in Figure 72

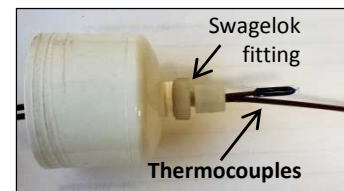


Figure 71: Thermocouples through Swagelok fitting

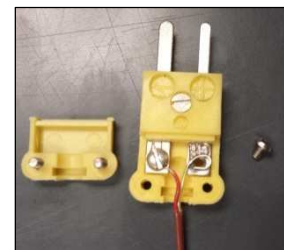


Figure 72: Thermocouple plug assembly



- j. Plug thermocouples into programmed dataloggers and screw PVC caps on with teflon tape
- 6) Assemble components of sampling port (x6 ports)
- a. Once geocomposite has been laid, place flange over port-hole in geocomposite
  - b. Install thermocouple and PVC thermocouple data logger housing
    - i. Use edging spike to create holes in geocomposite for porewater samplers and thermocouples, seen in Figure 73
    - ii. With guard-rod in sampler, push sampler 18" into one hole to create hole for thermocouple
    - iii. Use guard-rod to place thermocouple wire at desired depth
  - c. Set 1 ¼" PVC housing with data loggers into modified flange holes, as seen in Figure 74
  - d. Install water samplers and ports (x3)
    - i. With guard-rod in sampler, push sampler through hole, into sediments until top of sampler is ½" above geocomposite
    - ii. Install one sampler of each depth (1', 2', 3') per Figure 74
    - iii. Connect water port assembly in 1 ¼" pvc housing to sampler each sampler by fitting vinyl tubing over end of sampler
    - iv. Zip tie vinyl tubing to pushpoint sampler
  - e. Put washers on edging spikes and pound spikes into ground through bolt holes of PVC flange (x4) as seen in Figure 74
  - f. Set 1 ¼" PVC housing into modified flange holes, as seen in Figure 74
  - g. Mount 1 ¼" PVC housings to 6" pipe and flange (x4 per port)
  - h. Tighten hose clamps around two 1 ¼" PVC pipes opposite each other as well as 6" pipe, as illustrated in Figure 74
  - i. Repeat g. for remaining 2 tubes



Figure 73: Location of porewater sampler/thermocouple holes

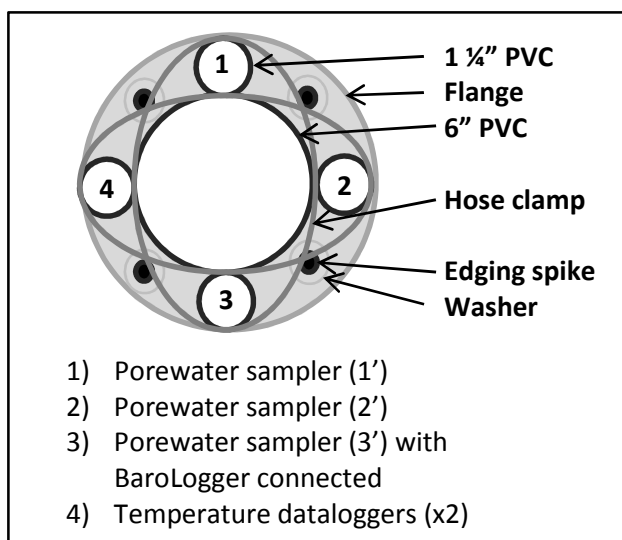


Figure 74: Top view schematic of sampling port

## Appendix H: Full-scale OBB product data sheets and construction photos

**product specifications**


### TENDRAIN II 91010-2

The drainage geonet is a boxed tri-planar structure consisting of vertically formed center ribs superimposed with horizontally formed top and bottom ribs. Open areas between the center ribs manage flow efficiently through continuous length, unobstructed channels. Geotextile intrusion into the channels is limited by the top and bottom ribs which are superimposed to, and lie perpendicular to the center ribs. This boxed tri-planar geonet provides high transmissivity in soil environments under high and low loading conditions. Tendrain II has properties conforming to the values and test methods listed below:

PROPERTY	TEST METHODS	UNITS	VALUE	QUALIFIER	TEST
<b>Geonet Core<sup>1</sup></b>					
• Thickness	ASTM D 5199	mil (mm)	300 (7.6)	±10%	50,000 sf
• Density	ASTM D 792	g/cm <sup>3</sup>	0.94 – 0.96	Range	50,000 sf
• Melt Flow Index	ASTM D 1238	g/10min	1.0	MAX	50,000 sf
• Carbon Black	ASTM D 4218	%	2-3	Range	50,000 sf
• Tensile Strength Ratio <sup>2</sup>	ASTM D 7179	-	1.0	MAV	50,000 sf
• Thickness Retained <sup>3</sup>	GRI-GC8	%	75		
• Creep Reduction Factor <sup>3</sup>	GRI-GC8	-	1.2		
<b>Geotextile<sup>1</sup></b>					
• Mullen Burst	ASTM D 3786	kPa (psi)	2900 (420)	MARV	100,000 sf
• Grab Tensile	ASTM D 4632	N (lbs)	900 (202)	MARV	100,000 sf
• Puncture Resistance	ASTM D 4833	N (lbs)	500 (112)	MARV	100,000 sf
• AOS	ASTM D 4751	mm (US Std Sieve)	0.21 (70)	MaxARV	500,000 sf
• Permittivity	ASTM D 4491	sec <sup>-1</sup>	0.2	MARV	500,000 sf
• Tear Strength	ASTM D 4533	N (lbs)	350 (79)	MARV	100,000 sf
• U.V. Resistance (500 hrs)	ASTM D 4355	%	50	-	Per formula
• Mass	ASTM D 5261	g/m <sup>2</sup>	350	MARV	100,000 sf
<b>Geocomposite</b>					
• Roll Size	12.5 ft x 200 ft (3.8 m x 61 m)				

Qualifiers: MARV=Minimum Average Roll Value (MARV), MAV=Minimum Average Value, MAX=Maximum Value, MaxARV=Maximum average roll value, MD=Machine Direction.

NOTES: 1. Geonet and Geotextile properties listed are prior to lamination. 2. Tensile strength ratio is calculated by dividing tensile strength in the cross machine direction by machine direction. 3. Thickness retained is based on 10,000 hour compressive creep test; under 15,000 psf load and 40°C temperature, creep reduction factor are determined by extrapolated to 30 years of design life 4. Geocomposite transmissivity is measured per ASTM D4716 with testing boundary conditions as follows: steel plate / Ottawa sand / geocomposite / 60mil geomembrane / steel plate, and seating period of 100 hours according to GRI-GC8. The side with circular apertures should be placed facing up, while the ribbed side should be placed facing down as indicated with "Top" / "Bottom" labels on the rolls.



4800 Pulaski Highway, Baltimore, MD 21224, USA

Phone 410.327.1070 800.874.7437

Fax 410-327-1078

www.synteccorp.com

6/24/2013

Figure 75: Geocomposite Product Sheet

NEW YORK STATE DEPARTMENT OF TRANSPORTATION  
MATERIALS BUREAU  
AGGREGATE TESTS  
PORTLAND CEMENT CONCRETE PLANT

PLANT <b>Hoffa</b>		LOCATION <b>PIT</b>		REGION	
DATE <b>7/12</b>		TIME OF SAMPLE <b>10:30</b>		CONCRETE CLASS	
INSPECTOR		TESTS: <input type="checkbox"/> routine <input type="checkbox"/> retest			
CHECK TEST(S) REPORTED ON THIS FORM		CONTRACTS SERVED:			
FINE AGGREGATE <input type="checkbox"/> gradation <input type="checkbox"/> minus #200 <input type="checkbox"/> fineness modulus <input type="checkbox"/> moisture <input type="checkbox"/> visual identification		COARSE AGGREGATE <input type="checkbox"/> gradation <input type="checkbox"/> visual identification <input type="checkbox"/> cleanliness <input type="checkbox"/> moisture			
CHECK SAMPLE LOCATION		COARSE AGGREGATE <input type="checkbox"/> belt <input type="checkbox"/> barge <input type="checkbox"/> stockpile <input type="checkbox"/> other <input type="checkbox"/> bin			

FINE AGGREGATE TESTS									
GRADATION					FINENESS MODULUS		VISUAL IDENTIFICATION		
SIEVE	WT.	% RETAINED	% PASSING	SPEC. LIMITS	SIEVE	100 - % PASS	Compares favorably to certified aggregate reference sample?		
3/8"			100	100			<input type="checkbox"/> Yes <input type="checkbox"/> No		
#4	1.1	2	99.8	90-100	#4	2	If "NO", explain:		
#8	24.1	4.8	95.0	75-100	#8	5.0			
#16	100.1	19.8	75.2	60-86	#16	24.8			
#30	115.7	22.5	52.9	25-60	#30	47.1			
#60	14.1	28.0	24.9	10-30	#60	75.1			
#100	90.5	18.0	6.9	1-10	#100	93.1			
#200	23.0	4.5	2.4	0-3					
PAN	12.2	2.4							
TOTAL	505.6	100			TOTAL	245.3			
ORIGINAL DRIED WEIGHT: 505.2					FM = TOTAL 100 100 245		FM (MIX DESIGN) 3.00		

## FINE AND COARSE AGGREGATE TESTS

MINUS #200 MATERIAL				FREE MOISTURE CONTENT			
AGGREGATE SIZE DESIGNATION				AGG. SIZE	FINE	NO. 1	NO. 2
WT. ORIGINAL SAMPLE (DRY) (A)				WT. (WET) (A)			
WT. AFTER WASHING (DRY) (B)				WT. (DRY) (B)			
WT. MINUS #200 MATL. (A-B)				% ABS. (C) *			
% MINUS #200 $\frac{(A-B)}{A} \times 100$				% FREE MOISTURE $\frac{(A-B \times 100) - C}{B}$			

\* From the Department's Approved List of Aggregate Sources

Figure 76: Sand gradation data





## TECHNICAL DATA SHEET

### RENO MATTRESSES

#### Reno Mattress

OT [Reno mattresses](#) are manufactured from hexagonal woven steel wire Mesh Type 60, commonly referred to as double twist wire mesh as per SANS 1580:2005 (Figure 1 and Table 1). [Reno mattresses](#) are filled with rock at the project site to form flexible, permeable, monolithic structures for river bank and scour protection, channel linings for erosion control and underwater pipeline protection.

The steel wire used during the manufacture of the mattress is heavily zinc coated, Class A as per SANS 675:1997. If required, a PVC coating is extruded over the galvanised wire to provide added protection for use in aggressive environments such as, acidic soils and water, salt water and in water carrying a high abrasive sediment load. The PVC coating has a nominal thickness of 0,5 mm. The properties and tolerances of steel wire and mesh are shown in Tables 1 and 2.

In order to reinforce the structure, all mesh panel edges are selvaged with a wire having a greater diameter than the mesh wire. [Reno mattresses](#) are partitioned into cells by means of diaphragms positioned at approximately 1m centers. Dimensions and sizes of Reno mattresses are shown in Table 3. When specifying [Reno mattresses](#) in the tender documents or bill of quantities, please refer to Table 4.

#### Filling and Lacing

[Reno mattresses](#) should be filled with rock ranging between 75 mm and 150 mm. The range in sizes may allow for a variation of 5% oversize and / or 5% undersize rock, provided it is not placed at the exposed surface. In all cases, oversize rock shall not be larger than 200 mm and the undersize rock shall not be smaller than 50 mm. Rocks shall be hard, angular to round, durable and of such quality that they shall not disintegrate on exposure to water or weathering during the life of the structure. Care should be taken when placing the stone to ensure that the PVC coating on the Reno mattress is not damaged. All visible faces should be carefully hand-packed for appearance purposes. For further information on the installation of mattresses, please refer to the [Installation Guidelines for Reno mattresses](#).

In place of lacing wire, lacing operations can be made by using a Spenax tool (Figure 4) available from our offices together with stainless steel rings (Figure 3A) having the following specifications:

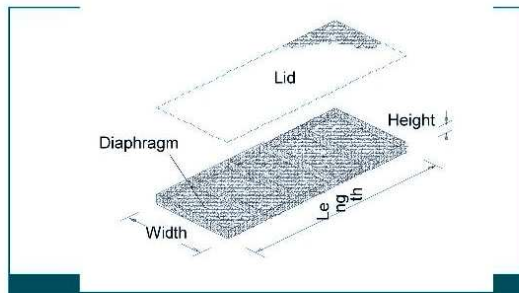
- diameter: 3mm
- tensile strength: 156-178 kg/mm<sup>2</sup>

Spacing of the rings or loops must not exceed that shown in Figure 3B.

#### Wire

All tests on wire are performed prior to manufacturing the mesh.

1. **Tensile strength:** The wire used for the manufacture of the [gabions](#) has a tensile strength between 350-575 N/mm<sup>2</sup> according to SANS 675:1997.
2. **Elongation:** Elongation is not less than 10% in accordance with EN 10223-3. Tests are carried out on a sample at least 25 cm long.
3. **Adhesion of zinc:** The adhesion of the zinc coating to the wire is such that, when the wire is wrapped six turns around a mandrel having four times the diameter of the wire, it does not flake or crack when rubbed with the bare fingers, in accordance with SANS 675:1997.
4. **Ductility:** The ductility of the zinc-coated wire is such that when the wire is wrapped at least eight times around a wire having the same diameter of the test specimen at a rate not exceeding 15 turns per minute and then unwrapped at the same rate, it does not show any sign of fracture of the underlying steel wire in accordance with SANS 675:1997.



#### STANDARD MESH-WIRE

Mesh Type 60	b	Tolerance (mm)	OD Wire Ø (mm)
Galvanised	60	-4 +10	2,2
Galvanised + PVC	60	-4 +10	2,2 / 3,2



#### MESH TOLERANCE

The tolerance on the opening of mesh "b" being the distance between the axis of two consecutive twists according to SANS 1580:2005.

Table 1

#### PROPERTIES OF WIRE

Use	Units	Lacing	Mesh	Selvage
Wire**				
Galvanised	Ø mm	2,2	2,2	2,7
Galvanised + PVC		2,2 / 3,2	2,2 / 3,2	2,7 / 3,7
Wire Tolerance*	Ø mm	±0,08	±0,08	±0,08
Quantity of zinc*	g/m <sup>2</sup>	245	245	275
Tensile strength*	N/mm <sup>2</sup>	350-575		

\* According to SANS 675:1997

\*\* According to SANS 1580:2005 and SANS 675:1997

Table 2



Figure 2



Diamond Wire Netting & Finished Products Company

Tel:0086-311-85962006 85964002 85280058

Fax:0086-311-83800997 Email:river@gabion-box.com

### PVC Coating Characteristics

The properties of the PVC material adheres to the following:

**Colour:** Grey RAL 7037 according to ASTM D1482-57T;

**Specific gravity:** 1,30-1,38 kg/dm<sup>3</sup> in accordance with ASTM D792 Table 1;

**Hardness:** between 55 and 65 Shore D, according to ASTM D2240;

**Tensile strength:** not less than 20,6 MPa, according to ASTM D412-92;

**Modulus of elasticity:** not less than 18,6 MPa, in accordance with ASTM D412-92;

**Abrasion resistance:** the percentage of the weight loss is less than 12%, according to ASTM D1242-92;

**Creeping corrosion:** max. penetration of corrosion of the wire from a square cut end is 25 mm when the specimen has been immersed for 2,000 hrs in a 5% solution HCl (hydrochloric acid 12 Be).

The accelerated aging tests are:

**Salt spray test:** test period 3,000 hours, test method ASTM B117-94;

**Exposure to UV rays:** test period 3,000 hours at 63°C, test method ASTM D1499-92a and ASTM G23-93 apparatus Type E;

**Brittleness temperature:** no higher than -9°C, or lower temperature when specified by the purchaser, when tested in accordance with ASTM D746.

The properties after aging tests are as follows:

**Appearance of coated mesh:** no cracking, stripping or air bubbles, and no appreciable variation in color;

**Specific Gravity:** variations do not exceed 6%;

**Hardness:** variations do not exceed 10%;

**Tensile strength:** variations do not exceed 25%;

**Modulus of elasticity:** variations do not exceed 25%;

**Abrasion resistance:** variations do not exceed 10%;

**Brittleness temperature:** do not exceed +18°C.

STANDARD RENO MATTRESS SIZES		
Length (m)	Width (m)	Height (m)
2,0*	1,0	0,30
3,0*	1,0	0,30
6,0	2,0	0,17
6,0	2,0	0,23
6,0	2,0	0,30

Tolerances : Height, Width: ±5%; Length: ±10%  
All sizes and dimensions are nominal.  
\* Lids pre-attached.

Table 3

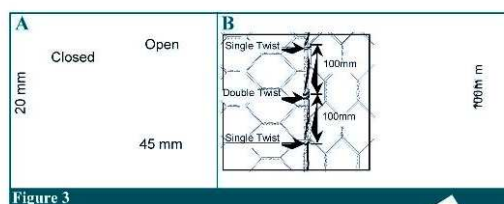


Figure 3

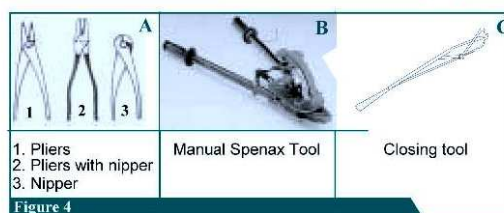


Figure 4

BILL OF QUANTITIES					
Item No.	Description	Unit	Quantity	Rate	Amount (R)
	GABIONS - SANS 1200DK:1995 (Double twist hexagonal wire mesh to SANS 1580:2005).				
1	<b>RENO MATTRESSES</b> (Including material and delivery).				
1.1	Mesh Type 60 with 2,2mm Class A Galvanised wire. Length x Width x Height	m <sup>3</sup>			
1.2	Mesh Type 60 with 2,2 / 3,2mm Class A Galvanised and PVC coated wire. Length x Width x Height	m <sup>3</sup>			
2	Surface preparation for bedding of <b>Reno mattresses</b> .	m <sup>2</sup>			
3	Installation of <b>Reno mattresses</b> (Including unfolding, placing, filling and lacing).	m <sup>3</sup>			
4	Rockfill.	m <sup>3</sup>			
5	<b>AG GEOTEXTILE</b> (Including material, delivery, unrolling, cutting and placing).				
	Continuous Polyester Filament Double Needle-Punched.				
5.1	AG150 - Minimum Energy Absorption of 4,0 kN/m	m <sup>2</sup>			
5.2	AG200 - Minimum Energy Absorption of 6,5 kN/m	m <sup>2</sup>			
5.3	AG300 - Minimum Energy Absorption of 10 kN/m	m <sup>2</sup>			
5.4	AG400 - Minimum Energy Absorption of 12 kN/m	m <sup>2</sup>			

Table 4

Diamond Wire Netting & Finished Products Company

Tel:0086-311-85962006 85964002 85280058 Fax:0086-311-83800997

Email:river@gabion-box.com

ADD:188 meters away from west of Wangdu Building, Anping town, Hebei, China

Figure 78: Reno mattress product sheet page 2/2



## The Duckbill

### Anchor Principle >>>

Saving time and labor, patented Duckbill® Anchors work like toggle bolts in the soil.

Duckbill Anchors are driven into the ground (with no holes, no digging and no concrete), providing a safe and environmentally sensitive installation.

An upward pull on the anchor tendon rotates the Duckbill Anchor into a perpendicular "load lock" position in undisturbed soil.

Duckbill Anchor systems offer the most effective, lightweight, economical solutions to any anchoring application, large or small.

## Models >>>

### Model 40

300 lbs. capacity in normal soils

### Model 68

1,100 lbs. capacity in normal soils

### Model 88

3,000 lbs. capacity in normal soils

### Model 138

5,000 lbs. capacity in normal soils

## How It Works >>>



Drive Anchor



Remove Drive Steel



Pull On Wire Rope



Load Locked

- ① Drive anchor into the soil using a hammer and drive steel rod (a small jack hammer can also be used with power drive steel).
- ② Once anchor is at the proper depth, remove the drive steel.
- ③ Set the anchor in the soil by pulling up on the wire rope.
- ④ The upward pull on the wire rope rotates the anchor into a perpendicular load locked position.

- > **Safe**
- > **Strong**
- > **Easy to Install**

Figure 79: Duckbill anchors product sheet

## MHE Products

3371 Sherman Rd.

East Tawas, MI 48730

(989) 362-5179



14" PushPoint (PP14) 1/8" diameter Sediment Research Sampler	\$50.00 US/Sampler	10% off for Government/Educational
27" PushPoint (PP27) 1/8" diameter Sediment Research Sampler	\$60.00 US/Sampler	10% off for Government/Educational
36" PushPoint (PPX36) 1/4" diameter Field Investigation Sampler	\$100.00 US/Sampler	10% off for Government/Educational
72" PushPoint (PPX72) 1/4" diameter Field Investigation Sampler	\$130.00 US/Sampler	10% off for Government/Educational
8" dia. Mild Steel (uncoated) or polycarbonate Sampling Platform	\$130.00 US/Platform	Each (special order)
Syringe Assemblies for 1/8" samplers	\$5.00 US	Each
Syringe Assemblies for 1/4" samplers (inc. 1/4" x 1/4" adapter)	\$6.00 US	Each
1/8" or 1/4" diameter Screen-Soks	\$4.00 US	Each

Figure 80: Porewater sampler product sheet





Figure 81: OBB construction materials





Figure 82: Temporary construction barriers





Figure 83: Reno mattress anchor installation





Figure 84: Digging a trench to integrate the edges of the reno mattress





Figure 85: Installation of the geocomposite, monitoring ports and sand





Figure 86: The completed OBB module

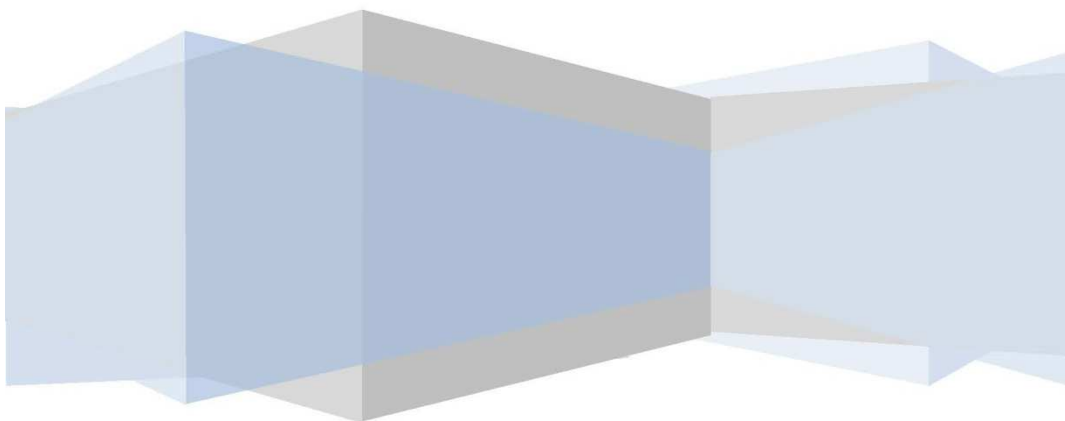
## Appendix I: 454 Pyrosequencing Data Analysis Methodology



### Data Analysis Methodology

Last Updated: 9/16/2014

The most recent version of this file can be downloaded from  
[http://www.researchandtesting.com/docs/Data\\_Analysis\\_Methodology.pdf](http://www.researchandtesting.com/docs/Data_Analysis_Methodology.pdf)





## Contents

Version Changelog .....	4
Version 2.2.3 (09/16/2014) .....	4
Version 2.2.2 (09/03/2014) .....	4
Version 2.2.1 (08/29/2014) .....	4
Version 2.2.0 (07/09/2014) .....	4
Version 2.1.1 (05/20/2014) .....	4
Version 2.1.0 (02/28/2014) .....	4
Version 2.0.0 (01/28/2014) .....	4
Term Definitions .....	5
Client Data Retention Policy .....	5
Data Analysis Methodology .....	6
Visual Overview of the Data Analysis Process .....	6
Overview of the Data Analysis Process .....	6
Denoising and Chimera Checking .....	7
Denoising .....	7
Chimera Checking .....	9
Raw Sequence Data File Formats .....	10
SFF File Generation (454 Only) .....	10
FASTQ File Generation .....	10
Microbial Diversity Analysis .....	12
Quality Checking and FASTA Formatted Sequence/Quality File Generation .....	12
Sequence Clustering .....	13
Tree Building .....	14
Taxonomic Identification .....	14
Diversity Analysis .....	15
Analysis description .....	16





## Data Analysis Methodology

Zip Archives.....	19
Zip Archive Names .....	19
Split Zip Archives.....	19
Windows .....	19
Linux / Mac.....	20
References .....	21



## Version Changelog

### Version 2.2.3 (09/16/2014)

- Updated the data archive to split files too large to fit on our webserver.
- Included instructions for how to handle split zip archives.

### Version 2.2.2 (09/03/2014)

- Added the OTUs folder to the Analysis archive.
- Moved OTUmap.txt from Analysis/OTUMap.txt to Analysis/OTUs/OTUMap.txt
- Added OTUs.fas to the Analysis/OTUs archive.
- Corrected the otus.tre file. All ';' within sequence definitions have been changed to '\_ '.

### Version 2.2.1 (08/29/2014)

- Added the customer data retention policy.

### Version 2.2.0 (07/09/2014)

- Added phylogenetic tree construction using MUSCLE and FastTree.
- Added Krona visualization to the Taxonomic Analysis pipeline.
- Added phylogenetic tree, multiple sequence alignment, and Krona visualizations to the analysis zip archive.
- Updated 454 and Ion Torrent PGM processing to run using the same workflow as MiSeq.
- Added description for the OTUMap.txt file in the Analysis Folder.

### Version 2.1.1 (05/20/2014)

- Updated OTU Selection. Trimming to shortest sequence now performed before UPARSE OTU Selection.

### Version 2.1.0 (02/28/2014)

- Updated denoiser to use PEAR for paired-end read merging in place of USEARCH.

### Version 2.0.0 (01/28/2014)

- Updated denoiser to use USEARCH 7, replacing USEARCH 5.
- Methodology now accounts for processing of 454, Ion Torrent PGM and Illumina MiSeq data.



### Term Definitions

Terms used within this guide are defined as follows:

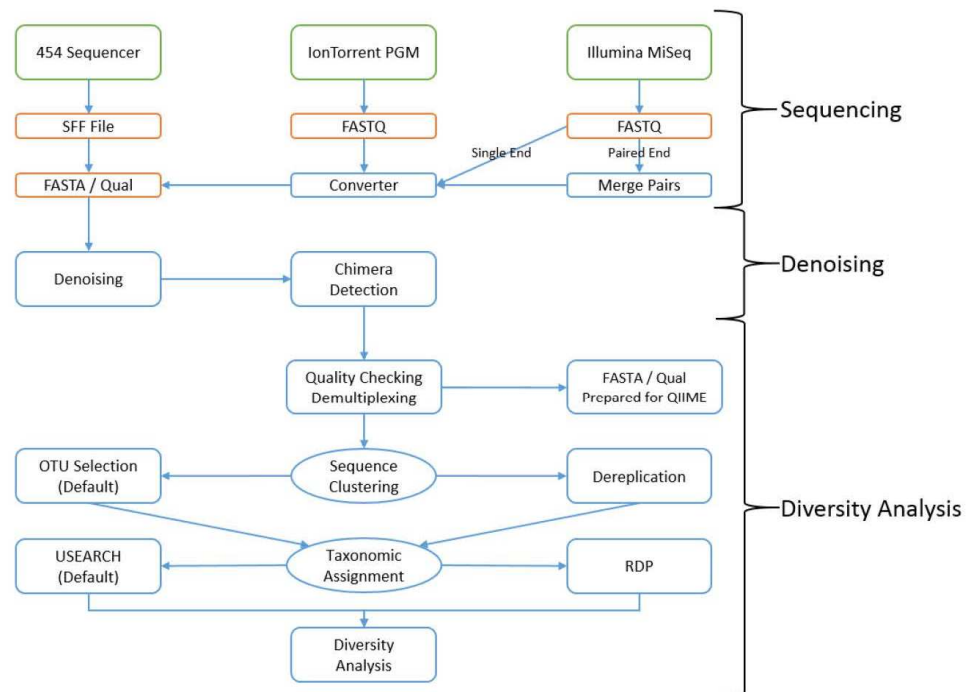
- Tag
  - The term tag refers to the 8-10 bp sequence at the 5' end of the sequence read.
  - The tag is also known as the barcode in some programs.
- ASCII value
  - ASCII (American Standard Code for Information Interchange) is a character encoding scheme based on the English alphabet to encode the following: the numbers 0-9, the letters a-z, the letters A-Z, basic punctuation, control codes (such as new line), and the blank space.
  - Each letter, number and punctuation mark on a keyboard is assigned a numeric value (mostly between 0 and 127) using the ASCII table in order to create a way of encoding/decoding character symbols into computer readable digital bit patterns.

### Client Data Retention Policy

Data will be made available for download (typically via a 12 month temporary link) upon completion of your project. RTL will make every reasonable effort to store all electronic data for your project for a period of 24 months from the date of notification that the project has been completed. If you have any questions regarding your data or if you need to discuss longer term storage, please contact us.

## Data Analysis Methodology

### Visual Overview of the Data Analysis Process



### Overview of the Data Analysis Process

Once sequencing of your data has completed, the data analysis pipeline will begin processing the data. The data analysis pipeline consists of two major stages, the denoising and chimera detection stage and the microbial diversity analysis stage. During the denoising and chimera detection stage, denoising is performed using various techniques to remove short sequences, singleton sequences, and noisy reads. With the bad reads removed, chimera detection is performed to aid in the removal of chimeric sequences. Lastly, remaining sequences are then corrected base by base to help remove noise from within each sequence. During the diversity analysis stage, each sample is run through our analysis



pipeline to determine the taxonomic information for each constituent read and then this information is collected for each sample. This stage is performed for all customers whose data is sequenced using primers targeting the 16S, 18S, 23S, ITS or SSU regions. Analysis can be performed on other regions but may require additional charges.

The data analysis pipeline is broken down into the following steps, each of which is discussed more thoroughly in the sections below:

- Denoising and Chimera Checking
  1. Denoising
  2. Chimera Checking
  3. SFF File Generation (454 only) – FASTQ File Generation (Ion Torrent & Illumina)
- Microbial Diversity Analysis
  1. Quality Checking and FASTA Formatted Sequence/Quality File Generation
  2. Sequence Clustering
  3. Taxonomic Identification
  4. Data Analysis

## Denoising and Chimera Checking

### Denoising

The process of denoising is used to correct errors in reads from next-generation sequencing technologies. According to the paper “Accuracy and quality of massively parallel DNA pyrosequencing” by Susan Huse, et al. and “Removing noise from pyrosequenced amplicons” by Christopher Quince, et al. the per base error rates from 454 pyrosequencing attain an accuracy rate of 99.5% [1] [2]. The paper “A tale of three next generation sequencing platforms: comparison of Ion Torrent, Pacific Biosciences and Illumina MiSeq sequencers” by Michael Quail, et al. states that the observed error rates generated by the Illumina MiSeq is less than .4% while the Ion Torrent PGM has an error rate of 1.78% [3]. Due to the large number of reads and even higher number of base calls per sequencing run, the total number of noisy reads can be quite substantial. In order to determine true diversity it becomes critical to determine which reads are good and which reads contain noise introduced by the experimental procedure. The Research and Testing Laboratory analysis pipeline attempts to correct this issue by denoising entire regions of data prior to performing any other steps of the pipeline.

The Research and Testing Laboratory analysis pipeline performs denoising by performing the following steps on each region:

1. The forward and reverse reads are taken in FASTQ format and are merged together using the PEAR Illumina paired-end read merger [4]. (Illumina MiSeq Paired End Sequencing Only)
2. The FASTQ (Illumina MiSeq and Ion Torrent PGM Only) and SFF (454 Only) formatted files are converted into FASTA formatted sequence and quality files.
3. Reads are run through an internally developed quality trimming algorithm. During this stage each read has a running average taken across the sequence and is trimmed back at the last base where the total average is greater than 25.
4. Sequence reads are then sorted by length from longest to shortest.
5. Prefix dereplication is performed using the USEARCH [5] algorithm. Prefix dereplication groups reads into clusters such that each sequence of equal or shorter length to the centroid sequence must be a 100% match to the centroid sequence for the length of the sequence. Each cluster is marked with the total number of member sequences. Sequences < 100bp in length are not written to the output file, however no minimum cluster size restriction is applied which will allow singleton clusters to exist in the output.
6. Clustering at a 4% divergence (454 & Illumina) or 6% divergence (IonTorrent) is performed using the USEARCH [5] clustering algorithm. The result of this stage is the consensus sequence from each new cluster, with each tagged to show their total number of member sequences (dereplicated + clustered). Clusters that contain <2 members (singleton clusters) are not added to the output file, thus removing them from the data set.
7. OTU Selection is performed using the UPARSE OTU selection algorithm [6] to classify the large number of clusters into OTUs.
8. Chimera checking, which is explained in more detail below in the section entitled "Chimera Checking", is performed on the selected OTUs using the UCHIME chimera detection software executed in *de novo* mode [7].
9. Each clustered centroid from step 6 listed above is then mapped to their corresponding OTUs and then marked as either Chimeric or Non-Chimeric. All Chimeric sequences are then removed.
10. Each read from step 3 is then mapped to their corresponding nonchimeric cluster using the USEARCH global alignment algorithm [5].
11. Using the consensus sequence for each centroid as a guide, each sequence in a cluster is then aligned to the consensus sequence and each base is then corrected using the following rules where C is the consensus sequence and S if the aligned sequence:
  - a. If the current base pair in S is marked to be deleted, then the base is removed from the sequence if the quality score for that base is less than 30.



- b. If the current position in S is marked to have a base from C inserted, then the base is inserted into the sequence if the mean quality score from all sequences that mark the base as existing is greater than 30.
  - c. If the current position in S is marked as a match to C but the bases are different, then the base in S is changed if the quality score for that base is less than 30.
  - d. If a base was inserted or changed, the quality score for that position is updated. If the base was deleted the quality score for that position is removed.
  - e. Otherwise, leave the base in S alone and move to the next position.
12. The corrected sequences are then written to the output file.

### Chimera Checking

As discussed in the paper “Chimeric 16S rRNA sequence formation and detection in Sanger and 454-pyrosequenced PCR amplicons” by Brian Haas, et al. the formation of chimeric sequences occurs when an aborted sequence extension is misidentified as a primer and is extended upon incorrectly in subsequent PCR cycles [8]. This can be seen in Figure 1, shown below.

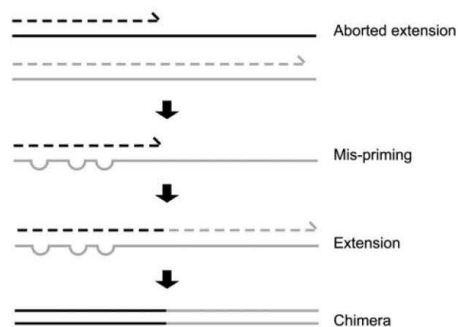


Figure 1.

Formation of chimeric sequences during PCR. An aborted extension product from an earlier cycle of PCR can function as a primer in a subsequent PCR cycle. If this aborted extension product anneals to and primes DNA synthesis from an improper template, a chimeric molecule is formed. Figure and description taken directly from “Chimeric 16S rRNA sequence formation and detection in Sanger and 454-pyrosequenced PCR amplicons” by Brian Haas, et al. [8].

Because amplification produces chimeric sequences that stem from the combination of two or more original sequences [7], we will perform chimera detection using the *de novo* method built into UCHIME.

The Research and Testing Laboratory analysis pipeline performs chimera detection and removal by executing UCHIME [7] in *de novo* mode on the clustered data that was output by our denoising methods. By using this method we can determine chimeras across entire region of data even after accounting for noise and removing low quality sequences.

## Raw Sequence Data File Formats

### SFF File Generation (454 Only)

A sff file is a binary file containing detailed information regarding each read in a single file. For each read, the sff contains a flowgram, quality score and sequence with defined lengths from QC measures performed by the machine. The sff represents the raw data and includes many reads that may have been excluded due to length or chimera detection or any other filter requested for custom processing. Since the files are binary, they cannot be opened with standard text editors. Special programs like Mothur [9] or BioPython [10] are able to load their data into human readable formats and output fasta, qual, flowgram or text (sff.txt) versions. Sff files or their derivatives can then be used for further processing of the data. Sff files provided may be of two forms. In the case of an entire region containing a single investigator's samples, the entire region plus mapping file is provided. In cases where multiple investigators had samples on a single region, each sample is demultiplexed from the sff file using the Roche sffinfo tool by providing its barcode, effectively eliminating it from any read extracted. The split sff can then be used for raw data or submitted directly to archives like the NCBI's SRA. In cases where a single sff for all samples is desired but an entire quadrant is not used, an investigator may request a single sff for a nominal charge. Alternatively, it is possible to use the provided split sff files for denoising/chimera removal by modifying the mapping files. Additional instructions are available if you wish to do so.

### FASTQ File Generation

FASTQ files are text based formatted data files that store the nucleotide sequences generated by the sequencer and their corresponding quality scores encoded as ASCII characters. A FASTQ file contains 4 lines per read that contain the following information:

- Line 1 contains the sequence ID (read definition) and is prepended with an at symbol, '@'.
- Line 2 contains the sequence data.
- Line 3 acts as a separator line between the sequence data and the quality score, it contains a single plus sign, '+'.
- Line 4 encodes the quality values for the sequence in line 2 with each quality score being represented by a single character. As such Line 2 and Line 4 must be the same length.

Decoding of the quality scores requires you to know the phred score offset that was used when the file was generated. Once you know the offset, you can take the ASCII value for the given character and subtract the offset value to obtain the quality score. For example, if the phred offset is +33 and the character 'B' is encountered, then the quality score for that position would be 33 as 'B' is represented by



the ASCII value 66 and the offset is 33 ( $66 - 33 = 33$ ). Using the same logic, 'A' (represented by the value 65) would be  $65 - 33 = 32$  meaning the 'A' character represents a quality score of 32. A free to view ASCII table can be found here: <http://www.ascii-code.com/>.

### Illumina MiSeq

The Illumina MiSeq produces FASTQ files with a phred offset of +33. While the FASTQ file(s) generated by a MiSeq do contain all of the raw sequence data generated by the sequencer, they **do not** contain any information regarding the primer (forward or reverse). Unlike other next generation sequencing technologies, the MiSeq does not sequence the primer, instead it begins sequencing at the first base pair following the forward or reverse primer. This can make processing of your data difficult if the post processing program you decide to use requires it be able to see the primer on the sequence, however most modern programs have removed this restriction due to the prevalence of Illumina data. FASTQ files generated by the Illumina MiSeq come in two forms depending on the sequencing – either paired end or single end. Single end reads are stored in a single FASTQ file with each read in the file representing a read from the sequencer. Paired end reads, however, are slightly more complex and are covered in following section. Reads from the Illumina MiSeq are stored per sequence and are demultiplexed by the Illumina Software, thus your raw data will be missing all barcode information.

### Paired End FASTQ Files

Paired end reads are stored in two FASTQ files with the first file storing the forward “half” of the read and the second file which stores the reverse “half” of the read. It should be noted that both reads are provided in forward order, meaning if you wish to link the two reads together you will first need to take the reverse complement of the reads in the second file. Depending on the insertion size and sequencing read length, the forward and reverse reads may or may not overlap at some point. Unlike other FASTQ files, the order of reads within these files must be kept in a specific order to avoid issues with most post processing programs. The reads within these two files must stay the same between the two files, meaning if you remove or move a sequence in one file, you must remove it or move it to same place in the other file to preserve the same order in both files.

Because the insert size for a paired end sequence matters, we provide two examples of how your sequences may, or may not, line up. In both examples it is assumed that you have already taken the reverse complement of the reverse reads.

**Example 1** – Insert Size approx. 500bp using a 2x300 kit.

Forward-----  
 ~250 BP Forward Only | ~50 BP Alignment | ~250 BP Reverse Only  
 -----Reverse



**Example 2** – Insert Size approx. 800bp using a 2x300 kit.



#### *IonTorrent PGM*

The IonTorrent PGM produces FASTQ files with a phred offset of +33. FASTQ files generated by the IonTorrent contain all of the raw reads stored in a single FASTQ file with barcode information available for demultiplexing. FASTQ files you receive from us from an IonTorrent will be merged into as few files as possible given the number of barcodes available if your samples were run on multiple IonTorrent chips.

#### **Microbial Diversity Analysis**

In order to determine the identity of each remaining sequence, the sequences must first be quality checked and demultiplexed using the denoised data generated previously. These sequences are then clustered into OTUs using the UPARSE [6] algorithm. The centroid sequence from each cluster is then run against either the USEARCH global alignment algorithm or the RDP Classifier against a database of high quality sequences derived from the NCBI database. The output is then analyzed using an internally developed python program that assigns taxonomic information to each sequence and then computes and writes the final analysis files.

#### **Quality Checking and FASTA Formatted Sequence/Quality File Generation**

The denoised and chimera checked reads generated during sequencing are condensed into a single FASTA formatted file such that each read contains a one line descriptor and one to many lines of sequence/quality scores. The Research and Testing Laboratory analysis pipeline takes the FASTA formatted sequence and quality files and removes any sequence which fails to meet the following quality control requirements:

1. Sequences must be at least ½ the expected length given the primer sets used.
2. Sequences must contain a valid error free barcode.

Sequences that pass the quality control screening are condensed into a single FASTA formatted sequence and quality file such that each read has a one line descriptor followed by a single line of



sequence/quality data. The descriptor line in both files has been altered to contain the samples name followed by the original descriptor line, separated with a unique delimiter (::).

This stage of the pipeline creates the FASTA reads archive which contains the following files:

1. The sequence reads from all samples concatenated into a single sequence file. The original tags have been removed from each sequence and an “artificial tag” has been added in its place. The title of the file will be <name>\_<order ID>.fas.
2. The quality scores from all samples concatenated into a single quality file. The scores are labeled with the corresponding sample name and will have a matching line in the .fas file. Since the original tags were removed from the sequence and an “artificial tag” was put into its place, the quality scores have been similarly altered such that the original scores for the tag have been removed and an “artificial quality tag” has been added in its place. The artificial quality tag consists of Q30s for the length of the tag. This file will be labeled <name>\_<order ID>.qual.
3. A mapping file consisting of sample names included in the analysis. This file contains the information for each sample such that each line has the sample name, tag and primer used for the sample. This file will be labeled as: <name>\_<order ID>.txt

### Sequence Clustering

OTU selection clusters sequences into clusters using either an OTU selection program or dereplication depending on the needs of the customer. By default, the OTU selection method is used to determine OTUs and uses the centroid sequence for each OTU to determine taxonomic information. However, if the customer requests that we use the dereplication method, then the clusters will instead represent 100% identity clusters and taxonomic information will be assigned to each of these cluster’s centroid sequence instead.

### OTU Selection (Default)

OTU selection is performed using the guidelines discussed in the paper “UPARSE: Highly accurate OTU sequences from microbial amplicon reads” by Robert Edgar [6]. In that paper, the following methodology is laid out in order to select OTUs:

1. Perform dereplication on the sequences.
2. Remove all singleton clusters from the data set and sort the data by abundance.
3. Trim all sequences to the same length.
4. Perform OTU clustering using UPARSE.

#### 5. Map original reads to the OTUs

Dereplication of sequences is performed using the USEARCH prefix dereplication method [5]. Once complete we removed all singleton clusters and sorted the remaining sequences by cluster size from largest to smallest. The sequences are then run through a trimming algorithm that trims each sequence down to the same size. It should be noted that the sequences are only trimmed for UPARSE and the final taxonomic analysis is based upon the full length sequences. Next we use the UPARSE algorithm to select OTUs [6]. Using the USEARCH global alignment algorithm [5] we then assign each of the original reads back to their OTUs and write the mapping data to an OTU map and OTU table file.

#### *Dereplication*

Some customers would prefer to not have their data go through UPARSE if they are interested in the taxonomic information of the singleton sequences. For these customers we have the pipeline replace the OTU selection stage with a dereplication step using the USEARCH prefix dereplication algorithm [5]. Once the dereplication is complete a dereplication mapping table and dereplication table (same format as the OTU table) are both created and the centroid sequences are written to a file for taxonomic assignment.

#### *Tree Building*

Once OTU selection has been performed, a phylogenetic tree in Newick format is constructed. In order to construct the phylogenetic tree, multiple sequence alignment must be done on the OTU sequences in order to generate equal length aligned sequences. The multiple sequence aligner MUSCLE [11] [12], developed by Robert Edgar, is used with a maximum of 2 iterations in order to perform the alignment of the OTU data. The finished multiple sequence alignment is then passed into FastTree [13] [14], developed by Morgan Price at the Lawrence Berkeley National Lab, a program used to infer approximately-maximum-likelihood phylogenetic trees from aligned sequence data. If you would like to learn more about how FastTree works, please visit the following link:

<http://www.microbesonline.org/fasttree/#How>.

#### *Taxonomic Identification*

In order to determine the taxonomic information for each remaining sequence, the sequences must be run through either the USEARCH global alignment program or the RDP classifier. By default the USEARCH based method is employed however the RDP classifier can be substituted if a customer has requested that we use the RDP classifier instead. In either case the data is identified using a database of





high quality sequences derived from NCBI that is maintained in house. If a customer would prefer we classify their data using a different database such as GreenGenes then we can substitute that database in place of our own. If a non-standard database is requested that requires Research and Testing Laboratory to spend time converting or creating, then a small fee may be charged.

### *USEARCH Global Search (Default)*

The global search method uses a mixture of the USEARCH global search algorithm along with a python program to then determine the actual taxonomic assignment that is assigned to each read. This method is described in the paper “An extensible framework for optimizing classification enhances short-amplicon taxonomic assignments” by Nicholas Bokulich, et al. [15]. The paper describes a methodology in which a high quality database is used in pair with USEARCH rapidly find the top 6 matches in the database for a given sequence. From these 6 sequences you then assign a confidence value to each taxonomic level (kingdom, phylum, class, order, family, genus and species) by taking the number of taxonomic matches that agree with the top match and then divide by the number of total matches, e.g. Bacteria is the top kingdom match and 5 hits state Bacteria and 1 hit shows another kingdom, this would assign a confidence of  $5/6 = .83$ . Once confidence values are assigned for each sequence an RDP formatted output file is generated to be used by our final analysis program.

### *RDP Classifier*

The RDP Classifier is naïve Bayesian classifier that can rapidly determine taxonomic information for sequences while automatically determining the confidence it has at each taxonomic level [16]. The RDP classifier is run against an internally maintained database or a customer requested database along with a taxonomic file to help determine confidence values by giving the classifier a taxonomic tree.

### *Diversity Analysis*

Regardless of the classifier that was used, the data next enters the diversity analysis program. This program takes the OTU/Derep table output from sequence clustering along with the output generated during taxonomic identification and begins the process of generating a new OTU table with the taxonomic information tied to each cluster. This updated OTU table is then written to the output analysis folder with both the trimmed and full taxonomic information for each cluster. For each taxonomic level (kingdom, phylum, class, order, family, genus and species) four files are generated which contain the number of sequences per full taxonomic match per sample, the percentage per full taxonomic match per sample, the number of sequences per trimmed taxonomic match per sample and the percentage per trimmed taxonomic match per sample. These files are all described in more detail below.

## Analysis description

The analysis archive you receive with your data will contain the following files:

- For each taxonomic level (<level>) where level is Kingdom, Phylum, Class, Order, Genus or Species.
  - FullTaxa.<level>.counts.txt
    - This file contains a table with the columns representing each sample in your order and the rows representing each unique taxonomic information for the top hit listed down to <level>, e.g. if <level> is Phylum then it will give each unique Kingdom/Phylum combination.
    - Each row/column intersection defines the number of sequences in the sample that matched that particular unique taxonomic information.
    - Keep in mind that the Full Taxa data shows only the taxonomic information for the top hit, regardless of what the confidence values were.
  - FullTaxa.<level>.percent.txt
    - This file contains a table with the columns representing each sample in your order and the rows representing each unique taxonomic information for the top hit listed down to <level>, e.g. if <level> is Phylum then it will give each unique Kingdom/Phylum combination.
    - Each row/column intersection defines the percent of sequences in the sample that matched that particular unique taxonomic information.
    - Keep in mind that the Full Taxa data shows only the taxonomic information for the top hit, regardless of what the confidence values were.
  - TrimmedTaxa.<level>.counts.txt
    - This file contains a table with the columns representing each sample in your order and the rows representing each unique taxonomic information for the top hit listed down to <level>, e.g. if <level> is Phylum then it will give each unique Kingdom/Phylum combination.
    - Each row/column intersection defines the number of sequences in the sample that matched that particular unique taxonomic information.
    - Keep in mind that the Trimmed Taxa data shows the taxonomic information after the confidence values are taken into account. The USEARCH method rejects the taxonomic information at a level if the confidence is below 51% while the RDPClassifier uses a minimum confidence of 80%.
  - TrimmedTaxa.<level>.percent.txt
    - This file contains a table with the columns representing each sample in your order and the rows representing each unique taxonomic information for the top

hit listed down to <level>, e.g. if <level> is Phylum then it will give each unique Kingdom/Phylum combination.

- Each row/column intersection defines the percent of sequences in the sample that matched that particular unique taxonomic information.
- Keep in mind that the Trimmed Taxa data shows the taxonomic information after the confidence values are taken into account. The USEARCH method rejects the taxonomic information at a level if the confidence is below 51% while the RDPClassifier uses a minimum confidence of 80%.

- OTU/Derep tables

- FullTaxa.otu\_table.txt

- This file contains a table with the columns representing each sample in your order and the rows representing each unique OTU or Dereplication Cluster. The final column contains the taxonomic information for that particular OTU/Cluster listed down to the Species level.
    - Keep in mind that the Full Taxa data shows only the taxonomic information for the top hit, regardless of what the confidence values were.

- TrimmedTaxa.otu\_table.txt

- This file contains a table with the columns representing each sample in your order and the rows representing each unique OTU or Dereplication Cluster. The final column contains the taxonomic information for that particular OTU/Cluster listed down to the Species level.
    - Keep in mind that the Trimmed Taxa data shows the taxonomic information after the confidence values are taken into account. The USEARCH method rejects the taxonomic information at a level if the confidence is below 51% while the RDPClassifier uses a minimum confidence of 80%.

- Krona Folder

- Raw Data Folder

- This folder contains the raw data files that were passed to Krona in order to generate the FullTaxa and TrimmedTaxa Krona HTML files. These files were derived directly from the FullTaxa.species.counts.txt and TrimmedTaxa.species.counts.txt files described above. These files are provided for transparency purposes regarding how your visualization data was created.

- FullTaxa.krona.html

- This file contains the Krona visualization of the FullTaxa.species.count.txt file discussed above. The visualization file is a standard HTML file and should be accessible using any web browser. This visualization was generated using the FullTaxa.species.counts.txt file described before and contains data on all

samples found in that file. You are able to switch between samples using the menu on the left hand side of the screen. Keep in mind that the “Collapse” checkbox is checked by default which can cause your taxonomic levels to look incorrect.

- **This file requires an internet connection in order to work.**

- TrimmedTaxa.krona.html

- This file contains the Krona visualization of the FullTaxa.species.count.txt file discussed above. The visualization file is a standard HTML file and should be accessible using any web browser. This visualization was generated using the TrimmedTaxa.species.counts.txt file described before and contains data on all samples found in that file. You are able to switch between samples using the menu on the left hand side of the screen. Keep in mind that the “Collapse” checkbox is checked by default which can cause your taxonomic levels to look incorrect.

- **This file requires an internet connection in order to work.**

- **OTUs Folder**

- OtuMap.txt

- This file contains the mapping of each OTU identification number used in the OTU Table files. Each line contains the following information separated by tabs: the OTU identification number, the number of sequences that make up the OTU, the sequence definition for the seed sequence and then the sequence definition for each member sequence.

- OTUs.fas

- This file contains the OTU sequences selected during sequence clustering in fasta format. For information regarding how this file was generated please see Sequence Clustering on page 13.

- **TreeData Folder**

- otu\_map.condensed.txt

- This file contains a condensed version of the OtuMap.txt file discussed above. Each line contains two columns separated by tabs. The first column gives the OTU identification number and the second column contains the sequence definition for the seed sequence.

- otus.msa

- This file contains the multiple sequence alignment for each OTU described in the OTU table and OTU map. This file was generated using MUSCLE as described above in the section titled Tree Building.

- otus.tre





- This file contains the phylogenetic tree in Newick tree format created using the otus.msa file described above. This file was generated using FastTree as described in the section titled Tree Building on page 14.

While each file is listed a .txt file, the files are actually tab separated variable files (tsv) and can be opened using any text editor (we suggest using Notepad++ for large file manipulation - <http://notepad-plus-plus.org>) or any spreadsheet editor such as Excel or OpenOffice Calc. Each file can be dragged and dropped into Excel or you may choose to right click on the file name, select “Open With” and choose Excel as the program. Each file contains information about all the samples. Sample names span the first row with the taxonomic designations at each respective taxonomic level listed in the first column.

## Zip Archives

### Zip Archive Names

The following archives will be passed along to you upon completion of your order:

- <Name>\_<OrderNumber>Raw<SequencingDate>.zip
  - This archive will contain the raw FASTQ (Illumina MiSeq) or raw SFF (Roche 454 and IonTorrent PGM).
- <Name>\_<OrderNumber>Fasta<SequencingDate>.zip
  - This archive will contain the denoised sequence data for your entire order in FASTA/Qual format.
- <Name>\_<OrderNumber>Analysis<SequencingDate>.zip
  - This archive contains the data described in the “Analysis description” section found on page 16.
  - This archive will only be sent if you used a standard primer set that we have a working database for. Custom assays will likely not be analyzed.

### Split Zip Archives

If any zip archive is larger than 10GB in size, we will be unable to upload the file to our file server without breaking the file into smaller chunks. In order for you to open these files you will need to download each file in the archives set (denoted with <ArchiveName>.zip.XXX where XXX is a number starting at 001 and counting upwards) and then stitch them back together prior to unzipping the archive. The following commands can be used to rebuild the zip file prior to unzipping.

### Windows

Stitching the files together in Windows requires you to do the following:



- Open a command/DOS prompt
  - In most versions of windows go to “Start menu” then type in cmd and run cmd.exe.
- Navigate to the folder you downloaded the files into.
- Type in the following: `copy /B ArchiveName.zip.* ArchiveName.zip`
- Unzip the ArchiveName.zip file as you normally would.

#### Linux / Mac

Stitching the files together in Linux or Mac requires you to do the following:

- Open a command terminal.
- Navigate to the folder you downloaded the files into.
- Type in the following: `cat ArchiveName.zip.* > ArchiveName.zip`
- Unzip the ArchiveName.zip file as you normally would.

## References

- [1] S. M. Huse, J. A. Huber, H. G. Morrison, M. L. Sogin and D. M. Welch, "Accuracy and quality of massively parallel DNA pyrosequencing.," *Genome Biology*, vol. 8, no. 7, 2007.
- [2] C. Quince, A. Lanzen, R. J. Davenport and P. J. Turnbaugh, "Removing Noise From Pyrosequenced Amplicons," *BMC Bioinformatics* , vol. 12, no. 38, 2011.
- [3] M. A. Quail, M. Smith, P. Coupland, T. D. Otto, S. R. Harris, T. R. Connor, A. Bertoni, H. P. Swerdlow and Y. Gu, "A tale of three next generation sequencing platforms: comparison of Ion Torrent, Pacific Biosciences and Illumina MiSeq sequencers," *BMC Genomics*, 2012.
- [4] J. Zhang, K. Kobert, T. Flouri and A. Stamatakis, "PEAR: A fast and accurate Illumina Paired-End reAd mergeR," *Bioinformatics*, 2013.
- [5] R. C. Edgar, "Search and clustering orders of magnitude faster than BLAST," *Bioinformatics*, pp. 1-3, 12 August 2010.
- [6] R. C. Edgar, "UPARSE: highly accurate OTU sequences from microbial amplicon reads," *Nature Methods*, vol. 10, pp. 996-998, 2013.
- [7] R. C. Edgar, B. J. Haas, J. C. Clemente, C. Quince and R. Knight, "UCHIME improves sensitivity and speed of chimera detection," *Oxford Journal of Bioinformatics*, vol. 27, no. 16, pp. 2194-2200, 2011.
- [8] B. J. Haas, D. Gevers, A. M. Earl, M. Feldgarden, D. V. Ward, G. Giannoukos, D. Ciulla, D. Tabbaa, S. K. Highlander, E. Sodergren, B. Methé, T. Z. DeSantis, The Human Microbiome Consortium, J. F. Petrosino, R. Knight and B. W. Birren, "Chimeric 16S rRNA sequence formation and detection in Sanger and 454-pyrosequenced PCR amplicons," *Genome Research*, 2011.
- [9] P. Schloss, S. L. Westcott, T. Ryabin, J. R. Hall, M. Hartmann, E. B. Hollister, R. A. Lesniewski, B. B. Oakley, D. H. Parks, C. J. Robinson, J. W. Sahl, B. Stres, G. G. Thallinger, D. J. V. Horn and C. F. Weber, "Introducing mothur: Open-source, platform-independent, community-supported software for describing and comparing microbial communities," *Appl Environ Microbiol*, vol. 75, no. 23, pp. 7537-41, 2009.

- [10] P. J. A. Cock, T. Antao, J. T. Chang, B. A. Chapman, C. J. Cox, A. Dalke, I. Friedberg, T. Hamelryck, F. Kauff, B. Wilczynski and M. J. L. d. Hoon, "Biopython: freely available Python tools for computational molecular biology and bioinformatics," *Bioinformatics*, vol. 25, no. 11, 2009.
- [11] R. C. Edgar, "MUSCLE: multiple sequence alignment with high accuracy and high throughput," *Nucleic Acids Research*, vol. 32, no. 5, pp. 1792-1797, 2004.
- [12] R. C. Edgar, "MUSCLE: a multiple sequence alignment method with reduced time and space complexity," *BMC Bioinformatics*, 2004.
- [13] M. N. Price, P. S. Dehal and A. P. Arkin, "FastTree: computing large minimum evolution trees with profiles instead of a distance matrix.," *Molecular biology and evolution*, vol. 26, no. 7, pp. 1641-1650, 2009.
- [14] M. N. Price, P. S. Dehal and A. P. Arkin, "FastTree 2 – Approximately Maximum-Likelihood Trees for Large Alignments," *PLOS One*, 2010.
- [15] N. A. Bokulich, J. R. Rideout, K. Patnode, Z. Ellett, D. McDonald, B. Wolfe, C. F. Maurice, R. J. Dutton, P. J. Turnbaugh, R. Knight and J. G. Caporaso, "An extensible framework for optimizing classification enhances short-amplicon taxonomic assignments," *Not Yet Published*, 2014.
- [16] Q. Wang, G. M. Garrity, J. M. Tiedje and J. R. Cole, "Naive Bayesian classifier for rapid assignment of rRNA sequences into the new bacterial taxonomy.," *Applied and Environmental Microbiology*, vol. 73, no. 16, pp. 5261-5267, 2007.

## Appendix J: Full-Scale OBB supplemental data

Table 16: Key for identifying aromatic hydrocarbons

No.	m/z	Abbreviation	Compound
1	120	AB	C <sub>3</sub> -alkylbenzenes
2	134		C <sub>4</sub> -alkylbenzenes
3	148		C <sub>5</sub> -alkylbenzenes
4	162		C <sub>6</sub> -alkylbenzenes
5	128	NAPH	C <sub>0</sub> -naphthalene
6	142		C <sub>1</sub> -naphthalenes
7	156		C <sub>2</sub> -naphthalenes
8	170		C <sub>3</sub> -naphthalenes
9	184	FL	C <sub>4</sub> -naphthalenes
10	166		C <sub>0</sub> -fluorene
11	180		C <sub>1</sub> -fluorenes
12	194		C <sub>2</sub> -fluorenes
13	208	BP	C <sub>3</sub> -fluorenes
14	222		C <sub>4</sub> -fluorenes
15	154		C <sub>0</sub> -biphenyl
16	168		C <sub>1</sub> -biphenyls + dibenzofuran
17	182	PHEN	C <sub>2</sub> -biphenyls + C <sub>1</sub> -dibenzofuran
18	178		C <sub>0</sub> -phenanthrene
19	192		C <sub>1</sub> -phenanthrenes
20	206		C <sub>2</sub> -phenanthrenes
21	220	PY	C <sub>3</sub> -phenanthrenes
22	234		C <sub>4</sub> -phenanthrenes
23	202		C <sub>0</sub> -pyrene/fluoranthene
24	216		C <sub>1</sub> -pyrenes/fluoranthenes
25	230	CHR	C <sub>2</sub> -pyrenes/fluoranthenes
26	244		C <sub>3</sub> -pyrenes/fluoranthenes
27	258		C <sub>4</sub> -pyrenes/fluoranthenes
28	228		C <sub>0</sub> -chrysene
29	242	BT	C <sub>1</sub> -chrysenes
30	256		C <sub>2</sub> -chrysenes
31	270		C <sub>3</sub> -chrysenes
32	284		C <sub>4</sub> -chrysenes
33	148	DBT	C <sub>1</sub> -benzothiophenes
34	162		C <sub>2</sub> -benzothiophenes
35	176		C <sub>3</sub> -benzothiophenes
36	190		C <sub>4</sub> -benzothiophenes
37	204	NBT	C <sub>5</sub> -benzothiophenes
38	184		C <sub>0</sub> -dibenzothiophene
39	198		C <sub>1</sub> -dibenzothiophenes
40	212		C <sub>2</sub> -dibenzothiophenes
41	226	MAS	C <sub>3</sub> -dibenzothiophenes
42	240		C <sub>4</sub> -dibenzothiophenes
43	234		C <sub>0</sub> -naphthobenzothiophene
44	248		C <sub>1</sub> -naphthobenzothiophenes
45	262	TAS	C <sub>2</sub> -naphthobenzothiophenes
46	276		C <sub>3</sub> -naphthobenzothiophenes
47	290		C <sub>4</sub> -naphthobenzothiophenes
48	253		Monoaromatic steranes
49	267	TAS	Monoaromatic steranes
50	239		Monoaromatic steranes
51	231		Triaromatic steranes
52	245		Triaromatic steranes

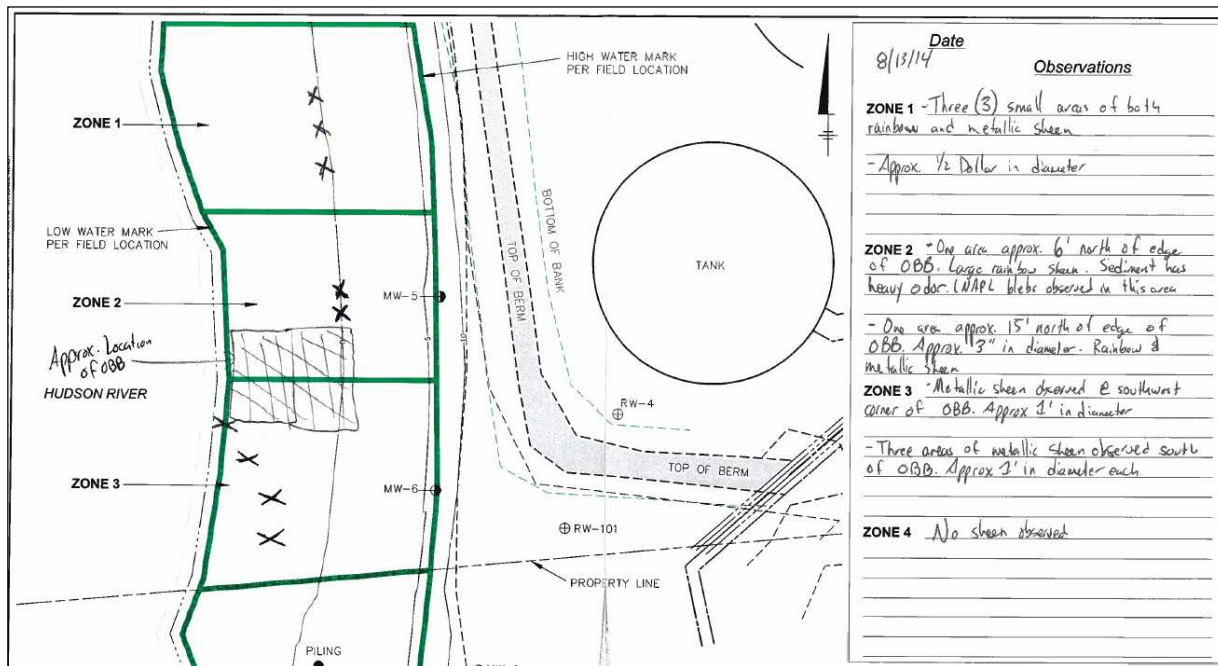





Figure 87: Record of sheen observation from 8/13/2014



Date	Component	Observation	Cause	Action Taken	Photo
1/16/14	Reno mattress wire basket	Lid opened and lifted	Ice Scour	Re-fastened lid to baskset with wire rings	 
5/14/14	Reno mattress wire basket	Basket corner split open by ice scour	Assumed Ice scour; observed after spring thaw	Repaired opening with wire rings	




5/14/14	Anchors	2/14 anchors moved/ loosened	Ice scour or Settlement of the OBB	None	
5/14/14	Monitoring Ports	Housing tubes shifted from original position to varying degrees. The Shift may have jeopardized sampling port connections.	Improper installation (No Hose clamps holding them in position)	None	
5/14/14	Monitoring Ports	Insert filled with clayey fine sediments and algae	Sedimentation, algae	None	
5/14/14	Monitoring Ports	Temperature datalogger housings lost waterproofing	Assumed temperature fluctuations or freeze/thaw	None	
8/12/14	Monitoring Port F	Water port cap fitting gone	Unknown. possibly river debris	None	



Table 17: Microbial DNA 454 pyrosequencing data from full-scale OBB study

	Geocomposite			Sediment			
	OBB A	OBB B	OBB E	Sed A	Sed B	Sed E	Adjacent
<b>Bacteria</b>							
<i>Acidobacterium sp</i>	11.2	10.0	10.5	30.6	24.1	11.4	19.2
<i>Flavobacterium sp.</i>	9.4	10.6	18.0	5.9	8.1	13.6	15.5
<i>Methylobacter sp.</i>	5.5	7.9	4.6				
<i>Rhodoferrax sp.</i>		3.7			4.5	6.2	
<i>Polaromonas sp</i>		3.8			4.7	5.7	
<i>Acidovorax sp.</i>		3.1			3.5	4.1	
<i>Geobacter sp</i>			3.0				5.6
<i>Methylothermus sp.</i>	3.8	4.0					
<i>Castellaniella sp</i>		5.2					
<i>Eubacterium sp.</i>				4.0			
<i>Cytophaga sp</i>			3.4				
<i>Nitrospira sp.</i>				3.0			
<b>Total Identified</b>	29.9	48.3	39.6	43.6	44.9	41.1	40.3
<b>Other</b>	70.1	51.7	60.4	56.4	55.1	58.9	59.7
<b>Archaea</b>							
<i>Methanosaeta sp.</i>	30.4	33.4	21.8	16.1	28.7	25.1	22.4
<i>Candidatus Nitrosopumilus sp</i>	29.2	17.1	24.4	14.9	8.6	14.0	33.8
<i>Nitrososphaera</i>		5.4	5.6	3.6	9.0	5.1	
<i>Thermoplasma sp.</i>		4.3	5.5			8.0	
<i>Candidatus Nitrososphaera</i>				6.0		5.1	
<i>Methanosarcina sp.</i>		3.0	4.8				
<b>Total Identified</b>	59.6	63.2	62.1	40.6	46.2	57.2	56.2
<b>Other</b>	40.4	36.8	37.9	59.4	53.8	42.8	43.8